Influence of Molecular Diffusion on the Transport of Passive Tracers in 2D Laminar Flows

DISSERTATION

zur Erlangung des akademischen Grades
Doctor rerum naturalium
(Dr. rer. nat.)
im Fach Physik
Spezialisierung:
Theoretische Physik

eingereicht an der
Mathematisch-Naturwissenschaftlichen Fakultät
Institut für Physik
Humboldt-Universität zu Berlin

von
Master of Science, Patrick Pöschke

October 28, 2018

Präsidentin der Humboldt-Universität zu Berlin:
Prof. Dr.-Ing. Dr. Sabine Kunst

Dekan der Mathematisch-Naturwissenschaftlichen Fakultät:
Prof. Dr. Elmar Kulke

Gutachter:

1. *Prof. Dr. Igor Sokolov*
2. *Prof. Dr. Benjamin Lindner*
3. *Prof. Dr. Marcin Magdziarz*

eingereicht am:	10.04.2018
Tag der mündlichen Prüfung:	18.10.2018

Abstract

In this thesis, we consider the advection-diffusion-(reaction) problem for passive tracer particles suspended in two-dimensional laminar flow patterns with small thermal noise. The deterministic flow comprises cells in the shape of either squares or cat's eyes. Rotational motion occurs inside them. Some of the flows consist of sinusoidal regions of straight forward motion. All systems are either periodic or are bounded by walls. One examined family of flows continuously interpolates between arrays of eddies and shear flows. We analyse extensive numerical simulations, which confirm previous theoretical predictions as well as reveal new phenomena. Without noise, particles are trapped forever in single building blocks of the flow. Adding small thermal noise, leads to largely enhanced normal diffusion for long times and several kinds of diffusion for intermediate times. Using continuous time random walk models, we derive analytical expressions in accordance with numerical results, ranging from subdiffusive to superballistic anomalous diffusion for intermediate times depending on parameters, initial conditions and aging time. We clearly see, that some of the previous predictions are only true for particles starting at the separatrix of the flow - the only case considered in depth in the past - and that the system might show a vastly different behavior in other situations, including an oscillatory one, when starting in the center of an eddy after a certain aging time. Furthermore, simulations reveal that particle reactions occur more frequently at positions where the velocity of the flow changes the most, resulting in slow particles being hit by faster ones following them.

The extensive numerical simulations performed for this thesis had to be done now that we have the computational means to do so. Machines are powerful tools in order to gain a deeper and more detailed insight into the dynamics of many complicated dynamical and stochastic systems. Thus, they will be of even greater importance in the future.

Keywords: diffusion, anomalous diffusion, laminar, flow, advection, reaction, tracer, noise, eddy, vortex, simulation, numeric, random, mean squared displacement, probability density function, continuous time random walk, CTRW, stochastic differential equation

PhySH terms:
Research areas:

1. Classical transport[1]
2. Anomalous diffusion
3. Continuous time random walk (CTRW)

Theoretical techniques:

1. Stochastic differential equations

[1] This term has been chosen as "primary" for both publications.

Kurzzusammenfassung

In dieser Arbeit betrachten wir das Strömungs-Diffusions-(Reaktions)-Problem für passive Markerteilchen, die in zweidimensionalen laminaren Strömungsmustern mit geringem thermischem Rauschen gelöst sind. Der deterministische Fluss umfasst Zellen in Form von Quadraten oder Katzenaugen. In ihnen tritt Rotationsbewegung auf. Einige der Strömungen bestehen aus wellenförmigen Bereichen mit gerader Vorwärtsbewegung. Alle Systeme sind entweder periodisch oder durch Wände begrenzt. Eine untersuchte Familie von Strömungen interpoliert kontinuierlich zwischen Reihen von Wirbeln und Scherflüssen. Wir analysieren zahlreiche numerische Simulationen, die bisherige theoretische Vorhersagen bestätigen und neue Phänomene offenbaren. Ohne Rauschen sind die Teilchen in einzelnen Bestandteilen des Flusses für immer gefangen. Durch Hinzufügen von schwachem thermischen Rauschen wird die normale Diffusion für lange Zeiten stark verstärkt und führt zu verschiedenen Diffusionsarten für mittlere Zeiten. Mit Continuous-Time-Random-Walk-Modellen leiten wir analytische Ausdrücke in Übereinstimmung mit den numerischen Ergebnissen her, die je nach Parametern, Anfangsbedingungen und Alterungszeiten von subdiffusiver bis superballistischer anomaler Diffusion für mittlere Zeiten reichen. Wir sehen deutlich, dass einige der früheren Vorhersagen nur für Teilchen gelten, die an der Separatrix des Flusses starten - der einzige Fall, der in der Vergangenheit ausführlich betrachtet wurde - und dass das System zu vollkommen anderem Verhalten in anderen Situationen führen kann, einschließlich einem Schwingenden beim Start im Zentrum eines Wirbels nach einer gewissen Alterungszeit. Darüber hinaus enthüllen die Simulationen, dass Teilchenreaktionen dort häufiger auftreten, wo sich die Geschwindigkeit der Strömung stark ändert, was dazu führt, dass langsame Teilchen von schnelleren getroffen werden, die ihnen folgen.

Die umfangreichen numerischen Simulationen, die für diese Arbeit durchgeführt wurden, mussten jetzt durchgeführt werden, da wir die Rechenleistung dafür besitzen. Maschinen sind mächtige Instrumente um tiefere und detailliertere Einblicke in die Dynamik vieler komplizierter dynamischer und stochastischer Systeme zu erhalten. Daher werden sie in Zukunft von noch größerer Bedeutung sein.

Schlagworte: anomale Diffusion, laminar, Advektion, Reaktion, Rauschen, numerisch, mittlere quadratische Verschiebung, Aufenthaltswahrscheinlichkeitsdichte, stochastische Differentialgleichung

Contents

Chapter 1

Introduction

1.1 Stochastic processes, random walks, and diffusion

In nature one can often find things behaving in a seemingly random way. But not only in nature, also in man made systems, like the development of the price of a company on the stock market, the changes of certain quantities are erratic. Whenever a phenomenon looks erratic and complicated enough, it might be reasonable to describe it with the use of random variables and random numbers. One such phenomenon is the Brownian motion of particles suspended in a fluid, i.e. a liquid or a gas. Inside these media, the particles change their direction of motion, because they constantly collide with the molecules of the surrounding medium. This motion is named after the botanist Robert Brown. Another such phenomenon is the motion of the molecules of the fluid itself. The motion is called *molecular diffusion*, because of the overall slow steady spreading of these media inside each other. Molecular diffusion can be described by a theoretical concept which uses random variables. This concept is called *thermal noise*, because the random motion of the molecules is connected to the temperature of the medium and when converting the changes of the positions over time into an acoustic signal, it sounds like noise. Although Brown was not the first who observed random motion, a historical cornerstone of this research area is his observation of the erratic motion of parts of pollen suspended in water in the year 1827. Later, in 1855, Adolf Fick [1] examined salt solved in water and measured the strength of its diffusion by making use of what we now call diffusion equation.

Another historical cornerstone is a paper of Albert Einstein [2] from 1905, where he connects the friction coefficient of suspended particles inside a medium and the temperature of the medium to the diffusion coefficient, while explaining the Brownian motion using the theory of molecular kinetics. This was an important contribution to statistical physics. The greatest feature of this special field of physics is the ability to derive averaged macroscopic quantities from given microscopic probabilistic models.

When describing the motion of continuous media or particles suspended in them, if there is no wind or stream, it often suffices to describe the motion solely with the help of random variables. However, when a stream, and thus an average drift, is present, one has to take both effects into account: the seemingly random part of the motion and the deterministic, that means non-random part of the motion. Mathematical models containing at least one random variable are called *stochastic processes*. A stochastic process, that describes a path of consecutive random steps in some mathematical space, is called a *random walk*. For a visualisation, one just has to think about a chart from the stock market. The value of the price of a stock goes erratically up and down over

time.

For a good introduction to the concept of random walks and the connection to combinatorics, see [3]. In it, Chandrasekhar derives the probability of a particle to be at an arbitrary place, if the particle moves one step to the left or to the right with equal probability after each unit time interval. For a review of stochastic models in natural sciences, see the exhaustive overview article [4] and references therein. Often in nature, the motion, of e.g. animals, is persistent. That means, it is more likely to continue the motion in the same direction. This leads to a description using correlated noise, see [5] and [6]. Some scientists also examined the diffusion of particles changing between two different states of motion, see [7] or [8]. A similar system has been studied in [9], in order to model the random flips of bent tiny rods being partially made of platinum and propelling themselves in a solution of hydrogen peroxide. Furthermore, anomalous diffusion has been examined on fractal networks and in other disordered media, see e.g. [10]. This research area is rich of many more examples of different systems.

1.2 Laminar flows

In this thesis, we consider the motion of particles inside two-dimensional flows. These flows all are assumed to possess a property we call *laminar*. This word, basically meaning *flat*, describes flows which are so smooth that the flow consists only of parallel layers sliding past each other without mixing occurring between them.

A more precise definition of laminar flows uses the dimensionless quantity called *Reynolds number*. This is a ratio of inertial to viscous forces. Flows are typically laminar, if the Reynolds number of the flow is smaller than a few thousands. For larger Reynolds numbers the flow is called *turbulent*. For an example, one just has to think of the wild motion of large flames. When they are rapidly changing their shape, then their motion can typically be regarded as a turbulent one within the rest of the air. This example is easier to spot as a turbulent motion than those consisting of only one medium. If water or air alone is moving in a turbulent way, it is hard to see for the human eye.

An *eddy*, also called *vortex*, describes a part of a flow pattern, in which the particles of the liquid or gas are whirling around in circles, or in a nearly elliptic motion, or in a very similar way. Since in this thesis one system is called the eddy lattice flow, we want to stick to the term *eddy*. A part of a flow, in which the particles move mostly straight forward in one direction, is called *jet*. In many flow patterns we regard in this thesis, there will be eddies. However, each eddy is considered to be so smooth, that it forms a construct one can imagine as an onion, consisting of several layers of cyclic motion. Much like the different layers of an onion, one can peel off after another, the different cyclic layers, enveloping each other, do not mix, as long as we neglect thermal noise. Only if we consider small noise to be present, particles rarely make a transition from one layer to a neighboring one. The particles are considered so small, that they do not disturb the flow itself. They would only show us the trace of the streamline, if noise was not present. That is, why we call them *passive tracer particles*. To quantify the motion of these tracer particles in laminar flows under the influence of small noise by using appropriate mathematical tools, that is what this thesis mostly is about.

Chapter 2

Basic terms and methods of stochastics

In order to make this thesis to a certain degree self-contained, in this chapter we discuss basic concepts and methods from the theory of stochastic processes that are used throughout this thesis. We also define the main quantities, we are interested in for this thesis. The reader is assumed to be familiar with the concept of complex numbers, as well as the differentiation and integration of functions with several variables.

2.1 Introduction to basic terms

Stochastic processes are mathematical objects containing at least one random variable. Often in physics, these random variables depend on time. This mathematical concept has been invented, in order to describe quantities evolving at least partially seemingly random over time, like stock prices, and also to describe diffusing macroscopic entities, like a part of space with a certain temperature surrounded by a space of different temperature, to name a few examples.

One equation commonly used for the description of stochastic processes is the *stochastic differential equation* (SDE)

$$\dot{x}_i(t) = U_i(\mathbf{x}) + V_{ij}\xi_j \quad ; i = 1, \ldots, n \tag{2.1}$$

in n dimensions. This equation is also typically called *Langevin equation* by physicists. It lets the state variables x_i, the elements of the vector $\mathbf{x}$, evolve over time t according to a deterministic part U_i, as well as a random part $V_{ij}\xi_j$, also called the *noise* term. One can regard U_i as a surrounding velocity stream field, when x has the meaning of a position, or as a surrounding force field, if x is considered to be a velocity. If we want to integrate the SDE, we have to make a discretisation. Then, V_{ij} can be considered a weight function, rescaling the width of the *probability density function* (PDF) of the increments of ξ_j. Often, one assumes these increments to be independent in each spatial dimension, independent from each other at different time steps and obeying all the same distribution. In many cases these random numbers are *normally distributed*. If all the above conditions are fulfilled, then ξ_j is called *Gaussian white noise*. Using this noise, the SDE is able to describe the random movement of molecules in water and in air very well.

Note, that only additive noise is used throughout this entire thesis, i.e. the function V_{ij} does not depend on $\mathbf{x}$. Because of this property, the SDE is already fully defined by itself. Contrary, in the opposite case, i.e. when using multiplicative noise, then we would have to care about the interpretation of the noise term. There are various possible ways one could do that. Fortunately, for this thesis this issue is completely irrelevant.

In systems described by the above mentioned SDEs in the long time asymptotic, the overall motion of the particles often is *normal diffusion*. It is characterised by the *mean squared displacement* (MSD)

$$\mathrm{MSD}(t) = \left\langle \sum_{i=1}^{n} (x_i(t) - x_i(t=0))^2 \right\rangle \tag{2.2}$$

growing linearly in time, i.e.

$$\mathrm{MSD}(t) = 2nD^* t. \tag{2.3}$$

These equations mean the following: The distance of the current position x_i from the position at the beginning of the observation is being squared. This involves all n spatial dimensions enumerated by i. This so called *squared displacement* is then being averaged over many particle trajectories, denoted by the angular brackets, i.e. an *ensemble average*. This MSD is proportional to the time t for many systems. Sometimes the square root of the MSD, i.e. the *root mean squared displacement* (RMSD) is used for the description.

The MSD is one of the most important mathematical quantities in stochastic processes, because it is a very well measurable quantity in all kinds of scientific fields, like particle physics, molecular chemistry, inner cell dynamics, behavioral science of animals and many more! For experimental studies measuring the MSD via tracking of trajectories see e.g. [9, 11, 12, 13]. Even if one regards purely deterministic systems, e.g. sufficiently complicated dynamical systems, but with random or complicated initial conditions, it might still be useful to calculate the MSD. Using stochastic differential equations and *random walks*, describing particles making random steps at different time instances, is a microscopic picture of diffusion. The macroscopic picture of diffusion corresponds to considering the probability density $p(\mathbf{x}, t)$ of the particles being the solution of the *Fokker-Planck equation* (FPE)

$$\frac{\partial p(\mathbf{x},t)}{\partial t} = -\sum_{i=1}^{n} \frac{\partial}{\partial x_i} \left[U_i(\mathbf{x}) p(\mathbf{x},t) \right] + \frac{1}{2} \sum_{i,j,k=1}^{n} V_{ik} V_{jk} \frac{\partial^2}{\partial x_i \partial x_j} p(\mathbf{x},t). \tag{2.4}$$

This is the FPE corresponding to the SDE (2.1). The terms U_i and V_{ij} are the same in both equations. The first term in both equations describes a mean drift - the second term the molecular diffusion. Note, that (2.4) is a deterministic differential equation. This means, that even though each particle moves randomly, their probability density is a deterministically spreading macroscopic medium, when interpreted as the concentration of many such non-interacting particles. One could say, that one essential task in the field of stochastic processes and statistical physics in general, is to find connections between microscopic and macroscopic descriptions of nature, e.g. by setting up an SDE, identifying the corresponding FPE, and then determining the characteristics of the solution of the FPE.

2.1.1 Simple one-dimensional example

In order to better understand the basic terms mentioned in the previous section, let us look at one of the simplest examples: a normally diffusing particle in one dimension, i.e. $n = 1$. Suppose there is no drift involved, i.e. $U_1 = 0$. Setting the width of the Gaussian distribution to the constant $V_{11} = \sqrt{2D}$ with *noise intensity* or *diffusivity* D, reduces the FPE to the normal diffusion equation

$$\frac{\partial}{\partial t} p(x,t) = D \frac{\partial^2}{\partial x^2} p(x,t), \tag{2.5}$$

with the solution being the Gaussian function

$$p(x,t) = \frac{1}{\sqrt{4\pi Dt}} \exp\left(-\frac{x^2}{4Dt}\right). \tag{2.6}$$

The specialty about this system is, that it is not just normally diffusive after a long time, but all the time. Here MSD = $2Dt$ holds for all times t.

2.1.2 Other kinds of diffusion

If one encounters the concept of normal diffusion for the first time, it is useful to compare it to something one already knows, namely the *ballistic movement*, i.e. a movement with a constant velocity. Suppose a particle moves with the constant velocity v always in the same direction, i.e. it changes its position over time according to $x = vt$. Then we can calculate the mean squared displacement of many such particles flying in different directions. This is the preferred quantity in this field. However, the square root of it, the RMSD, is in this case the more intuitive one. We obtain

$$\text{MSD} = v^2t^2 \tag{2.7}$$

$$\text{RMSD} = |vt|. \tag{2.8}$$

Compared to the straight forward motion, of e.g. a bullet, a diffusing particle's root mean square position is not proportional to time, but only to the square root of it and is thus spreading more slowly. One has to keep in mind, that *ballistic diffusion*, contrary to ballistic movement, also allows frequent changes of direction, typically resulting in segments of straight motion between turning points. Thus the MSD corresponding to ballistic diffusion typically has a decreased prefactor, however has the same exponent in time as the ballistic movement.

It is convenient to generalise the idea of diffusion, in order to summarise the previous two kinds (normal and ballistic) together with other ones. This can be done in the following way: Let us regard movements of particles for which

$$\text{MSD} = Kt^\alpha \tag{2.9}$$

holds. The two constants are called *(anomalous) diffusion coefficient* K and *(anomalous) diffusion exponent* α. The latter assumes the value two in the ballistic case, respectively unity in the case of normal diffusion. Before we come to the more sophisticated types, let us first consider a very trivial example: Suppose several particles started at the same place, then all moved a bit away from their original positions in the exact same way and finally all stayed forever at the same place. Here, the MSD turns out to be constant, beginning from the time when the particles reached their resting positions. That means, the diffusion exponent is zero.

Between these three cases, standing still ($\alpha = 0$), normal diffusion ($\alpha = 1$), and ballistic movement ($\alpha = 2$), additionally exists *subdiffusion*, with $0 < \alpha < 1$, as well as *superdiffusion*, with $\alpha > 1$. Particles moving subdiffusively are spreading in the first place, contrary to resting, but slower than in the normal case, whereas particles spreading superdiffusively, do so faster than the normally diffusive ones. All situations in which the anomalous diffusion exponent is not unity are called *anomalous diffusion*. For them one can use an FPE containing *fractional derivatives* [14], in order to model the movement of the particles. These generalised derivatives can be calculated in a

similar way to (2.25) using integral transforms. Of course, one can also use a microscopical picture to describe anomalous diffusion. For these situations, there are SDEs with the noise ξ not being Gaussian white noise, but with a PDF possessing tails in shape of power laws which asymptotically decrease more slowly.

2.2 Fourier and Laplace transforms

2.2.1 Definition

In this section we will define two integral transforms. They will turn out to be very useful and essential for calculations involving random walks.

The *Fourier transform* of a function depending on the one-dimensional space x is defined as

$$\mathscr{F}\{f(x)\} = f(k) = \int_{-\infty}^{\infty} f(x)e^{ikx}\,dx. \tag{2.10}$$

For the transformed function we use the same symbol, but with the *wave number* k, also called *Fourier variable*, as its argument. Throughout the entire thesis, this transformation is only applied to functions of the one-dimensional position x. The argument of the transformed function is always denoted k. For the inverse operation

$$\mathscr{F}^{-1}\{f(k)\} = f(x) = \frac{1}{2\pi}\int_{-\infty}^{\infty} f(k)e^{-ikx}\,dk \tag{2.11}$$

holds. There are other possibilities on how to define this integral transform. One can split e.g. the prefactor and distribute it between $\mathscr{F}$ and $\mathscr{F}^{-1}$. Also, one can rescale the exponent. This can include a different convention for the sign of the exponent. However, when dealing with stochastic processes, it is common to choose this definition. That is, because if the function is a probability density $p(x)$, then the transformed function can be written as the average

$$p(k) = \left\langle e^{ikx} \right\rangle \tag{2.12}$$

over all positions x. Also note, that for PDFs the Fourier transformed function $p(k)$ always exists due to their nice mathematical properties[1].

A similar integral transform exists for functions defined on the positive half-axis, e.g. for *waiting time probability density functions* (WTD), since waiting times are not negative. The *Laplace transform* of a function $f(t)$ which vanishes for negative times t is defined as

$$\mathscr{L}\{f(t)\} = f(s) = \int_{0}^{\infty} f(t)e^{-st}\,dt. \tag{2.13}$$

In this thesis, the Laplace transform is only applied to probability densities depending on time t. For them this transformation always exists. The transformed variable s is called *frequency* or *Laplace variable*. The inverse Laplace transform can be calculated as the following contour integral in the complex plane

$$\mathscr{L}^{-1}\{f(s)\} = f(t) = \frac{1}{2\pi i}\int_{c-i\infty}^{c+i\infty} f(s)e^{st}\,ds, \tag{2.14}$$

[1]The needed property is the absolute integrability, which follows in this case from the positivity and the normalisability of probability density functions.

where one integrates along a parallel to the imaginary axis with the constant c chosen such that this parallel possesses a real part greater than the real parts of all the singularities of $f(s)$, i.e. all isolated points with the absolute value of $f(s)$ being infinite, lie left from this parallel. Since the inverse operation is rather complicated, mathematiciens transformed various typical functions and tabulated the results. Thus, the inverse transform of most common functions can then be found by looking them up in these tables, see e.g. [15]. The most important one of these pairs of functions for the theory of continuous time random walks (CTRWs) is, that the Laplace transform of a power law WTD is another power law

$$\mathscr{L}^{-1}\left\{1-\tau^{\alpha}s^{\alpha}\right\} = \frac{\alpha\tau^{\alpha}}{\Gamma(1-\alpha)}t^{-1-\alpha}, \tag{2.15}$$

where Γ is the gamma function, see [16] or (B.11), and τ a time constant used for normalisation. This holds asymptotically for large waiting times t and small Laplace variables s. For very small t the shape of a WTD is different, such that it is normalisable, of course. This law is used several times in this thesis and is called *Tauberian theorem*. A special case that deserves mentioning is the case $\alpha = 1/2$. We then obtain

$$\mathscr{L}^{-1}\left\{1-\sqrt{\tau s}\right\} = \frac{1}{2}\sqrt{\frac{\tau}{\pi}}t^{-3/2}. \tag{2.16}$$

This is useful for the Laplace transform of the WTD of a particle starting at the origin and normally diffusing until it leaves one half-space. The observation that normally diffusing particles possess these waiting times inside half the n-dimensional space is called *normal Sparre-Andersen behavior*, see [17] and references therein. This is a very important result in the field of statistical physics and can not be stressed enough! That is, because this gives us the WTDs for being inside each building block of the flows and thus also the starting point for important analytical calculations. In the following, we will examine the properties of these two integral transforms relevant to us.

2.2.2 Properties

Moments

After having learned how to calculate the Fourier and Laplace transforms, we want to look at the most important properties needed in this thesis. First of all, these two integral transforms are related to the moments $M_n = \langle x^n \rangle$ of a PDF $p(x)$. The first moment equals the mean. If that one equals zero, the second moments equals the variance. To see this relation, one simply replaces the exponential function appearing in the Fourier transform by its Taylor series expansion.

$$\begin{aligned} p(k) &= \left\langle e^{ikx}\right\rangle = \int_{-\infty}^{\infty} e^{ikx}p(x)\,dx = \int_{-\infty}^{\infty}\sum_{n=0}^{\infty}\frac{(ik)^n x^n}{n!}p(x)\,dx && (2.17)\\ &= \sum_{n=0}^{\infty}\frac{(ik)^n}{n!}\int_{-\infty}^{\infty}x^n p(x)\,dx = \sum_{n=0}^{\infty}\frac{(ik)^n}{n!}M_n && (2.18)\\ &= 1 + i\langle x\rangle k - \frac{\langle x^2\rangle}{2}k^2 + \ldots && (2.19) \end{aligned}$$

The constant term $p(k = 0) = 1$ results from the normalisation. Similarly, when a PDF is defined for positive times only, e.g. a WTD, the following derivation can be done:

$$p(s) = \langle e^{-st} \rangle = \int_0^\infty e^{-st} p(t)\, dt = \int_0^\infty \sum_{n=0}^\infty \frac{(-s)^n t^n}{n!} p(t)\, dt \tag{2.20}$$

$$= \sum_{n=0}^\infty \frac{(-s)^n}{n!} \int_0^\infty t^n p(t)\, dt = \sum_{n=0}^\infty \frac{(-s)^n}{n!} M_n \tag{2.21}$$

$$= 1 - \langle t \rangle s + \frac{\langle t^2 \rangle}{2} s^2 + \ldots \tag{2.22}$$

Again, the constant term $p(s = 0) = 1$ corresponds to the normalisation. Note, that in these two expansions not necessarily all moments have to exist. In fact, not any moment has to exist at all. On the contrary, the Fourier and Laplace transforms always exist for PDFs! If the moments exist, often one is only interested in the first two moments in space and the first moment in time. If the first spatial moment vanishes, then a PDF assumes approximately the form

$$p(k, s) \approx 1 - \langle t \rangle s - \frac{\langle x^2 \rangle}{2} k^2. \tag{2.23}$$

In this case one can easily show, that one can calculate the MSD from the PDF in the following way

$$\mathrm{MSD}(s) = \left[-\frac{\partial^2}{\partial k^2} p(k, s) \right]_{k=0}. \tag{2.24}$$

Derivatives and integrals

Another important property is, that derivatives with respect to space, respectively time can be replaced by multiplications with powers of the Fourier, respectively the Laplace variable.

$$\mathscr{F}\left\{ \frac{\partial^n}{\partial x^n} f(x, t) \right\} = (-ik)^n f(k, t) \tag{2.25}$$

$$\mathscr{L}\left\{ \frac{\partial}{\partial t} f(x, t) \right\} = s f(x, s) - f(x, t = 0) \tag{2.26}$$

$$\mathscr{L}\left\{ \frac{\partial^2}{\partial t^2} f(x, t) \right\} = s^2 f(x, s) - s f(x, t = 0) - \left[\frac{\partial}{\partial t} f(x, t) \right]_{t=0} \tag{2.27}$$

$$\mathscr{L}\left\{ \int_0^t f(x, t')\, dt' \right\} = \frac{1}{s} f(x, s) \tag{2.28}$$

Furthermore, if we transform WTDs, we can make use of the fact that they are normalised. Let e.g. $p(t)$ be a probability density that a random walker does not move until time t, then $\int_0^t p(t')\, dt'$ is the probability that the walker makes a step until time t and $\int_t^\infty p(t')\, dt'$ is the complementary probability, i.e. that the walker makes a step after time t. Using this together with (2.28), it is straight forward to show that

$$\mathscr{L}\left\{ \int_t^\infty p(t')\, dt' \right\} = \frac{1 - p(s)}{s} \tag{2.29}$$

holds. These properties are used very often to solve differential equations, since these integral transforms turn them into equations, which often can be solved algebraically

by rearranging terms and solving for the sought function. Furthermore, these integral transforms also allow one to define several kinds of fractional derivatives. They can be used in order to construct differential equations, which yield solutions describing the probability density evolving in systems that show anomalous diffusion. Integral transforms are usually the only way of calculating fractional derivatives.

Convolution theorem

Admittedly, when first being introduced to integral transforms, the idea might seem convoluted, complicated and a bit far fetched. However, there is one property that shows that the realm of Fourier transformed space and Laplace transformed time is exactly the intuitive concept for understanding random walks. The reason for this is, that these transforms replace a sequence of often used, but rather complicated integrals into a very graspable and interpretable simple product of functions, as we will see and use in Appendix C. This property is known as the fact that a so called *convolution integral* of two functions turns into a product of two functions of the transformed variable, i.e.

$$\mathscr{F}\left\{\int_{-\infty}^{\infty} f(x')g(x-x')\,dx'\right\} = f(k)g(k) \tag{2.30}$$

$$\mathscr{L}\left\{\int_{0}^{t} f(t')g(t-t')\,dt'\right\} = f(s)g(s). \tag{2.31}$$

These two formulas are referred to as *convolution theorem*. In order to illustrate why the Fourier transform is so intuitive, when it comes to random walks, let us consider Pearson's random walk on a line, see [14]. Imagine a walker starts at the origin on the x-axis and makes steps with step lengths drawn independently from the PDF $q(x)$ at each step. Now we want to know the probability density $P_n(x)$ for the walker to be at position x after n steps. Per definition, we have $P_0(x) = \delta(x)$ and $P_1(x) = q(x)$, where $\delta(x)$ is the Dirac delta distribution, see Chap. 29 in [16]. In order to obtain the probability density after two steps one has to calculate the convolution integral

$$P_2(x) = \int_{-\infty}^{\infty} q(x')q(x-x')\,dx'. \tag{2.32}$$

More steps involve even more convolution integrals.

$$P_3(x) = \int_{-\infty}^{\infty} q(x-x'')\int_{-\infty}^{\infty} q(x')q(x''-x')\,dx'dx'' \tag{2.33}$$

$$P_4(x) = \int_{-\infty}^{\infty} q(x-x''')\int_{-\infty}^{\infty} q(x'''-x'')\int_{-\infty}^{\infty} q(x')q(x''-x')\,dx'dx''dx''' \tag{2.34}$$

In the Fourier representation the result is simply

$$P_n(k) = (q(k))^n\,. \tag{2.35}$$

For each step there is a factor. The latter equation is therefore so intuitive, that it would have been a lot easier to write down the equation in the Fourier space in the first place! Analogously, if we make the generalisation that the step lengths are drawn from different distributions $q_1(x), q_2(x), \ldots$ in each step, then we obtain formulas like

$$P_3(x) = \int_{-\infty}^{\infty} q_3(x-x'')\int_{-\infty}^{\infty} q_1(x')q_2(x''-x')\,dx'dx'' \tag{2.36}$$

and so on, compared to

$$P_3(k) = q_1(k)q_2(k)q_3(k) \tag{2.37}$$

in Fourier representation.

Similarly to the previous example, we can also look at a process in time. Consider a walker starting at time $t = 0$. It makes steps after times independently drawn from the same WTD $\phi(t)$. We want to know the PDF $P_n(t)$ of the nth step occurring exactly at time t. Again per definition we have $P_1(t) = \phi(t)$. The next ones are calculated via convolutions

$$P_2(t) = \int_0^t \phi(t')\phi(t-t')\,dt' \tag{2.38}$$

$$P_3(t) = \int_0^t \phi(t-t'') \int_0^{t''} \phi(t')\phi(t''-t')\,dt'dt''. \tag{2.39}$$

In Laplace representation the result is again the very intuitive formula

$$P_n(s) = (\phi(s))^n\,, \tag{2.40}$$

i.e. one factor for each step. For a process involving space and time, see Appendix C.

Chapter 3

The eddy lattice flow and the Young-Pumir-Pomeau flow

3.1 Introduction and definition of the models

Cellular flows, i.e. two-dimensional flows of liquids moving around in eddies or vortices within cells, often have been named as typical examples of models showing anomalous diffusion, especially subdiffusion, on intermediate time scales, see [18, 19]. A simple explanation, e.g. in [19], compares these systems to comb models. In a comb, diffusion on a backbone along one spatial dimension is interrupted by diffusion in the teeth along another dimension. The movement along the backbone can then be described by a CTRW with waiting times distributed according to a power law. This movement is subdiffusive and, like other CTRWs with power law waiting times, shows aging and weak ergodicity breaking, see e.g. [20]. Furthermore, the properties of this diffusion strongly depend on the initial conditions.

The similarity between the cellular flow and the comb comes from the fact, that being trapped inside an eddy cell, the particle can not take part in the macroscopic spreading, unless it manages to return to the separatrix between cells. Thus, the coarse-grained picture of the macroscopic motion for both systems is the CTRW. In this sense, cellular flows correspond to combs with finite teeth, since the WTD has an exponential cutoff, because of the finite size of the cell. Eventually, each particle trapped inside a cell will have diffused through it - typically after a certain finite time. After this time scale, the system can be regarded in a coarse-grained way as a discrete time random walk on a lattice moving randomly from one neighboring cell to another. That is, why the final asymptotic behavior of the transport in cellular flows should be diffusive, with the final effective diffusion coefficient $D^* \propto D\mathrm{Pe}^{1/2}$, where D is the coefficient of molecular diffusion, and Pe the Péclet number, see [21]-[25]. The mathematical approaches used in studies until now in this field were mostly based on homogenisation, see e.g. [26] and references therein, and on the large deviation theory [27]. The final normally diffusive regime has already been investigated numerically, and results have been compared to analytical predictions.

However, remarkably, the intermediate subdiffusive time scale has not been investigated in such great detail. This time regime is often stated as a typical example of a situation where aging and ergodicity breaking occur, see e.g. [28, 29], without realising the greater details of the motion caused by the complicated dynamics inside a cell. The transport in cellular flows has been measured experimentally, see [30]-[32]. However, to the knowledge of the author, there is neither an existing work containing extensive

numerical simulations of the SDEs for these systems nor a comparison of numerics with the theoretical predictions in [21] and subsequent works even for the simplest initial condition, corresponding to starting at the separatrix, i.e. on the boundary of a cell, nor is there any work considering aging and convergence to ergodic behavior in these systems. This thesis is dedicated to filling this gap.

In this chapter two standard variants of cellular flows are considered: the *eddy lattice* (EL) flow in two dimensions, see e.g. [25], with the *stream function* given by

$$\psi_{\mathrm{EL}}(x,y) = ua \sin\left(\frac{x}{a}\right)\sin\left(\frac{y}{a}\right), \tag{3.1}$$

and a flow corresponding to a one-dimensional arrangement of cells along the x-axis, with no-slip boundary conditions at the walls, $y = 0$ and $y = \pi a$. The model stream function is

$$\psi_{\mathrm{YPP}}(x,y) = ua \sin\left(\frac{x}{a}\right)\left(\frac{y}{\pi a}\right)^2\left(1-\frac{y}{\pi a}\right)^2. \tag{3.2}$$

Introduced in [21], this flow is referred below to as the *Young-Pumir-Pomeau* (YPP) flow. In both cases u is the characteristic velocity, and πa is the length and width of a cell. Both flows show the intermediate-time subdiffusive behavior crossing over to normal diffusion at longer times. The comparison of these two flows is of considerable interest, since the transport behavior in them is very similar in certain respects, but very different in other ones.

The particle motion under the influence of the flow and of molecular diffusion is described by the SDE

$$\dot{\mathbf{r}} = \mathrm{rot}\,(0,0,\psi(\mathbf{r})) + \sqrt{2D}\boldsymbol{\xi}. \tag{3.3}$$

Here $\mathbf{r}$ is the instantaneous two-dimensional particle position, and $\boldsymbol{\xi} = (\xi_x, \xi_y)$ is a vector of two independent Gaussian noises with zero mean, noise intensity D, and with $\langle \xi_x(t)\xi_x(t')\rangle = \langle \xi_y(t)\xi_y(t')\rangle = \delta(t'-t)$. The term rot is the curl operator. Taking a as the unit length and $t_2 = a^2/D$ as time unit, we can rewrite this equation as

$$\dot{\mathbf{r}} = \mathrm{Pe}\ \mathrm{rot}\,(0,0,\Psi(\mathbf{r})) + \sqrt{2}\boldsymbol{\xi} \tag{3.4}$$

with

$$\Psi(x,y) = \begin{cases} \sin(x)\sin(y) & \text{for EL flow} \\ \sin(x)\left(\frac{y}{\pi}\right)^2\left(1-\frac{y}{\pi}\right)^2 & \text{for YPP flow} \end{cases} \tag{3.5}$$

with $\mathrm{Pe} = ua/D$ being the *Péclet number* of the flow. This quantity is the ratio of the advective transport rate to the diffusive transport rate and thus describes how much stronger the flow is compared to the diffusion. Throughout this entire thesis, we look at small molecular diffusion compared to the deterministic velocity, i.e. $\mathrm{Pe} \gg 1$. An example trajectory of the EL flow is shown in Fig. 3.1. Explicitly writing out the components for the eddy lattice flow, we obtain the equations

$$\dot{x} = \mathrm{Pe}\frac{\partial \Psi_{\mathrm{EL}}}{\partial y} + \sqrt{2}\xi_x = \mathrm{Pe}\sin(x)\cos(y) + \sqrt{2}\xi_x \tag{3.6}$$

$$\dot{y} = -\mathrm{Pe}\frac{\partial \Psi_{\mathrm{EL}}}{\partial x} + \sqrt{2}\xi_y = -\mathrm{Pe}\cos(x)\sin(y) + \sqrt{2}\xi_y. \tag{3.7}$$

In the same way one can obtain

$$\dot{x} = \mathrm{Pe}\frac{\partial \Psi_{\mathrm{YPP}}}{\partial y} + \sqrt{2}\xi_x = \mathrm{Pe}\sin(x)\frac{2y}{\pi^2}\left(1-\frac{y}{\pi}\right)\left(1-\frac{2y}{\pi}\right) + \sqrt{2}\xi_x \tag{3.8}$$

$$\dot{y} = -\mathrm{Pe}\frac{\partial \Psi_{\mathrm{YPP}}}{\partial x} + \sqrt{2}\xi_y = -\mathrm{Pe}\cos(x)\left(\frac{y}{\pi}\right)^2\left(1-\frac{y}{\pi}\right)^2 + \sqrt{2}\xi_y \tag{3.9}$$

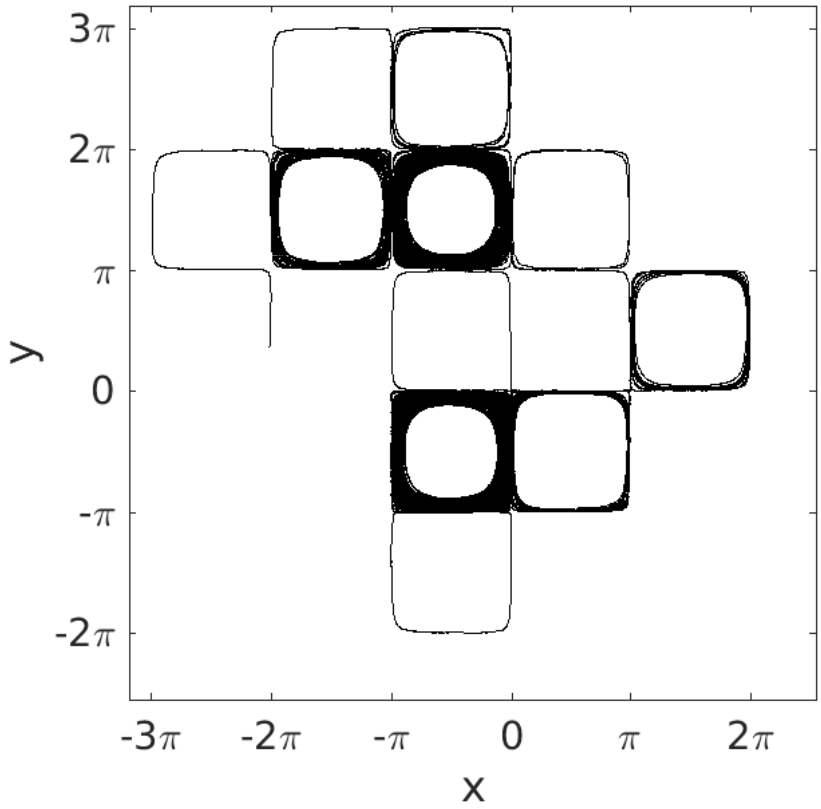

Figure 3.1: A typical trajectory of a passive tracer particle in the EL flow for Pe = 10^4 starting at the origin, obtained from integration of (3.4). The flow consists of eddies in quadratic cells. The flow in neighboring cells is rotating around in opposite directions, i.e. in an infinitely large chess board pattern.

as the equations for the YPP flow. This flow is shown in Fig. 3.2. Note also, that for the EL flow, there is the simple coordinate transform $x_\pm = x \pm y$ turning the equations in the simpler form

$$\dot{x}_+ = \mathrm{Pe} \sin x_- + 2\xi_{x_+} \tag{3.10}$$

$$\dot{x}_- = \mathrm{Pe} \sin x_+ + 2\xi_{x_-}, \tag{3.11}$$

where $\xi_{x_\pm}$ are again Gaussian white noises with the same properties as ξ_x and ξ_y. Note, that the two Gaussian noises do not add up linearly, but according to the law of the propagation of uncertainties, i.e. the resulting standard deviation is the square root of the sum of the squares of the standard deviations for each spatial dimension.

The remainder of this chapter is organised as follows: Below, in Sect. 3.2 we review the subdiffusion dynamics from the point of view of characteristic time scales. The numerical procedures for direct simulation of stochastic differential equations are introduced in Sect. 3.3. Results, concerning different aspects of transport, are presented in Sect. 3.4. Finally, in Sect. 3.5 we summarise our findings. The results of this chapter have been published in [33].

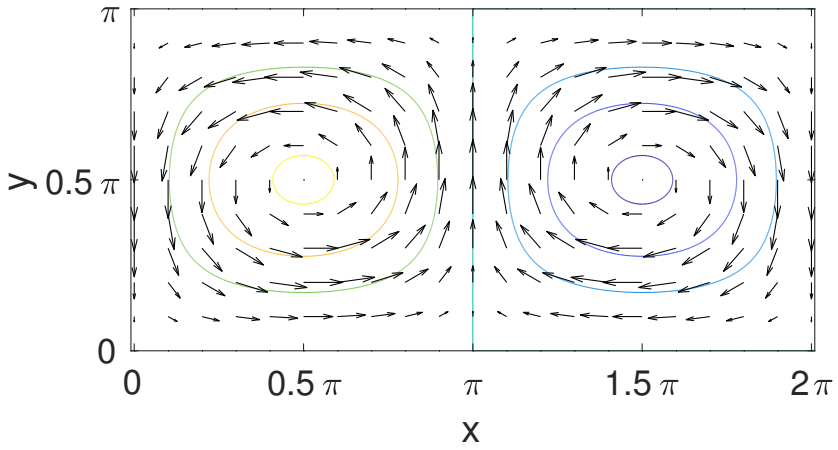

Figure 3.2: Visualisation of one periodic unit, i.e. two cells, of the YPP flow: contour plot of Ψ_{YPP}, Eq. (3.5), and a vectorfield plot of (3.8) and (3.9). Close to the parallel walls at $y = 0$ and $y = \pi$ the velocity is very small, contrary to the separatrix $x = n\pi$ with $n \in \mathbb{Z}$. Thus, this flow has fewer symmetries than the EL flow.

3.2 Characteristic times

In this section we look at which diffusion exponents the two flows possess and between which characteristic times the subdiffusion can be observed. A similar discussion can be found in [21]. Here we only look at the essential steps. The results in this section are not new, but they are important for understanding the results of this work.

A particle can be regarded as trapped inside a cell, when it is far enough inside it. This is because, once having entered the cell, the particle can not leave it until it has slowly diffused back to the periphery of the cell. Let us denote the direction normal to the streamlines by z with $z = 0$ corresponding to the separatrix. Then this particle motion along the z direction can be obtained by averaging the diffusion-advection equation along the streamlines [21]. The averaged equation has the form of the diffusion equation

$$\frac{\partial}{\partial t}p(z,t) = \frac{\partial}{\partial z}\left[D(z)\frac{\partial}{\partial z}p(z,t)\right]. \tag{3.12}$$

The functional dependence of the diffusion coefficient D is influenced by the boundary conditions at the edges of the cell and is therefore different for both flows. For the free boundaries, i.e. infinitely wide and free space, of the EL flow $D(z)$ can be taken constant and equal to the coefficient of molecular diffusion. In case of the no-slip boundary conditions at the two horizontal walls of the YPP flow one has to assume $D(z) \simeq z^{-1}$ for $z \ll a$, i.e. close to the walls, see [21].

The intermediate and final asymptotic behavior of the WTD for the jumps from one separatrix to the next can be obtained by first solving Eq. (3.12) for the probability $p(0,t)$ of being at the origin and utilising its connection to the first return probability, assuming that the process is Markovian, by solving the integral equation $p(0,t) = \delta(0)\delta(t) + \int_0^t \phi(t')p(0,t-t')dt'$, which can easily be done using Laplace transforms. The power law $p(0,t) \propto t^{-\gamma}$ then yields

$$\phi(t) \propto t^{\gamma-2} \tag{3.13}$$

for the first return-time probability density. Note, that this discussion is only valid in the case, where the particle starts on the separatrix, i.e. at $z = 0$, or very close to it and

holds for all transitions between cells. The first waiting time differs in all other cases, i.e. for different initial conditions, e.g. starting at the center of a cell or after having aged, [14].

The probability at being at the origin behaves as

$$p(0,t) \propto \begin{cases} t^{-1/2} & \text{for the EL flow} \\ t^{-1/3} & \text{for the YPP flow,} \end{cases} \tag{3.14}$$

which translates into $\phi(t) \propto t^{-3/2}$, i.e. normal Sparre-Andersen behavior, for the EL flow and into $\phi(t) \propto t^{-5/3}$ for the YPP flow, respectively. With these WTDs the corresponding CTRWs between cells with steps length πa result in subdiffusion described by

$$\mathrm{MSD}(t) \propto t^{1-\gamma} = \begin{cases} t^{1/2} & \text{for the EL flow} \\ t^{2/3} & \text{for the YPP flow,} \end{cases} \tag{3.15}$$

see [34] and references therein. The power law given by (3.13) only holds for intermediate times $t_1 < t < t_2$, bounded by the two characteristic times, t_1 and t_2. After the larger time $t_2 \sim a^2/D$, respectively

$$t_2 = 1 \tag{3.16}$$

in rescaled units, the particle will have been able to move through an entire cell via free molecular diffusion. For $t > t_2$ the WTD $\phi(t)$ possesses an exponential cutoff [21].

The smaller time t_1 is the characteristic time of deterministically moving along close to the boundary of a cell over the length of one cell, thus traversing it. Because of the different boundary conditions, it is different for the two flows. Note, that this minimal time needed to cross a cell defines the normalisation constant of the WTD $\phi(t)$. Since $\phi(t)$ vanishes rapidly for $t \ll t_1$ and $t \gg t_2$ we can approximate the cutoffs as being immediate ones, i.e.

$$\int_{t_1}^{t_2} \phi(t)dt \simeq 1, \tag{3.17}$$

where the upper bound is irrelevant, if $t_2 \gg t_1$, because of the integrability of $\phi(t) \simeq t^{\gamma-2}$. Thus

$$\phi(t) \simeq (1-\gamma)t_1^{1-\gamma}t^{\gamma-2} = \begin{cases} \frac{1}{2}\sqrt{t_1}\,t^{-3/2} & \text{for the EL flow} \\ \frac{2}{3}t_1^{2/3}t^{-5/2} & \text{for the YPP flow.} \end{cases} \tag{3.18}$$

Therefore, the smaller time defines the anomalous diffusion coefficient in the intermediate time regime

$$\mathrm{MSD}(t) \simeq \frac{\pi^2 a^2}{\Gamma(2-\gamma)\Gamma(\gamma)}\left(\frac{t}{t_1}\right)^{1-\gamma} \tag{3.19}$$

$$= \begin{cases} 2\pi\sqrt{\mathrm{Pe}}\,t^{1/2} & \text{for the EL flow} \\ \frac{\pi^2}{\Gamma(1/3)\Gamma(5/3)}\sqrt{\mathrm{Pe}}\,t^{2/3} & \text{for the YPP flow.} \end{cases} \tag{3.20}$$

up to a numeric constant, with t_1 from (3.25) using (3.16). This can be shown by using the Montroll-Weiss formula, see [14],

$$p(k,s) = \frac{1-\phi(s)}{s}\frac{1}{1-\lambda(k)\phi(s)} \tag{3.21}$$

together with (2.24) and with the step length distribution of the one-dimensional lattice

$$\lambda(k) = \cos(\pi a k) \approx 1 - \frac{1}{2}\pi^2 a^2 k^2, \tag{3.22}$$

since one is moving from one separatrix to another always over a distance of πa. For the EL flow the minimal time needed to travel through a cell is defined by the characteristic velocity of the flow and is of the order of $t_1 = a/u$. For the no-slip boundary condition of the YPP flow this does not hold, since the velocity vanishes at the boundary, see Fig. 3.2.

Let us consider a particle in the YPP flow entering a cell, without loss of generality, on its left side. During the time $t \sim a/u$ of travel along the vertical border of the cell the particle typically diffuses in the horizontal direction to the distance $\delta \sim \sqrt{Dt} \simeq (Da/u)^{1/2} \propto a\mathrm{Pe}^{-1/2}$. This is the thickness of the boundary layer, as discussed in Appendix C of [21]. The streamline at such a distance from the vertical boundary is characterised by the value of its stream function $\psi \simeq Au\delta$ with a numeric constant A. When moving parallel to the horizontal boundary say[1], for $x = \pi/2$, where $\psi = By^2$, a tracer passes at the distance $y \propto \sqrt{a\delta}$ from it. The typical velocity at this horizontal part of the streamline is $v_x \simeq u(y/a) \sim u\sqrt{\delta/a}$. Therefore, the typical transport time in the horizontal direction is

$$t_1 \simeq \frac{a}{v_x} \propto \frac{a}{u}\mathrm{Pe}^{1/4}. \tag{3.23}$$

The ratio of the times t_2, defining the end of the subdiffusive regime and thus also the transition to the normal diffusion, and t_1,

$$\frac{t_2}{t_1} \propto \frac{a^2}{D}\frac{u}{a}\mathrm{Pe}^{-1/4} = \mathrm{Pe}^{3/4} \tag{3.24}$$

is an increasing function of the Péclet number. This means, that the Péclet number has to be large enough, in order for an intermediate regime to establish. According to the simulations for both systems, $\mathrm{Pe} \geq 10^3$ is needed in order to see it clearly, i.e. stretching over one order of magnitude in time. Note, that transitions between regimes take their time too. Summarising these findings, we have

$$\frac{t_2}{t_1} \simeq \begin{cases} \mathrm{Pe} & \text{for the EL flow} \\ \mathrm{Pe}^{3/4} & \text{for the YPP flow.} \end{cases} \tag{3.25}$$

Again, the anomalous diffusion in these two systems is only pronounced in the case of large Péclet numbers.

The existence of the upper cutoff time guarantees the mean waiting time t^* inside a cell to be finite. It is given by

$$t^* = \int_{t_1}^{t_2} t\phi(t)dt \simeq t_1^{1-\gamma}t_2^{\gamma} \tag{3.26}$$

$$= t_2\left(\frac{t_2}{t_1}\right)^{\gamma-1} = \frac{a^2}{D}\left(\frac{t_2}{t_1}\right)^{\gamma-1} \tag{3.27}$$

for $t_2 \gg t_1$ and $0 < \gamma < 1$. The normal diffusion coefficient in the final regime is then

$$D^* \simeq \frac{a^2}{t^*} = D\left(\frac{t_2}{t_1}\right)^{1-\gamma}. \tag{3.28}$$

Inserting the expression for t_2/t_1 (3.25) and the respective values of

$$\gamma = \begin{cases} 1/2 & \text{for the EL flow} \\ 1/3 & \text{for the YPP flow,} \end{cases} \tag{3.29}$$

[1]Note, that there are two typos in the corresponding equations in [33].

we arrive at

$$D^* \simeq D\mathrm{Pe}^{1/2} \tag{3.30}$$

for both flows. This form of D^* guarantees the smooth transition from the anomalous diffusion on intermediate time scales given by (3.19) to the normal diffusion given by MSD $\sim D^* t$ at the upper crossover time t_2.

Note, that for initial conditions different from starting on the separatrix, and in situations when starting the observation after a certain aging time, the distribution $\phi_1(t)$ of the waiting time until the first jump between cells differs from $\phi(t)$ for all consecutive steps and can not, in general, be obtained by the approach based on streamline averaging.

3.3 About the numerical method

By numerically integrating the SDE (3.4), one obtains trajectories $\mathbf{r}(t) = (x, y)$ of tracer particles. These trajectories are used to compute the MSD from the initial position. For the integration the stochastic Heun method has been used. This second-order Runge-Kutta method is an efficient algorithm for the integration of stochastic differential equations with additive noise [35]. For an example of a fast implementation, see Appendix A. The size of the time step was chosen sufficiently small to ensure that the deviations of the deterministic part of (3.4) from its exact solution are negligible. Note, that without noise the stream function Ψ is conserved. For both flows choosing a time step of $\Delta t = 10^{-3}\mathrm{Pe}^{-1}$ turned out to be sufficient for all parameter values in all regimes of interest, until the maximum simulation time $t_{\max} = 100$. The simulations were done in the range of Péclet numbers from 10^2 to 10^5. Throughout the thesis, we focus mainly on the results for $\mathrm{Pe} = 10^4$.

This value has been chosen, because then the intermediate regime is already long enough to see it clearly - about two orders of magnitude in time - but on the other hand does not require too long trajectories. Therefore shorter, and thus more, simulations could be made in a still acceptable amount of time, yielding smooth curves for the MSDs. With smooth curves one can better see slopes, i.e. diffusion exponents and thus also crossover times. Usually, it is desirable to make ensemble averages over 10^4 different realisations for the MSD. This has been achieved for $\mathrm{Pe} = 10^4$.

In the next section we will also investigate an *aged MSD*. It still depends on the observation time t. However, first the system is prepared in one of the initial conditions, and afterwards ages for a certain aging time t_a. Then, at that moment, the observation starts with $t = 0$. This means, we have

$$\mathrm{MSD}(t, t_a) = \langle (\mathbf{r}(t_a + t) - \mathbf{r}(t_a))^2 \rangle \tag{3.31}$$

for the formula for the aged MSD. Of course, the ordinary MSD is reproduced by setting $t_a = 0$. Furthermore, when analysing if a system is ergodic, i.e. if an ensemble average equals a time average, we need the *time averaged mean squared displacement* (TAMSD)

$$\mathrm{TAMSD}(\Delta, T) = \frac{1}{T - \Delta} \int_0^{T-\Delta} [\mathbf{r}(t' + \Delta) - \mathbf{r}(t')]^2 \, dt', \tag{3.32}$$

with the *time delay* $\Delta > 0$. In addition to that, we also consider the ensemble average of these TAMSDs, the *ensemble averaged time averaged mean squared displacement*

(EATAMSD)

$$\mathrm{EATAMSD}(\Delta, T) = \frac{1}{T-\Delta}\int_0^{T-\Delta} \langle [\mathbf{r}(t'+\Delta) - \mathbf{r}(t')]^2 \rangle \, dt'. \tag{3.33}$$

Because of the effective one-dimensional transport in the YPP flow, for our analysis, we only consider displacements along the x-axis.

3.4 Results

In this section we look at the results of the extensive numerical simulations and compare them to analytical calculations. First of all, let us define the considered initial conditions.

3.4.1 Definition of the initial conditions

For both flows it is insightful to look at the following same three initial conditions.

1. First initial condition: starting homogeneously distributed at the separatrix between neighboring cells. For the EL flow this refers to all four edges of a quadratic cell. In the case of the YPP flow this only includes the vertical edges between cells, excluding the edges at the walls. Because of symmetry reasons, for both flows it is enough to set $x(t = 0) = 0$ and drawing $y(0)$ equally distributed between 0 and π.

2. Second initial condition: starting from a *"flooded"* cell. When taking the orientation into account, a full periodic unit of the flow would have a periodicity of 2π in both dimensions. However, because of symmetry reasons, it is enough to restrict oneself to the length of π in both dimensions. This simply means, that the particles start homogeneously distributed over one whole cell. This can be achieved by choosing $x, y \in [0, \pi]$ equally distributed.

3. Third initial condition: starting in the middle of an eddy. Here all particles start δ-distributed in the exact geometric center of one cell. For both flows this corresponds to e.g. $(x(0), y(0)) = (\pi/2, \pi/2)$.

Later on, for the YPP flow, we will also shortly look at a fourth initial condition similar to the first one, starting homogeneously at a wall, e.g. at $y(0) = 0$. This initial condition corresponds to a simple model of the atmosphere where dust or gases, like CO_2, are emitted at the surface of the earth and spread parallel to the surface, i.e. in the x-direction.

3.4.2 MSD and probability density on intermediate times

The results for the main quantities of interest are shown in Figs. 3.3 to 3.5 and 3.7. In these figures, (a) always presents the results for the EL flow, whereas (b) displays the results for the YPP flow. Remember, that for the EL flow the regarded distance for the measuring of the MSD is the usual two-dimensional Euclidean distance from the starting position, whereas for the YPP flow only the horizontal distance, i.e. along the x-axis, is considered.

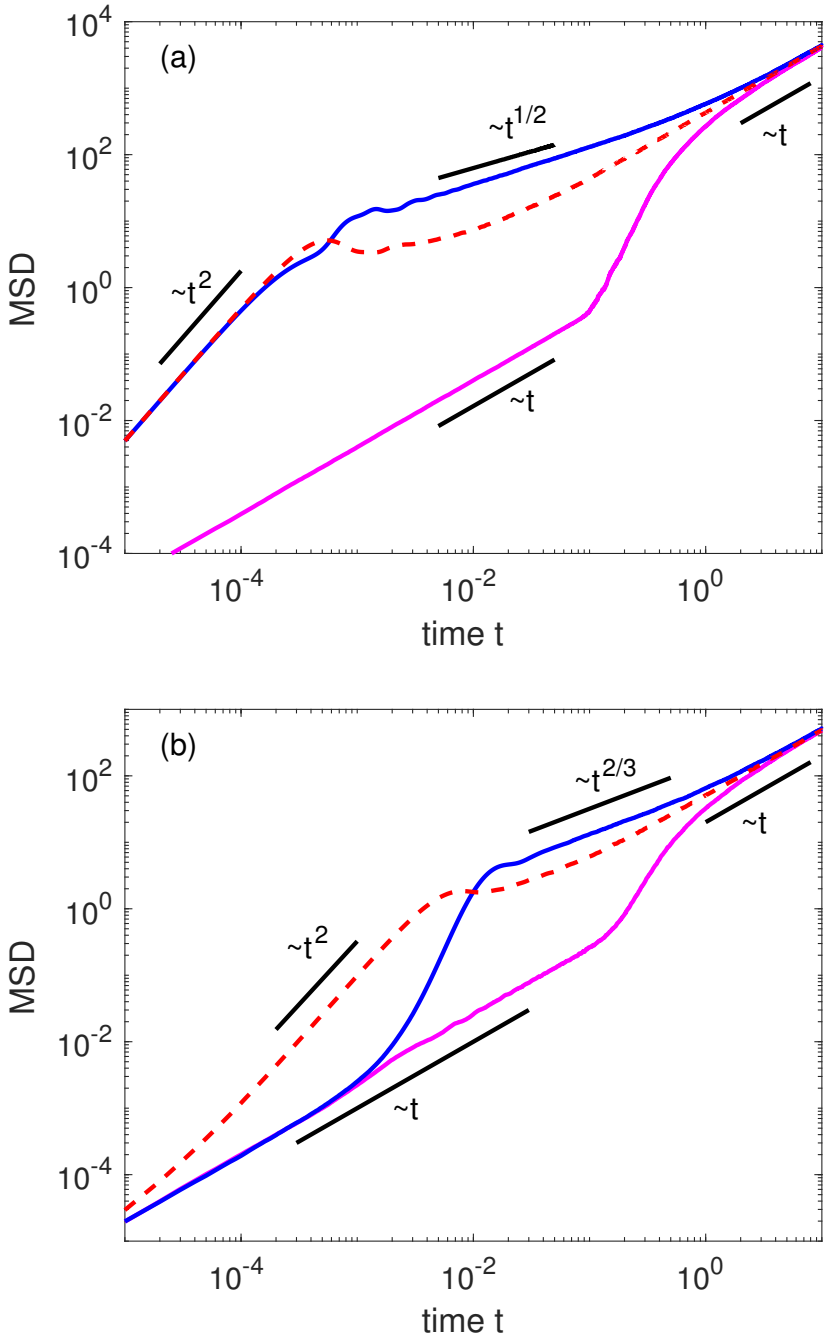

Figure 3.3: Simulated MSD of 10^4 walks for Pe $= 10^4$ for (a) the EL flow and (b) the YPP flow for starting at the separatrix (upper, solid blue), the flooded case (dashed red), and starting at the center of a cell (lower, solid magenta). The black bar indicating $t^{1/2}$ is a plot of Eq. (3.20).

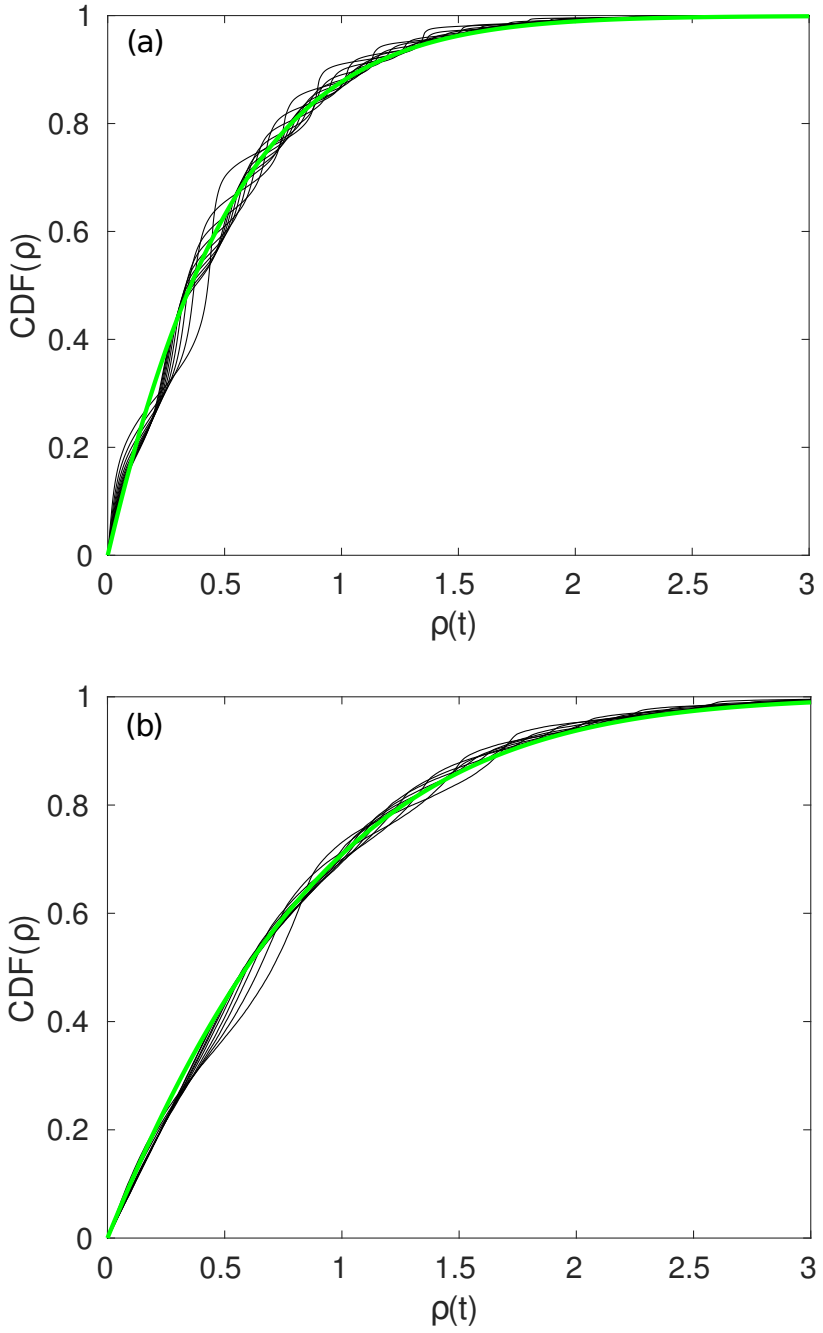

Figure 3.4: (a) CDF depending on the rescaled distance ρ for EL in subdiffusive regime: 10^6 simulated walks with time $t \in [0.01, 0.1]$ in steps of 0.01 (thin, black) compared to the predictions of CTRW (thick, green), Eq. (3.38). (b) The same for the YPP flow: 10^5 simulated walks with time $t \in [0.1, 0.5]$ in steps of 0.05. Note, that no adjustable parameters were used to obtain these two plots. Most particles are contained in a surrounding of three standard deviations around their initial position, since there the CDF is almost unity already.

Figure 3.3 shows the MSD for the three initial conditions defined above. The upper (solid blue) curves correspond to the first initial condition, i.e. starting at the separatrix. The red dashed curves show the MSD for the particles being homogeneously distributed over a cell at the beginning of the observation. This second initial condition is referred to as the "flooded case". The lower curves (solid magenta) correspond to starting at the center of a cell.

Let us first discuss the behavior of the MSD for the initial condition which has been researched most in the past, i.e. starting at the boundary of a cell, at or near the separatrix. For $t > t_1$ the MSD is well described by a CTRW. The two characteristic times define three different time regimes, i.e. an initial regime[2] for $t < t_1$, an intermediate one for $t_1 < t < t_2$, and a final one for $t > t_2$. In the EL flow the motion for $t < t_1$ is dominated by the ballistic transport at the periphery of a cell, contrary to the YPP flow, for which the motion for short times is the normal diffusion. The transition from this domain to the next one corresponds to a superballistic motion, since the transport velocity grows when the particle diffuses into the interior of the cell. On intermediate times scales, particles in both flows experience subdiffusion described by MSD $\propto t^{1/2}$ for the EL flow and MSD $\propto t^{2/3}$ for the YPP flow, as predicted by the CTRW model. In the final regime, i.e. when $t > t_2$, the motion is a normally diffusive one for both flows.

The time evolution of tracer particles starting at the separatrix, or close enough to it, is indeed well-described by a CTRW with the waiting time densities $\phi(t) \propto \tau^\alpha t^{-1-\alpha}$ as given by Eq. (3.18), with the characteristic time τ being of the order of t_1 and $\alpha = 1-\gamma$. With the given WTD $\phi(t)$ for each step of the length of order πa, the PDF of the particles displacement can be formulated in the form

$$p(k,s) = \frac{\tau^\alpha s^{\alpha-1}}{\frac{1}{2}\pi^2 a^2 k^2 + \tau^\alpha s^\alpha} \tag{3.34}$$

in the Fourier-Laplace representation, see (3.21), for small k and s, which corresponds to the long time and large scale limit in the space-time domain, see e.g. Chap. 4 of Ref. [14]. Note, that for intermediate times $t < t_2$ one can neglect the upper cutoff of the WTD at t_2. That means, in order to gain the intermediate asymptotics, we calculate the long time asymptotics of a process for which the power law of the waiting times goes on forever. When calculating the PDF $p(x,t)$ for both systems, we only look at one spatial dimension, i.e. x. The PDF is an even function of x and scales as a function of $\rho(t) = x(t)/\mathrm{RMSD}(t)$, with RMSD = MSD$^{1/2}$. That means, we have

$$p(x,t) \propto f_\alpha(|x(t)/\mathrm{RMSD}(t)|), \tag{3.35}$$

with the scaling function $f_\alpha(\rho)$ depending on the parameter α, which is different for both flows. For the YPP flow the integrals can be solved using Bessel functions of fractional order, see [21], yielding

$$f_{2/3}(\rho) \propto \mathrm{Ai}(\rho), \tag{3.36}$$

where Ai(ρ) is the Airy function, see Chap. 10 in [16] and note, that $\rho \geq 0$. In the case of the EL flow to our knowledge no closed form is known, but there is a useful integral representation[3], see Chap. 6 of Ref. [14], which helps to find $p(x,t)$, and thus $f_{1/2}(\rho)$,

[2] Of course, at very short times, before our "initial regime", there is always the very first time scale on which the transport by molecular diffusion is stronger than the flow, resulting in the same normal diffusion with coefficient D for all initial conditions.

[3] For alternative representations, see Appendix B.

numerically:

$$p(x,t) = \int_0^\infty \frac{1}{2\pi\sqrt{K\omega t}} \exp\left(-\frac{x^2}{4K\omega} - \frac{\omega^2}{4t}\right) d\omega \tag{3.37}$$

with K being proportional to the anomalous diffusion coefficient defining the MSD. K is obtained by calculating the MSD from (3.37) and comparing it to the simulated MSD. Knowing $f_\alpha(\rho)$ we can calculate the corresponding normalised *cumulative distribution function* (CDF)

$$\mathrm{CDF}(\rho) = F_\alpha(\rho) = \frac{\int_0^\rho f_\alpha(z)\,dz}{\int_0^\infty f_\alpha(z)\,dz} \tag{3.38}$$

of the rescaled absolute displacements ρ and compare it to the numerical results, see Fig. 3.4. Note, that for the EL flow, only the displacement along the x-direction is considered. The theoretical curves obtained in this way are shown as thick green lines on top of the curves representing the numerical results. The latter are represented as thin black lines for rescaled distances at different times during the subdiffusive regime. They follow indeed the predictions of CTRW model approximately but have additional small oscillations, which are not errors or artefacts but stem from the internal dynamics of the particles within the cells, which is not resolved on the longer time scales on which one can apply the CTRW approach. Locally larger slopes of the CDF correspond to local maxima of the PDF. They appear at the boundaries of the cells. Since the particles invade each cell beginning from the boundary, this is where the concentration is higher compared to the interior of the cells. This means, by counting the oscillations one can roughly count the number of invaded cells. This also shows, that the number of invaded cells in the subdiffusive regime is still relatively small, i.e. typically only half a dozen for most particles. It is exactly this intracell dynamics which makes the anomalous diffusion in cellular flow different from the one in combs with finite teeth. Also note, that the theoretical curves of the CDF(ρ) for different not too small Pe should all coincide as well respectively for both systems. We checked this to hold for ten times larger Pe, i.e. Pe = 10^5.

Let us return to the discussion of Fig. 3.3. When starting at the center of the cell (lower, solid magenta curves), there is no intermediate subdiffusive regime. The behavior in both flows makes a fast superballistic transition from an initial normal diffusion with diffusion coefficient D to a final normal diffusion with coefficient $D^* \simeq D\mathrm{Pe}^{1/2}$.

In the flooded case, i.e. when starting homogeneously distributed in one cell (red dashed curve), the final regime is the same as in the other two cases. However, it is reached significantly earlier. That is, why it is preferable to simulate this situation, when determining the final diffusion coefficient numerically. The motion at short times is ballistic, which for the EL flow coincides with the one for starting at the separatrix. Also note, that in the flooded case there is no intermediate regime with constant anomalous diffusion exponent. In the transition from the initial ballistic to the final diffusive regime only a slight oscillation occurs.

A similar behavior of the MSD for the considered initial conditions can be observed for other Péclet numbers as well, ranging from 10^2 to 10^6, i.e. for all simulated values; not shown.

For the YPP flow we also take a fourth initial condition of starting at a wall into consideration, i.e. $y = 0$ with $x \in [0, \pi]$ equally distributed. This initial condition is equivalent to starting at the separatrix with a vanishing advection flow and it corresponds to a pollution model of the atmosphere with dust being initially on the surface

of the earth. The MSD for this initial condition, see the lowest black dotted curve in Fig. 3.5 (b), is very similar to the initial condition of starting at the separatrix, see lowest solid blue curve.

3.4.3 Aging

The strong dependence on the initial conditions is the reason for aging and for non-ergodic behavior of the MSD at intermediate times, see e.g. the discussion in [36]. That is, why we look at both: the aging and the time averages.

Let us begin with the analysis of the aging behavior of the MSD. Since the homogeneous distribution of particles in the system is invariant under motion caused by the flow and molecular diffusion, the MSD in the flooded case does not age, i.e. $\mathrm{MSD}(t, t_a) = \mathrm{MSD}(t)$. For all other initial conditions aging is present, as shown in Fig. 3.5. The MSD for flooded cells acts as a limiting curve for the aged MSD for large aging times, i.e. $t_a \to \infty$. When starting at the separatrix, this limiting curve is approached from above for both flows, for intermediate times corresponding to sub-diffusion. In the short time domain there is a difference between the EL and the YPP flows caused by different relative positions of the MSD curves discussed above. Since for the EL flow the short time behavior for starting at the separatrix, and the flooded case coincide, the MSD at short times does not age. On the contrary, for the YPP flow the MSD for the initial time regime becomes considerably larger after aging. For the fourth initial condition of starting at a wall in the YPP flow, the MSD ages very similarly to that for starting at the separatrix.

Aging for starting at the center of a cell

When starting at the center of a cell, considerable aging effects can always be observed. For the EL flow the initial aged MSD is always ballistic and approaches the asymptotic initial ballistic MSD from below, whereas for the YPP flow, the aged MSD changes from diffusive to ballistic for short times.

Since the aged MSD is most interesting for intermediate times, i.e. $t_1 \ll t \ll t_2$, and for starting at the center of a cell, we investigate this situation in greater detail. The behaviour is very similar for both flows. As one can see in Fig. 3.5, the values of the aged MSD in this time domain for not too large aging times, i.e. $t_a \ll t_2$, are small compared to the cell area $\pi^2 \approx 10$. For that reason the MSD is dominated by the rotating motion within a single eddy and shows oscillations, whose amplitude decays slowly with an increase in both t and t_a. This kind of aging behavior is not observed in a comb which does not show any internal dynamics within the trapped state. The oscillations of the aged MSD are due to the fact, that the tracer position after aging time t_a is not at the center of a cell but at a finite distance from it. The further motion of the tracer approximately follows a closed streamline around the center of the cell, and indeed the frequency of the oscillations corresponds to the angular velocity of such rotations, which follows from the solution of the deterministic part of Eq. (3.4) in rescaled units for $\mathbf{r}$ close to the center of the cell. These frequencies are $\omega = \mathrm{Pe}$ for the EL flow and $\omega = (4\pi)^{-1}\mathrm{Pe}$ for the YPP flow. The simulations confirm the corresponding time periods $T = 2\pi/\omega$ of the circulations for the examined Pe values. The decay of these oscillations is caused by the dephasing of the motion: In the course of time more and more particles move away from the center of the cell. The rotation frequency depends on the distance from the center and decays to zero at its periphery.

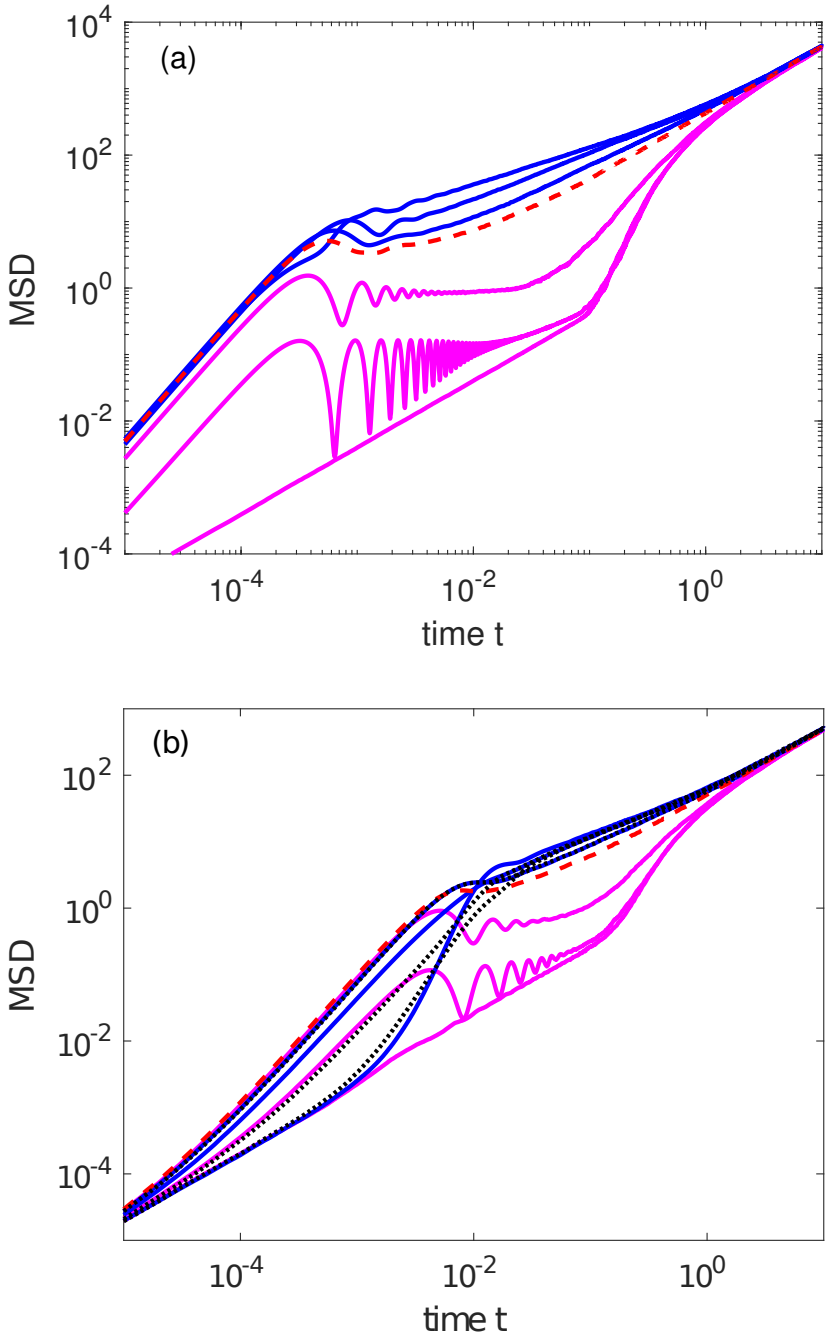

Figure 3.5: Same as Fig. 3.3 with aging times $t_a = 0$, 10^{-2}, and 10^{-1} (upper, solid blue and lower, solid magenta curves) compared to flooded case (dashed red). In (b) we show in addition the initial condition of starting at a wall, i.e. at $y = 0$ (dotted).

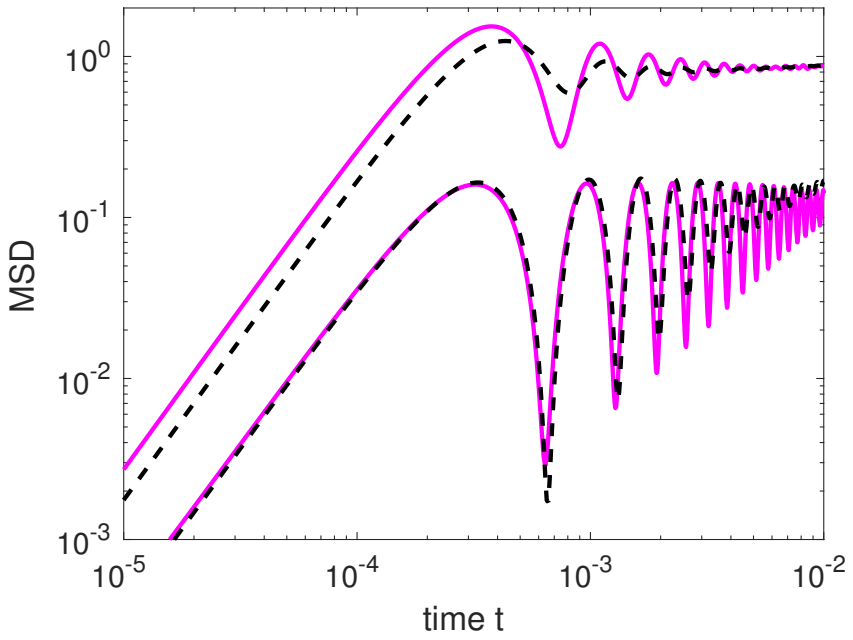

Figure 3.6: Zoom in on Fig. 3.5 (a), i.e. MSD(t, t_a) of the EL flow with $t_a = 10^{-2}$ (lower, solid magenta) and $t_a = 10^{-1}$ (upper, solid magenta), compared to approximate expression Eq. (3.46) (black dashed).

For the EL flow an approximate formula for the oscillatory part of the MSD can be derived in the following way: Sufficiently close to the center of the cell, the streamlines are nearly circular, and the diffusion occurs basically in the radial direction, whereas angular distributions are practically uniform. Let the particles at time $t = -t_a$ be δ-distributed at the center of the cell. At $t = 0$ their probability density is then given by the two-dimensional Gaussian distribution

$$p(r) = \frac{1}{4\pi D t_a} \exp\left(-\frac{r^2}{4Dt_a}\right) \tag{3.39}$$

with $D = 1$ in our units. Since we only look at large Péclet numbers, the diffusion is assumed to be much slower than advection. Thus, let us for the moment "freeze" the diffusion completely. We fix this distribution and assume that the tracers are uniformly advected along their respective circular streamlines. Then the evolution of the MSD is governed by the non-isochronicity of rotations. The larger the radius r, the longer the period $T(r)$. At time t, the instantaneous MSD for the infinitesimally thin ring of radius r equals

$$2r^2(1 - \cos(\omega(r)t)) \times 2\pi r p(r)\, dr \tag{3.40}$$

with $\omega(r) = 2\pi/T(r)$. Thus, the MSD equals

$$\mathrm{MSD}(t) = 4\pi \int_0^\infty r^3 p(r)(1 - \cos(\omega(r)t))\, dr. \tag{3.41}$$

When shifting the origin of the coordinates to the center of a cell, i.e. with $x = \pi/2 + U/2$ and $y = \pi/2 + V/2$, the equations $\dot{\mathbf{r}} = \mathrm{Pe}\ \mathrm{rot}(0, 0, \Psi(\mathbf{r}))$ become $\ddot{U} + \mathrm{Pe}^2 \sin(U) = 0$ and $\ddot{V} + \mathrm{Pe}^2 \sin(V) = 0$. Solutions of these pendulum equations are elliptic functions. For the oscillation of variable U with amplitude U_0, the period equals

$$T(r) = \frac{4}{\mathrm{Pe}} K(1 - \cos(U_0)), \tag{3.42}$$

with $K(m)$ being the complete elliptic integral of the first kind, see Chap. 17 in [16]. For sufficiently small amplitudes the period obeys

$$T(r) = \frac{2\pi}{\mathrm{Pe}}\left(1 + \frac{1}{8}U_0^2 + \frac{19}{768}U_0^4 + \dots\right), \tag{3.43}$$

with $U_0 = 2r$. Considering only terms up to quadratic order in r, we end up with

$$\omega(r) = \frac{2\pi}{T(r)} = \mathrm{Pe}\left(1 - \frac{r^2}{2}\right). \tag{3.44}$$

Substituting this and (3.39) into the expression for the MSD (3.41) and performing the integration yields

$$\mathrm{MSD}(t, t_a) = 8t_a + \frac{8t_a}{(1 + 4\mathrm{Pe}^2 t^2 t_a^2)^2}[(4\mathrm{Pe}^2 t^2 t_a^2 - 1)\cos(\mathrm{Pe}\, t) - 4\mathrm{Pe}\, t t_a \sin(\mathrm{Pe}\, t)]. \tag{3.45}$$

Now we "unfreeze" the diffusion stopped at t_a, i.e. we replace t_a by $t_a + t$, yielding

$$\begin{aligned}\mathrm{MSD}(t, t_a) &= 8(t_a + t) + \frac{8(t_a + t)}{(1 + 4\mathrm{Pe}^2 t^2 (t_a + t)^2)^2} \\ &\quad \times[(4\mathrm{Pe}^2 t^2 (t_a + t)^2 - 1)\cos(\mathrm{Pe}\, t) - 4\mathrm{Pe}\, t(t_a + t)\sin(\mathrm{Pe}\, t)].\end{aligned} \tag{3.46}$$

After the oscillations die out, the approximate expression becomes linear in time. Then the approximation does not hold any longer, since further terms in the expansion of the elliptic integral should be taken into account. Furthermore, the relevant streamlines of the EL flow are not circular anymore. However, for small times and small aging times, this approximation describes the MSD quite well, as we can see in Fig. 3.6, where the oscillating part of the aged MSD from Fig. 3.5 (a) is compared to our obtained formula. Summarising one can say, that this approximation only holds for small enough times and aging times, i.e. $t, t_a \ll 1$, and for aging times strongly exceeding one period, i.e. $t_a \gg 2\pi/\mathrm{Pe}$. A similar derivation for the YPP flow leads to much more complicated expressions, since the streamlines are not circular even in the vicinity of the center.

3.4.4 Time averages

The behavior of the time averaged MSD (3.32) strongly depends on the *total averaging time* T. Here we regard the results for $T \gg t_2 = 1$. For this case the ensemble averaged TAMSD for particles starting at the separatrix displays a behavior changing from ballistic at short times to diffusive at long times, as shown by the solid black curves in Fig. 3.7, very similar to the behavior observed for initially flooded cells. This intermediate stage disappears for low Pe, when t_1 and t_2 get too close. The overall type of the behavior can be explained by the discussion of a single trajectory, as shown in Fig. 3.1. Building TAMSD with longer T corresponds to averaging over all possible positions which the particle assumes during its motion taken as initial position. The distribution of these positions, folded back periodically to a single cell, is relatively homogeneous. Since for $T \gg t_2$ the system homogenizes, the dependence on T, as well as the dependence on initial conditions, disappear, and the distribution of TAMSD around its ensemble average is relatively narrow. The situation here is similar to the case of CTRW with truncated power law WTD as discussed in [28]. For T of about order unity, see the green dashed and blue curves in Fig. 3.7, the ensemble averaged TAMSD is also already very similar to the MSD for the flooded case. For $T \ll t_2$ the typical ergodicity breaking behavior should be present, but the dependence on the initial conditions and the complicated internal dynamics within the trapped state make the situation much more involved than the one for pure CTRW, see [28, 29].

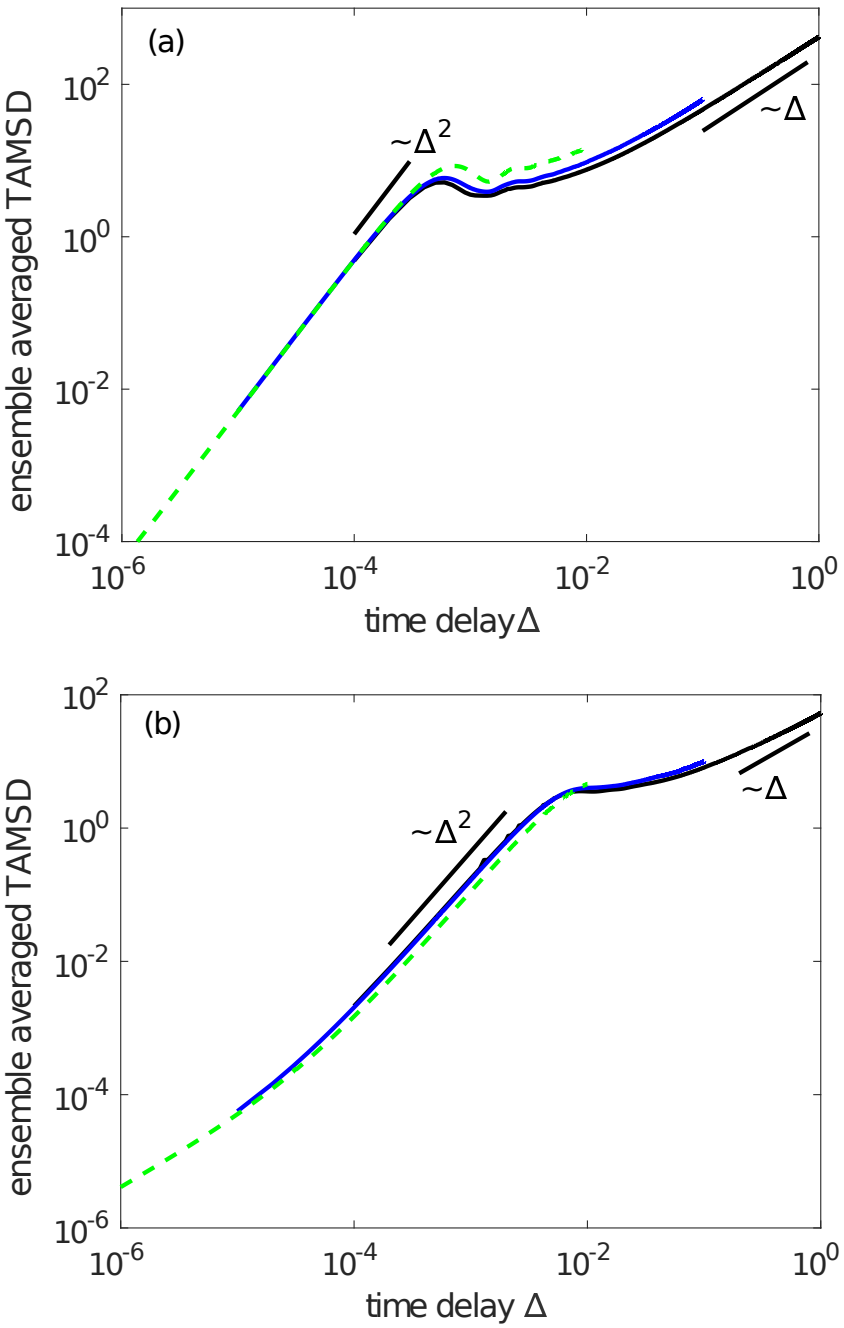

Figure 3.7: EATAMSD(Δ, T) according to Eq. (3.33) starting at the separatrix averaged over 10^2 walks (a) for the EL flow and (b) the YPP flow for $T = 10$ (solid black), $T = 1$ (solid blue) and $T = 0.1$ (green dashed).

3.5 Summary

We have considered the diffusion-advection problem in two simple cellular flow models that differ with respect to the boundary conditions at the edges of the cells. One consists of an infinitely vast two-dimensional lattice of eddies, the eddy lattice flow - the other one being a one-dimensional lattice of eddies bounded by two infinitely long parallel walls with no-slip boundary condition, the Young-Pumir-Pomeau flow. Without molecular diffusion each particle is trapped forever inside a single cell. Adding small thermal noise, leads to several effects like enhanced normal diffusion for long times. The models, often referred to as typical examples for subdiffusive tracer motion, were hardly investigated in detail until now. We focused on the intermediate time range, in which the tracer motion indeed shows subdiffusion in some cases. This could be shown by deriving expressions for the particle concentration (PDF, respectively its integral - the CDF) and the mean squared displacement (MSD) using a continuous time random walk (CTRW) model. Extensive numerical simulations of the systems under different initial conditions confirm established results, like expressions for the final diffusion coefficient, and show that the intermediate time subdiffusive regime, which has been predicted in the past, is only evident, if the particles start at the boundary between neighboring cells, i.e. at the separatrix, and is less pronounced or absent for other initial conditions, e.g. when particles initially are homogeneously distributed within the cell or are injected in the center of a cell. The complex motion of the particles within the single cell leads to interesting aging properties of the system in this intermediate time domain, and is also reflected in the behavior of the time averaged mean squared displacement for single trajectories. Such behavior is not captured by classical models based on CTRWs that possess no dynamics in the trapped state. However, we derived an approximate expression describing the aged motion for particles starting in the center of an eddy for a limited time range.

Chapter 4

The cat's eye flow

4.1 Introduction

Similarly to the previous chapter, we look again at two-dimensional flows. Regions of circulations, i.e. eddies, as well as far reaching jets belong to the basic building blocks of many two-dimensional flow patterns. For that reason, now we examine flows, which are made up of both - eddies and jets, making the model more complex and containing one of our previously examined flows consisting only of eddies, as a special case.

In hydrodynamics, the global transport properties of complex flow patterns are often derived from spatial averages over the local geometry, i.e. the exact shape of these building blocks, of the velocity field. In laminar jets, the particles are transported over long distances via advection, whereas a particle inside an eddy stays there localised for a long time - even forever in absence of thermal noise. Sir William Thomson, also known as Lord Kelvin, once examined a one-dimensional array of eddies with a *cat's eye* border pattern between them and jets at both sides of the array [37]. When researching two-dimensional flows, it is reasonable to extend this system to a temporally stationary and spatially periodic arrangement of stripes of jets enclosing stripes of eddies. In this chapter we therefore use the *"cat's eye flow"*, already introduced in [38]. This model is a family of flows, each of them differing by the value of one parameter. By varying this real number, we can tune the relative areas occupied by the eddies and by the jets. In the one limit the eddy lattice flow is reproduced, consisting only of eddies. The other extreme leads to a shear flow of alternating jets. For values in between we have flows containing one-dimensional arrays of eddies, all having the shape of nearly elliptic *"cat's eyes"*, with sinusoidal jets in between. Like before in the case of the EL flow, we find again that there are characteristic times, see e.g. [39], defining different time scales - initial and intermediate ones, on which the starting position matters as well as a final regime, on which a memory of the starting configuration has effectively erased by diffusion. These time scales correspond e.g. to typical times needed for the deterministic circulation within a cat's eye, as well as to average times needed to diffusive through various building blocks of the flow.

In cellular flows with small molecular diffusion, see [21]-[25], the intermediate and final asymptotics are most interesting. The final asymptotics, as predicted by homogenisation theory [26], is diffusive, and this chapter focuses on the quantitative description. In flows without jets, like in [21] or in the eddy lattice flow, see [33] or chapter 3, the intermediate asymptotics is subdiffusive [34, 40]. In flows with jets, called channels in the terminology of [41], this intermediate asymptotics corresponds to Lévy walks interrupted by rests. Before scientific research turns to the complex geometry of

experimentally available flows [11, 12, 13], it seems reasonable to study simpler models in detail first. Such a model is the cat's eye flow [41, 37, 38]. Similar to the previous chapter about the EL flow, in this chapter we look at the results of extensive numerical simulations of particle transport in the flow and comparison with theoretic results of an intermediate time *Lévy walk* (LW) model, with eddies inside the cat's eyes playing the role of traps and jets regarded as the transport mode in the LW, see [42] and references therein. Theoretical estimates confirm, that the LW model indeed describes the MSD of particles inside the flow for intermediate times. However, like in the two models of the previous chapter, the flow possesses a more complex behavior than the simple LW model suggests, which is indicated by the very different aging properties. Contrary to the well understood aging of Lévy walks [43, 44], the cat's eye flow shows an aging similar to the one of the EL flow for most parameter values, depending strongly on the initial conditions. When looking at aging times corresponding to times being smaller than the first waiting time in an eddy or in a jet, depending in which the walker starts, the LW interrupted by rests only performs one rest or one step of ballistic motion with constant speed, whereas the motion inside the cat's eye flow is much more complex and corresponds to nearly elliptic motion for most parameter values. That means, like in the EL flow, transport by the flow is richer than its random walk model! To the knowledge of the author, there have been no extensive numerical simulations nor comparisons of them with analytical results until now for this system.

The remainder of this chapter is organised as follows: Below, in Sec. 4.2 we look at the shape of the different parts of the flow, in order to gain a certain intuitive understanding of how the flow works in principle. The subsequent Sec. 4.3 focuses on the different time scales for the MSD. In Sec. 4.4 we go through the numerical and analytical result, comparing and discussing them. Finally, in Sec. 4.5 we sum up the findings. The results of this chapter have been published in [45].

4.2 Definition and geometric properties of the model

4.2.1 Definition of the flow

We define the cat's eye flow similarly to the previous chapter, using the same SDE

$$\dot{\mathbf{r}} = \mathrm{rot}\,(0, 0, \psi_{\mathrm{Cat}}(\mathbf{r})) + \sqrt{2D}\boldsymbol{\xi}, \tag{4.1}$$

but with a different two-dimensional[1] stream function

$$\psi_{\mathrm{Cat}}(x, y) = u\,a\left[\sin\left(\frac{x}{a}\right)\sin\left(\frac{y}{a}\right) + A\cos\left(\frac{x}{a}\right)\cos\left(\frac{y}{a}\right)\right], \tag{4.2}$$

where again u is the characteristic velocity, D is the molecular diffusivity and $\boldsymbol{\xi} = (\xi_x, \xi_y)$ is a vector of Gaussian noises with zero mean and $\langle \xi_x(t)\xi_x(t')\rangle = \langle \xi_y(t)\xi_y(t')\rangle = \delta(t' - t)$. The deterministic part of the flow pattern is periodic with respect to both coordinates and consists of elementary cells of the length and width πa. By taking a as the spatial unit and the temporal unit as a^2/D like before, we have the same definition of the Péclet number $\mathrm{Pe} = u\,a/D$, which turns the equations into

$$\dot{\mathbf{r}} = \mathrm{Pe}\ \mathrm{rot}\,(0, 0, \Psi_{\mathrm{Cat}}(\mathbf{r})) + \sqrt{2}\boldsymbol{\xi} \tag{4.3}$$

$$\Psi_{\mathrm{Cat}}(x, y) = \sin x \sin y + A\cos x \cos y. \tag{4.4}$$

[1] The original stream function in [38] was three-dimensional. For our purposes the description in a plane suffices.

That means, this time the system possesses the second parameter A additionally to Pe. Throughout this entire thesis, we look at small molecular diffusion compared to the deterministic velocity, i.e. Pe $\gg 1$. The deterministic part of the velocity of the flow (4.3) is given by

$$\begin{aligned} \mathrm{Pe}^{-1}\dot{x} &= \frac{\partial \Psi_{\mathrm{Cat}}}{\partial y} = \sin x \cos y - A \cos x \sin y \\ \mathrm{Pe}^{-1}\dot{y} &= -\frac{\partial \Psi_{\mathrm{Cat}}}{\partial x} = -\cos x \sin y + A \sin x \cos y. \end{aligned} \tag{4.5}$$

This flow can be thought of as a solution of the two-dimensional Navier-Stokes equation for an incompressible fluid with kinematic viscosity ν and a spatially periodic force of e.g. $\mathbf{F} = 4\nu \sin x \cos y\,(\mathbf{e}_x + A\mathbf{e}_y)$.

4.2.2 About parameter values and fixed points

In principle, the parameter A can assume arbitrary real values of either sign. However, it is sufficient to restrict analysis to the interval $0 \leq A \leq 1$. A transformation $x \to \pi - x$ (or $y \to \pi - y$) is equivalent to the change of the sign of A, whereas a shift $x \to x + \pi/2$, $y \to y + \pi/2$ with simultaneous rescaling of time units by the factor A is equivalent to the transformation $A \to 1/A$. For numerical investigations, we take the following values of A: 10^{-3}, 10^{-2}, 10^{-1}, 0.25, 0.5, 0.75, 0.9, and 1.

Regardless of the value of A, the flow possesses stagnation points at $(x, y) = (\pi m, \pi n)$, and at $(x, y) = (\pi/2 + \pi m, \pi/2 + \pi n)$, where $m, n \in \mathbb{Z}$. At $|A| < 1$, the former points are hyperbolic fixed points, i.e. saddles, and the latter ones are elliptic fixed points, i.e. centers. At $|A| > 1$, the fixed points interchange their roles. Exchange of stability between stagnation points occurs in the course of degenerate global bifurcation at $|A| = 1$. At this parameter value, the straight lines $y = x + \pi n$, $n \in \mathbb{Z}$ turn into invariant continua of stagnation points, see straight red lines in Fig. 4.1 (a). In that case the system is transformed into a shear flow: The plane is partitioned into alternating regions of ballistic motion in opposite directions. Contrary, at $A = 0$, the jets are absent and the entire plane is covered by cells with closed streamlines: the eddy lattice flow [33].

4.2.3 Special streamlines: separatrix and center of the jet

Isolines of the stream function (4.4) for several values of A are presented in Fig. 4.1. The black dashed curves, obtained by shifting the curve

$$y(x) = \arctan\left(-A \cot(x)\right), \quad x \in [0, \pi] \tag{4.6}$$

by integer multiples of π along both spatial coordinates, are the *central lines* of the jet regions in which ballistic motion takes place. Along them, $\Psi_{\mathrm{Cat}}(x, y)$ vanishes. These jet regions are separated from the closed elliptic orbits by the isolines $|\Psi_{\mathrm{Cat}}| = A$. These *separatrices* are obtained by translating

$$y_{\pm}(x) = \arccos\left[\frac{A^2 \cos x \pm \sqrt{1 - A^2}\sin^2 x}{A^2 \cos^2 x + \sin^2 x}\right], \quad x \in [0, \pi] \tag{4.7}$$

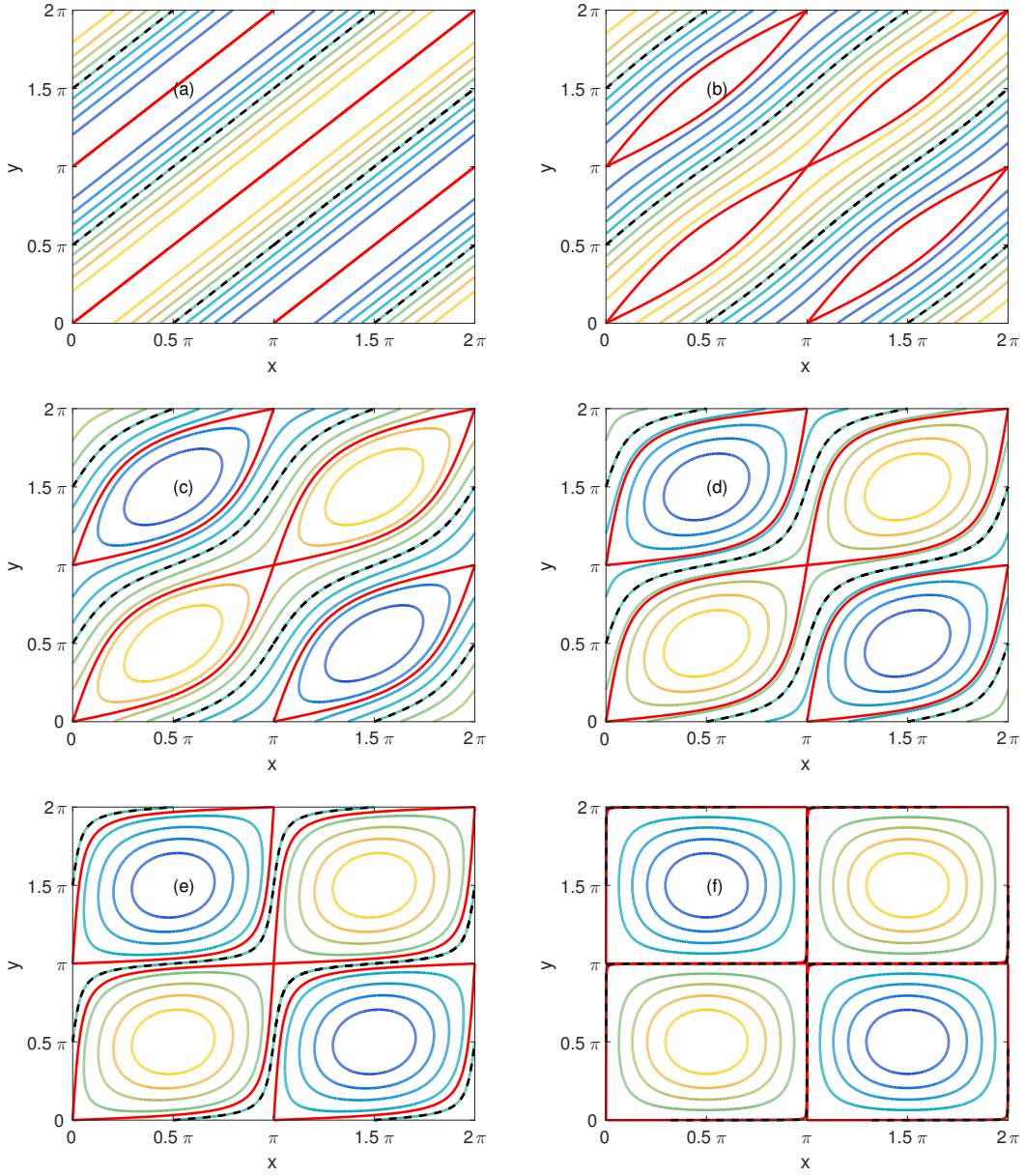

Figure 4.1: Contour plot of stream function (3.18) for (a) $A = 1$, (b) $A = 0.9$, (c) $A = 0.5$, (d) $A = 0.25$, (e) $A = 10^{-1}$, and (f) $A = 10^{-3}$. Yellow closed streamlines, e.g. lower left vortex, denote counter-clockwise motion. Blue closed streamlines denote clockwise motion. For $A \to 1$ separatrices (red) between jets and eddies merge pairwise, the eddies cease to exist, and a shear flow with a sinusoidal velocity profile emerges. For $A \to 0$ pairs of separatrices (red) merge with the central line of the jet (black dashed) and become the edges of quadratic cells.

along both coordinates with π-periodicity, see the red curves that form the border of the cat's eyes in Fig. 4.1. Here the plus (respectively minus) sign corresponds to the lower (respectively upper) boundary of the cat's eye. At non-zero small values of A the narrow curvy jets with alternating directions of unbounded motion are formed between the cells, see Fig. 4.1 (f). As A grows, these jets become thicker, see Fig. 4.1 (e), (d), and so on.

4.2.4 Main axis and width of the jet

The flow is anisotropic. It possesses an axis of faster transport, called *"the axis"* throughout this thesis. Its direction corresponds to one of the coordinates obtained by rotating the system (x, y) around the origin by $\pi/4$. In these rotated coordinates, the equations of motion are significantly simpler. In terms of $x_\pm = x \pm y$, their deterministic parts simplify to[2]

$$\dot{x}_\pm = \mathrm{Pe}\,(1 \pm A) \sin x_\mp. \tag{4.8}$$

For $A = 1$ the coordinate x_- is conserved in the deterministic case, i.e. without noise, and the plane is covered by a continuum of invariant straight streamlines. The velocity of motion along each of these lines is sinusoidally modulated across the continuum. In presence of diffusion, the longitudinal motion along x_+ has both deterministic and diffusive components, whereas the transverse motion along x_- is purely diffusive. Contrary, at $A = 0$, the pattern (4.8) turns into the EL flow. In terms of x_+ and x_-, the separatrix (4.7) then becomes

$$x_- = \pm \arccos\left[\frac{(1-A)\cos x_+ + 2A}{1+A}\right], \tag{4.9}$$

thus the maximal width of the eye, measured in length units of the original coordinates x and y, is

$$\sqrt{2}\arccos\frac{3A-1}{1+A}. \tag{4.10}$$

It can be shown that the local velocity v_s along the separatrix can be expressed as

$$v_\mathrm{s}^2(x_+) = 2\mathrm{Pe}^2(1-A)\left[(A-1)\cos^2 x_+ - 2A\cos x_+ + A + 1\right]. \tag{4.11}$$

For the width of the jet we take the distance between the separatrices measured along the local normal to the central line of the jet, also measured in length units of the original coordinates. When making the slight approximation[3] that the central line is parallel and equally distant to its two neighboring separatrices, this yields the lengthy expression

$$\begin{aligned} w_\mathrm{j}(x_+) \;=\; & \left[\arcsin\left(\frac{2A+(1-A)\cos x_+}{1+A}\right) + \arcsin\left(\frac{2A-(1-A)\cos x_+}{1+A}\right)\right] \\ & \times\sqrt{\frac{(1+A)^2-(1-A)^2\cos^2 x_+}{2((1+A)^2-(1-A)^2\cos 2x_+)}}. \end{aligned} \tag{4.12}$$

[2]Note, that there is a typo concerning a sign in the corresponding formula in [45].

[3]This assumption is violated around the saddle points. However, exactly at these points, i.e. when the normal to the central line goes through a saddle, the formula yields the exact width of the jet. Around them the correction, i.e. the root factor, to the width measured along x_- is still small. Thus one can neglect deviations.

As a function of the coordinate x_+, along the axis, the width of the jet oscillates between the sharp maximum

$$w_{\max} = \frac{1}{\sqrt{2}} \arccos\left(\frac{1-3A}{1+A}\right) \tag{4.13}$$

and the minimum

$$w_{\min} = \frac{1+A}{\sqrt{1+A^2}} \arcsin\left(\frac{2A}{1+A}\right) \tag{4.14}$$

measured in units of the original coordinates. Both reproduce the exact width $\pi/\sqrt{2}$ of the jet for $A = 1$.

At small values of A the width displays a broad plateau around its minimal value. There, the minimum

$$w_{\min} \approx 2A + \frac{A^3}{3} + \dots \tag{4.15}$$

can be used as a "typical" jet width. The linear approximation, i.e. $w_{\min} \approx 2A$, suffices for our purposes. At $A = 1$ the deviation is 22%. For $A \leq 0.9$ it is 4% or less, fitting better for smaller values of A. As we will see later on, this approximation of the minimal jet width will turn out to be very useful in estimating one of the characteristic times. The minimum of the jet width is especially important, since it is likely there, where the particles make a transition from one eddy to another.

4.3 Mean squared displacement

4.3.1 Characteristic times

Most central to the analysis of the cat's eye flow are the three characteristic time scales it possesses. The first two are exactly the same as for the EL flow, see [33] or chapter 3. Now the second one just has a slightly different interpretation. Because of the existence of jets, now an additional third time has to be considered, making the dynamics more complex. The three characteristic times of the cat's eye flow are the following:

1. The first characteristic time is the time a particle typically needs to deterministically cross a cat's eye, i.e. an eddy, by being transported by the flow. In dimensional units, i.e. the units of (4.2), respectively rescaled units of (4.3), i.e. with $a \to 1$, $D \to 1$, and $u \to \mathrm{Pe}$, it is

$$t_1 \simeq \frac{a}{u} = \frac{1}{\mathrm{Pe}}. \tag{4.16}$$

2. The second characteristic time for this system is the time typically needed to diffuse along a length of a periodic unit with distance of order πa. This contains both: the time to diffuse across an eddy plus the time to diffuse across a neighboring jet. This way, the time is always the same independent of the width of either of these building blocks of the flow. After this time the particles perform random walks from eddy to eddy, respectively from moving along a jet in one direction to a jet in the opposite direction. Thus, after this time the final normal diffusion sets in. This time equals in the two respective units

$$t_2 \simeq \frac{a^2}{D} = 1. \tag{4.17}$$

3. The third characteristic time t_3 is the one needed to diffusive across a jet only. It is given by

$$t_3 \simeq t_2 w^2 \tag{4.18}$$

where w is the characteristic width of the jet measured in units of a, i.e. the parameter w itself is dimensionless. Applying (4.15), this yields

$$t_3 = w^2 \approx 4A^2 \tag{4.19}$$

in our normalised units. Note that t_3 is always either of the order of t_2 or smaller.

The waiting times in an eddy are given by a power law probability density function, i.e. the normal Sparre-Andersen behavior

$$\phi(t) \propto t^{-3/2} \tag{4.20}$$

between the smaller cutoff time t_1 and the larger cutoff time t_2. The waiting times in a jet are given by the same power law, but with the upper cutoff time being t_3. The time t_1 corresponds to the time resolution of the random walk scheme: The behavior at shorter times is dominated by the local dynamics.

4.3.2 Transport regimes

In this section we qualitatively describe the three transport regimes observed when starting at the separatrix of the flow. Quantitative details are considered in the next subsection that presents the results of the numerical simulations.

Initial regime

When a particle starts at the separatrix or close enough to it, except for the immediate surrounding of a saddle point, for short times[4] $t < t_1$, it moves along the streamline with the local velocity close to v_s (4.11) and the average velocity v of the order of Pe. This motion is independent on whether the instantaneous position of the tracer particle is inside the jet or inside the eddy, because the flow is very similar on both sides of the separatrix. The motion is ballistic, i.e. $\mathrm{MSD}(t) \simeq v^2 t^2$. The simulations confirm that for large Pe the typical velocities on both sides close to the separatrix coincide and are of the order of the Péclet number, i.e. $v \approx \mathrm{Pe}$.

Intermediate time regime

After the time t_1 the second transport regime begins, if both times t_2 and t_3 are considerably larger than t_1, i.e. $\mathrm{Pe}\, w^2 \gg 1$. Like in the previous regime, we have again ballistic transport, but a slower one: The prefactor is reduced to a quarter of its original size. At this time scale, the particles typically move along several eddies. The motion inside a jet can be modelled approximately by the transport mode in a Lévy walk, whereas the rotational motion inside an eddy corresponds to the resting phase, i.e. macroscopically seen, standing still. Both modes can be recognised, when looking at the trajectories in Fig. 4.2. There the linear slopes correspond to the straight motion, whereas the plateaus

[4] Of course, at very short times, before our "initial regime", there is always the very first time scale on which the transport by molecular diffusion D is stronger than the flow, resulting in the same normal diffusion for all initial conditions.

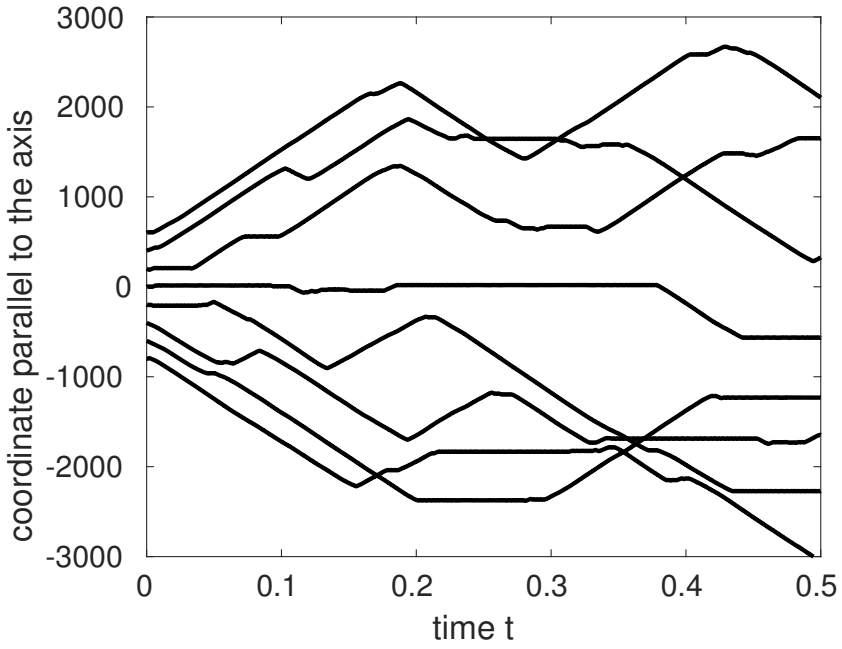

Figure 4.2: Coordinate parallel to the axis of the system at Pe $= 10^4$ and $A = 0.5$ for a simulation of eight tracer particles starting at the separatrix at intermediate time scales: $t_1 \ll t < t_3 \approx t_2$. Inclined straight segments: ballistic motion. Plateaus: trapping events. To resolve the trajectories optically at small values of t, a fictitious vertical shift between them has been introduced.

correspond to standing still. The waiting time densities of being in either of the two modes follows the power law $\phi(t) \propto t^{-3/2}$. Such a Lévy walk yields, after a lengthy calculation of applying the formalism, see Appendix C, the ballistic expression of the MSD:

$$\mathrm{MSD}(t) = \frac{1}{4} v^2 t^2. \tag{4.21}$$

The two regimes of ballistic transport for several values of A are presented in Fig. 4.3. The crossover between them is visualised in Fig. 4.4, where it can be seen that the theoretical estimate for the change in the prefactor of one quarter, given by Eq. (4.21), is well matched by the simulations. The transport in the system is strongly anisotropic, since the motion is dominated by the longitudinal movement along the axis of the system, whereas the motion in direction normal to the axis still takes place within just one eddy or jet. This motion inside an eddy can not be captured by a coarse-grained random walk model, and will be discussed in the next section on the basis of numerical results.

The time dependence of the MSD between the two times t_3 and t_2 is non-universal, i.e. it depends on the parameter A, see the two different intermediate slopes in Fig. 4.3, but also especially on the initial conditions, see Figs. 4.5 and 4.6. In contrast, the final diffusion regime that begins at long times $t > t_2$ is universal, i.e. does not depend on initial conditions, but is a lot larger for larger A, since then the jets are enhancing the final diffusion a lot.

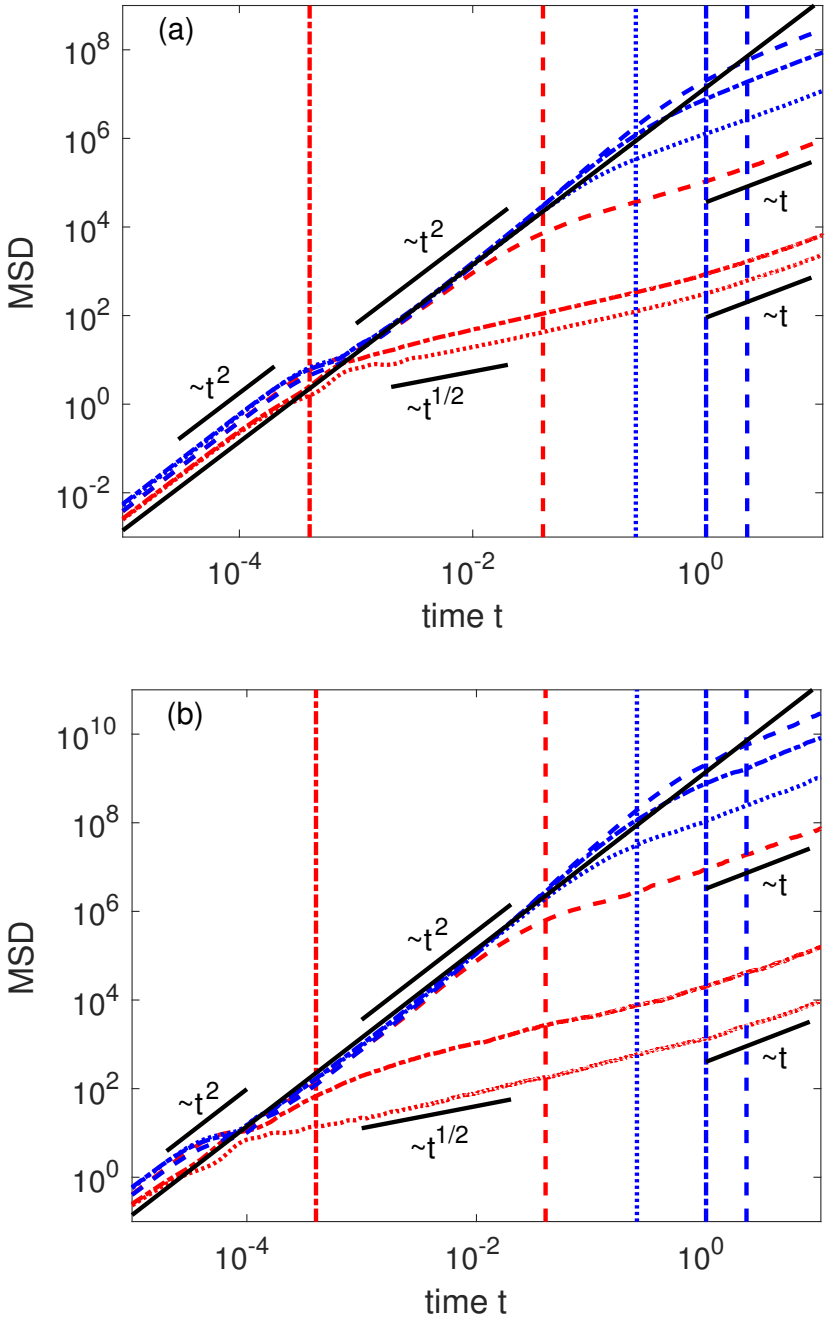

Figure 4.3: Temporal evolution of the simulated MSD for ensembles of tracers starting on the separatrix between the jet and the vortex at, respectively, $A = 10^{-3}$ (lowest curve), $A = 10^{-2}$, $A = 10^{-1}$, $A = 0.25$, $A = 0.5$ (center curves), and $A = 0.75$ (uppermost curve), compared to the asymptotic theory, Eq. (4.21) (black continuous). Time t_3, Eq. (4.19), is indicated by vertical lines in the same style as the curves they belong to. Panel (a): 10^4 walks at Pe $= 10^4$. Panel (b): 10^3 walks at Pe $= 10^5$. The velocity in both plots varies slightly with A around $v \approx 0.75\,\mathrm{Pe}$. The intermediate ballistic regime occurs only if $t_3 \gg t_1 \approx 1/\mathrm{Pe}$. Note, that the curves in (a) are the black dashed lines in Figs. 4.5 (a-d) and 4.6 (a-b).

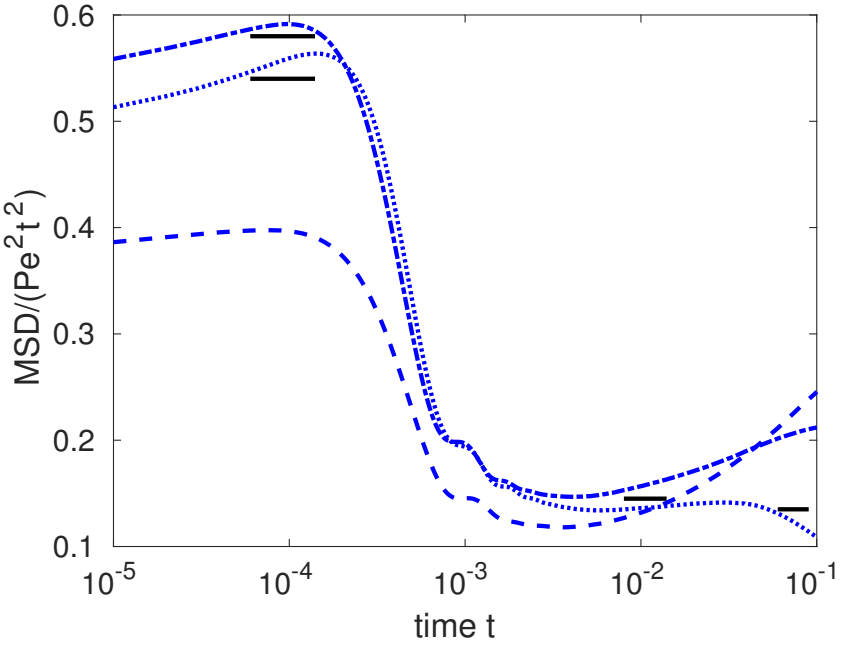

Figure 4.4: Crossover in prefactor of MSD between two regimes of ballistic transport for Pe = 10^4. Rescaled curves from Fig. 4.3 (a) for $A = 0.25$ (dotted), $A = 0.5$ (dash-dotted), and $A = 0.75$ (dashed). Horizontal lines indicate the values: 0.58, 0.54, 0.145, and 0.135. The MSD during the intermediate ballistic regime is about one quarter of its value during the initial ballistic regime $t < 10^{-4}$, as predicted by theory, Eq. (4.21).

Final regime

In the remainder of this section we reproduce the estimates for the diffusion coefficients in the final regime for the two main directions of the flow, derived in [41]. The basic idea is the following: Knowing the diffusivities in each of the building blocks of the flow, their widths and how these building blocks are arranged, one can identify the diffusivities of the flow with conductivities, i.e. inverse resistances, and then calculate the diffusivity of the whole system according to the rules of electric circuits. These conductivities and resistances have to be weighted with the respective width of the part of the flow.

At the time and length scales of the final regime, the structure of the flow can be thought of as a layered one - an array of parallel jets and rows of eddies whose exact shapes hardly matter. The final diffusion coefficients strongly depend on the structures in which the particles spend most of their time. A simple estimate assumes a constant thickness for those parallel layers: The exact form and the variation of the thickness influence only numerical prefactors. For small A we have isotropic diffusion in the eddy lattice (EL) layers with the diffusion coefficient

$$D_{\mathrm{EL}} \simeq \sqrt{uaD} = D\,\mathrm{Pe}^{1/2}. \tag{4.22}$$

The diffusion in the jet is strongly anisotropic. In the direction normal to the axis

$$D_\perp = D \tag{4.23}$$

holds, whereas in the parallel direction we have

$$D_\parallel \simeq u^2 t_3 = u^2 \frac{a^2 w^2}{D} = D\,\mathrm{Pe}^2 w^2. \tag{4.24}$$

For the final diffusion for the direction normal to the axis, the particles have to diffusive through an eddy and through a jet one after another. When particles move along the axis, they can move either in an eddy or a jet being next to each other. Thus we end up with sequential, respectively parallel switching of the diffusivity in an eddy and one of the respective two diffusivities inside a jet.

The final diffusion coefficient in the direction normal to the main axis is then given by the weighted harmonic mean of the corresponding local coefficients, i.e. it corresponds to a sequential switching of diffusivities (conductivities), analog to adding up electric resistances

$$D_\perp^* \simeq \left(\frac{w}{D_\perp} + \frac{1-w}{D_{\mathrm{EL}}}\right)^{-1} = \frac{D}{w + (1-w)\mathrm{Pe}^{-1/2}}. \tag{4.25}$$

For large Pe it is dominated by the first term in the denominator, resulting in

$$D_\perp^* \simeq \frac{D}{w} \simeq \frac{D}{A}. \tag{4.26}$$

This effect takes place for $w > \mathrm{Pe}^{-1/2}$, which in the units $u = a = 1$, used in [41], translates into $A > \sqrt{D}$. The final diffusion coefficient parallel to the axis is the one for a parallel switching of diffusivities (conductivities), analog to adding up electric conductivities

$$D_\parallel^* \simeq D_\parallel w + D_{\mathrm{EL}}(1-w) = D[\mathrm{Pe}^2 w^3 + \mathrm{Pe}^{1/2}(1-w)]. \tag{4.27}$$

For large Pe this is dominated by the first term provided $w > \mathrm{Pe}^{-1/2}$ again, resulting in

$$D_\parallel^* \simeq D\mathrm{Pe}^2 w^3 = D\mathrm{Pe}^2 A^3. \tag{4.28}$$

In this way, the result of [41] is reproduced, since there $\mathrm{Pe} \equiv 1/D$, it follows

$$D_\parallel^* \simeq A^3/D. \tag{4.29}$$

The simple ansatz above does not allow us to analyse the intermediate time behavior or the aging which both strongly depend on the non-trivial dynamics inside each of the building blocks of the flow. This can be achieved numerically.

4.4 Results of the simulations

The numerical method is exactly the same as the one used in the previous chapter, see section 3.3. This time we integrate again (4.3), but with the stream function of the cat's eye flow (4.4). For an efficient algorithm making use of the simpler form of the deterministic part the equations, (4.8), after rotating and stretching the coordinate system, see Appendix A. In order to use the computational resources more efficiently, it is actually enough to go to the maximal simulation time of $t_{\max} = 10$. This suffices to confirm the final diffusion coefficients derived in the last section. Furthermore, because we already know at which Péclet numbers the intermediate regimes last long enough in order to be able to examine them, it is enough to restrict the analysis to Pe ranging from 10^3 to 10^5. Again, larger Péclet numbers need smaller time steps, which result in longer and thus fewer simulations. That is, why the curves in Fig. 4.3 (b) are a bit less smooth than in Fig. 4.3 (a).

4.4.1 Definition of the initial conditions

For the cat's eye flow we consider basically the same three initial conditions from the eddy lattice flow. The first one for starting at the separatrix just has to be defined in different way, because here the separatrix looks more complicated. Furthermore there is an insightful fourth initial condition merging with the first one in the limit of the EL flow.

1. First initial condition: starting homogeneously distributed at the separatrix between eddies and jets. For simplicity, the particles are already very homogeneously distributed, when taking the average of the following two conditions: once setting $x(t = 0)$ equally distributed between 0 and π each time obtaining $y(x)$ according to (4.7) and in the other case taking $y(0)$ homogeneously and obtaining $x(y)$ by the inverse of (4.7). However, simulations showed that only the exact shape of the MSD at the transition between the initial and intermediate regime about the time t_1 changes, when just taking one of the two initial conditions. This means, it is enough to take $x(0)$ homogeneously from $[0, \pi]$ and $y(x(0))$ according to (4.7). Half the particles start at the curve y_+ and the other half at the other curve y_-.

2. Second initial condition: starting from a flooded periodic unit. Because of similar symmetry reasons like the ones for the EL flow, it is enough to take exactly the same initial condition as for the EL flow, i.e. choosing $x, y \in [0, \pi]$ equally distributed.

3. Third initial condition: starting at the exact geometric center of an eddy. This also coincides with the initial condition for the EL flow, e.g. $x(0) = y(0) = \pi/2$. Note however, that for the extreme case of the shear flow, i.e. $A = 1$, eddies cease to exist and the former centers of eddies lie then on the separatrix. That means in that case the two initial conditions coincide.

4. Fourth initial condition: starting homogeneously distributed at the central line of the jet. Because of symmetry reasons, it is enough to choose $x(0)$ homogeneously from $[0, \pi]$ and $y(x(0))$ according to (4.6). In the other extreme case of approaching the EL flow, i.e. $A \to 0$, this initial condition converges to the one for starting at the separatrix.

The results for different values of A are plotted in Figs. 4.3 to 4.6. For most situations the component of the MSD parallel to the axis dominates, see dashed lines in Figs. 4.5 and 4.6, often covered by the solid lines for the overall MSD. Only for small values of A or when starting inside the cat's eye for short time intervals the two components are approximately equal, see the dashed and dotted lines being nearly identical.

4.4.2 Starting at the separatrix

When starting from the separatrix, the MSD shows an initial ($t < t_1$) and an intermediate time ($t_1 < t < t_3$) ballistic regime, see Fig. 4.3. One can see clearly, that the intermediate ballistic regime occurs only if the third characteristic time, indicated by the vertical lines in the same style as the corresponding curves, obeys $t_3 \gg t_1 \approx 1/\mathrm{Pe}$.

In the other case, when A is very small so that the flow pattern is very close to the EL flow, the intermediate time ($t_1 < t < t_2$) diffusion exponent is 1/2, see also [34, 40].

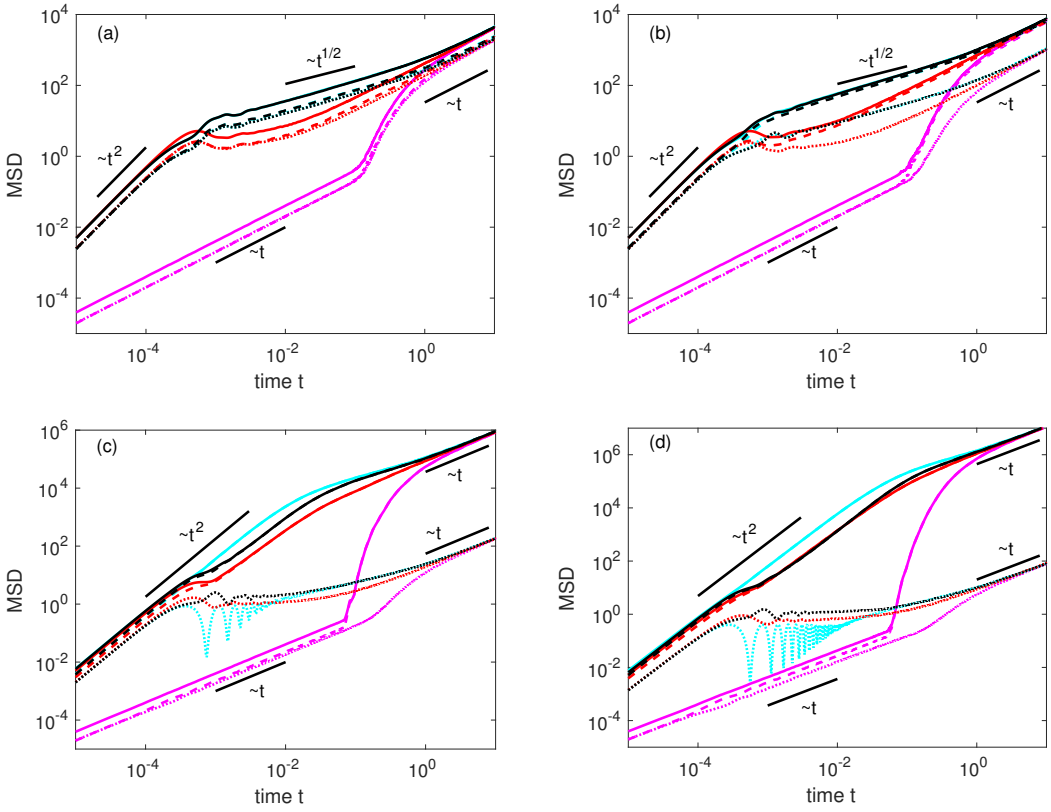

Figure 4.5: Temporal evolution of the simulated MSD for 10^4 walks at Pe $= 10^4$. Solid lines: total MSD, dashed lines: MSD parallel to the jet, dotted lines: MSD orthogonal to the jet. Starting positions are denoted by coloring from dark to light colors: separatrix between jet and eddy (black), flooded (dark red), center of an eddy (magenta), and the central streamline of a jet (light cyan). Panels: (a) $A = 10^{-3}$, (b) $A = 10^{-2}$, (c) $A = 10^{-1}$, and (d) $A = 0.25$. Note, that in (a) and (b) the jet region is so thin that the MSD for the first and last initial condition (black and cyan) almost coincide. For (a) the parallel and the perpendicular components of the MSDs are almost equal, and the eddy lattice flow [33] is reproduced. Note also, that in (d) the MSD for the start on the separatrix (black) and the flooded case (red) are very similar.

4.4.3 Other initial conditions

For most initial conditions and not too small values of A the overall MSD is almost identical to the MSD parallel to the axis. That means the MSD perpendicular to the axis is negligible. Both components of the MSD possess a final normal diffusion for times $t \gg t_2$. However, the MSD parallel to the axis is several orders of magnitude larger than the perpendicular part for not too small A. The simulations confirm the observation that the corresponding final diffusion coefficients $D^*_{\parallel}$ and $D^*_{\perp}$ indeed possess the functional dependences, (4.29) and (4.26), derived above, see [41]. The simulations indicate that these relations hold not only for $A \ll 1$ but approximately also in the broader range $A \leq 0.5$.

One has to point out, that for the value of $A = 0.25$ two initial conditions are approximately the same, see the almost identical black and red curves in Fig. 4.5 (d). In that case the width $w \approx 2A$ of the jet is about half the width of an eddy, see Fig. 4.1 (d). Interestingly, this seems to be a value, where the jet is exactly so much thinner than an eddy that when starting flooded, about the right ratio of particles start in the

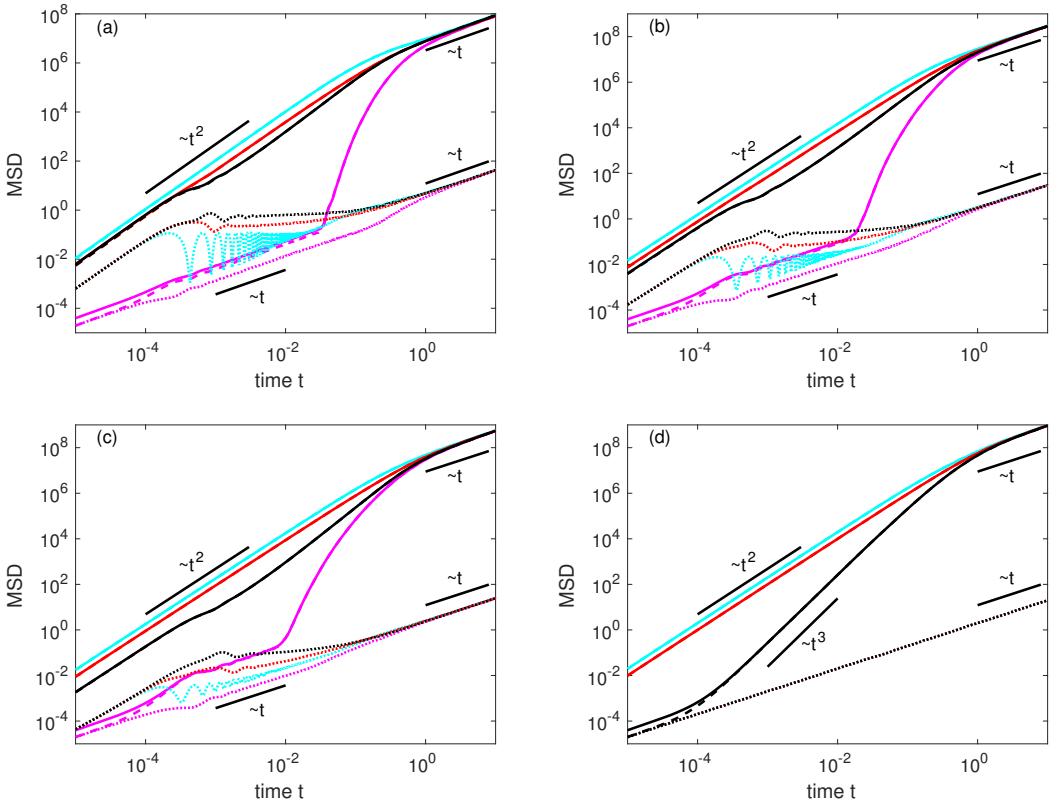

Figure 4.6: Same as Fig. 4.5 with (a) $A = 0.5$, (b) $A = 0.75$, (c) $A = 0.9$, and (d) $A = 1$. Note, that in the flow pattern of (d) there are no eddies, and the corresponding initial condition (magenta) has converged to the one for a start at the separatrix (black).

jet, so that the ensemble average with the ones starting in the eddy results in an MSD comparable to the one for starting at the separatrix right at the border between jet and eddy. Therefore $A = 0.25$ is a very useful parameter value, since on the one hand, some quantities, like the intermediate MSD, can be calculated well for starting at the separatrix, whereas on the other hand, the flooded scenario is experimentally easier accessible. Here the MSDs for both initial conditions are about the same.

Note, that the same should hold for larger Péclet numbers. This was tested to hold also for $\mathrm{Pe} = 10^5$. There, the plot of the MSD over time is exactly the same, with the only difference that the squared speed, and thus the initial ballistic and the parallel part of the MSD are hundred times larger and that the characteristic bending between the initial and the intermediate regime happens an order of magnitude earlier.

Starting in the cat's eye

The MSD for starting at the separatrix, see also the black curves in Figs. 4.5 and 4.6, are quantitatively very similar to the other initial conditions, see red and cyan curves, except for a start at the center of a cat's eye, see magenta curves. For this initial condition an initial normally diffusive regime turns after a sudden and short superballistic regime into a final normally diffusive regime. Furthermore, there is an intermediate normally diffusive regime for moderate values of A, i.e. if $0.25 \leq A \leq 0.9$.

Special case: shear flow

When the parameter A approaches unity, the flow turns into a shear flow with a sinusoidal velocity profile. At $A = 1$, the equations of motion in terms of the coordinates $x_+ = x + y$ and $x_- = x - y$ become

$$\dot{x}_+ = \mathrm{Pe} \sin x_- + \sqrt{2}\,(\xi_x + \xi_y) \tag{4.30}$$

$$\dot{x}_- = \sqrt{2}\,(\xi_x - \xi_y). \tag{4.31}$$

In the stripe where $\sin x_- \approx x_-$ holds, this is approximately the linear shear flow [46]. Note, that this is the case for $t \ll t_2$. The MSDs along both coordinates are well known [47] and read in our notation

$$\mathrm{MSD}_\parallel = \frac{1}{2}\left\langle x_+^2 \right\rangle = \frac{8}{3}\mathrm{Pe}^2 t^3 \tag{4.32}$$

$$\mathrm{MSD}_\perp = \frac{1}{2}\left\langle x_-^2 \right\rangle = 2t, \tag{4.33}$$

where $D = 1$ has been used. Indeed, numerics show that for $\mathrm{Pe} = 10^3$ to 10^5 the MSDs are well fitted by $\mathrm{MSD}_\parallel^{\mathrm{sim}} = 2\mathrm{Pe}^2 t^3$ and $\mathrm{MSD}_\perp^{\mathrm{sim}} = 2t$. This means, that for $A = 1$ the system is close to a linear shear flow.

Note, that for tracers starting close to the separatrix at $A \to 1$, the intermediate regime becomes a superballistic one. That is, because a transition towards the shear flow $\mathrm{MSD}_\parallel \propto t^3$, see Eq. (4.32) and Fig. 4.6 (c,d), is established.

4.4.4 Aging

When choosing the center of the cat's eye as the initial position, we also consider the aged MSD obtained by starting at $x = y = \pi/2$, letting the tracers evolve for the aging time t_a, and then commencing the observation, i.e. then $t = 0$. Figures 4.7 and 4.8 show these simulated aged MSDs. Note, that the asymptotic slopes are the same as in Figs. 4.5 and 4.6. The MSDs for other initial conditions are already close to that for the flooded case and therefore hardly age. That is, why aging for these initial conditions is not shown.

Recall that for $A = 1$ there are no eddies anymore. Their former centers, as well as the former hyperbolic points, lie exactly on the separatrix which, in its turn, becomes a straight line that entirely consists of degenerate stagnation points. For this situation we show in Fig. 4.8 (d) the process of aging for starting on that straight line.

For $A \neq 1$ the aged MSD as a function of time is oscillating. As shown in section 3.4.3, see also [33], for sufficiently small A and not too large values of times and aging times $t, t_a \ll 1$, the leading terms for the aged MSD are given by

$$\begin{aligned}\mathrm{MSD}(t, t_a) \approx\ & 8(t + t_a) + \frac{8(t + t_a)}{\left[1 + (2\Omega\, t(t + t_a))^2\right]^2} \\ & \times \left\{\left[(2\Omega\, t(t + t_a))^2 - 1\right]\cos(\Omega\, t) - 4\Omega\, t(t + t_a)\sin(\Omega\, t)\right\}\end{aligned} \tag{4.34}$$

i.e. (3.46), where the frequency of oscillations $\Omega \approx \mathrm{Pe}\sqrt{1 - A^2}$ is a monotonically decreasing function of A. For this approximation to work well, the aging time should strongly exceed one period: $t_a \gg 2\pi/\Omega$.

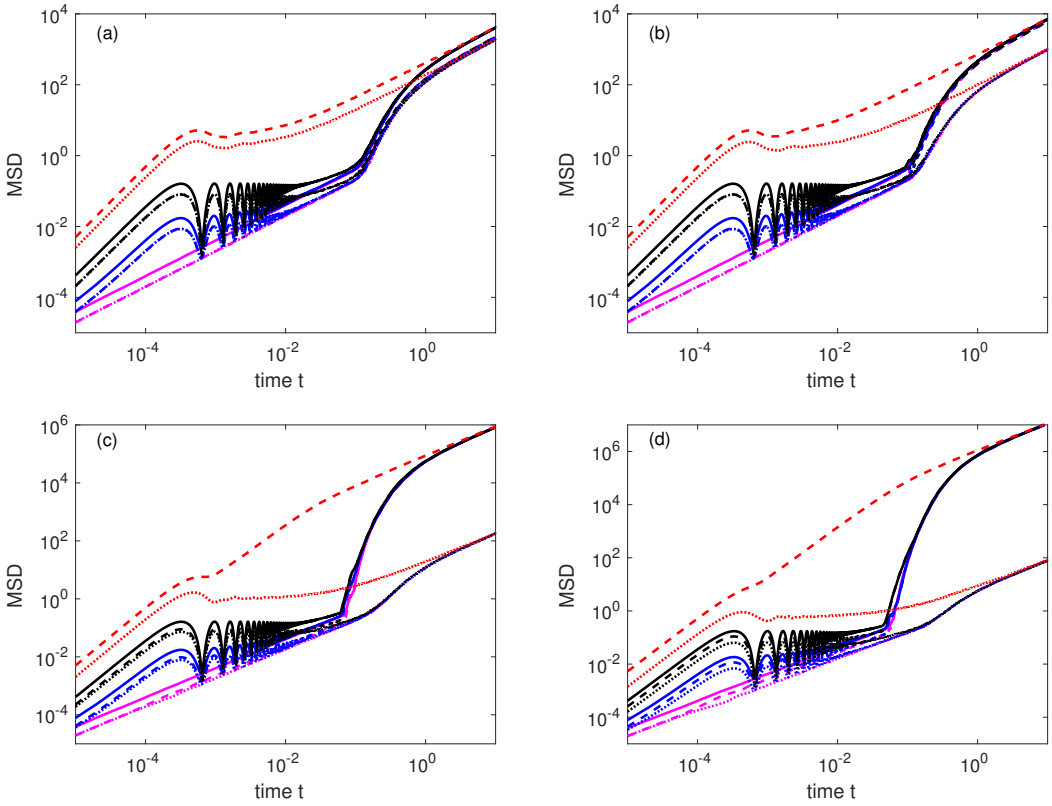

Figure 4.7: Simulated aged MSD for 10^4 walks starting at the eddy center at Pe = 10^4. Solid lines: total MSD, dashed lines: MSD parallel to the jet, dotted lines: MSD orthogonal to the jet. Aging times: $t_a = 0$ (magenta), $t_a = 10^{-3}$ (blue) and $t_a = 10^{-2}$ (black). Panels: (a) $A = 10^{-3}$, (b) $A = 10^{-2}$, (c) $A = 10^{-1}$, and (d) $A = 0.25$. For $t_a \gg t_2$ the MSD converges to the flooded case (red dashed) respectively to its orthogonal part (red dotted). In (a) the jet region is so thin, that the eddy lattice flow is reproduced. Here the parallel and the orthogonal components are approximately the same.

4.5 Summary

We considered the advection-diffusion problem for tracer particles in the cat's eye flow. This two-dimensional flow consists of two different elements: jet regions having shapes of meandering stripes next to eddies having shapes of cat's eyes, thus making the geometry of the flow more complex than our previously studied flows. However, the family of the cat's eye flows is conveniently parametrised by only a single parameter, and interpolates between the eddy lattice flow, without jets, and a shear flow with sinusoidal velocity profile, without eddies. In the absence of molecular diffusion, the tracers are either carried away ballistically by jets, or stay trapped in eddies forever. Adding small thermal noise, enables the transitions between eddies and jets, and, at long times, leads to anisotropic diffusion with the diffusion coefficient in the direction of the jet much larger than the one in the perpendicular direction. This long time regime seems to be the only one which was discussed theoretically in considerable detail until now. At intermediate time scales the transport can be modelled by a stochastic scheme corresponding to Lévy walks interrupted by rests. The transport phase of the walk corresponds to the motion in a jet, and rests to trapping inside eddies. This scheme however only applies for initial conditions corresponding to starting close to the separatrix. The behavior for other initial conditions may be vastly different. This is especially the

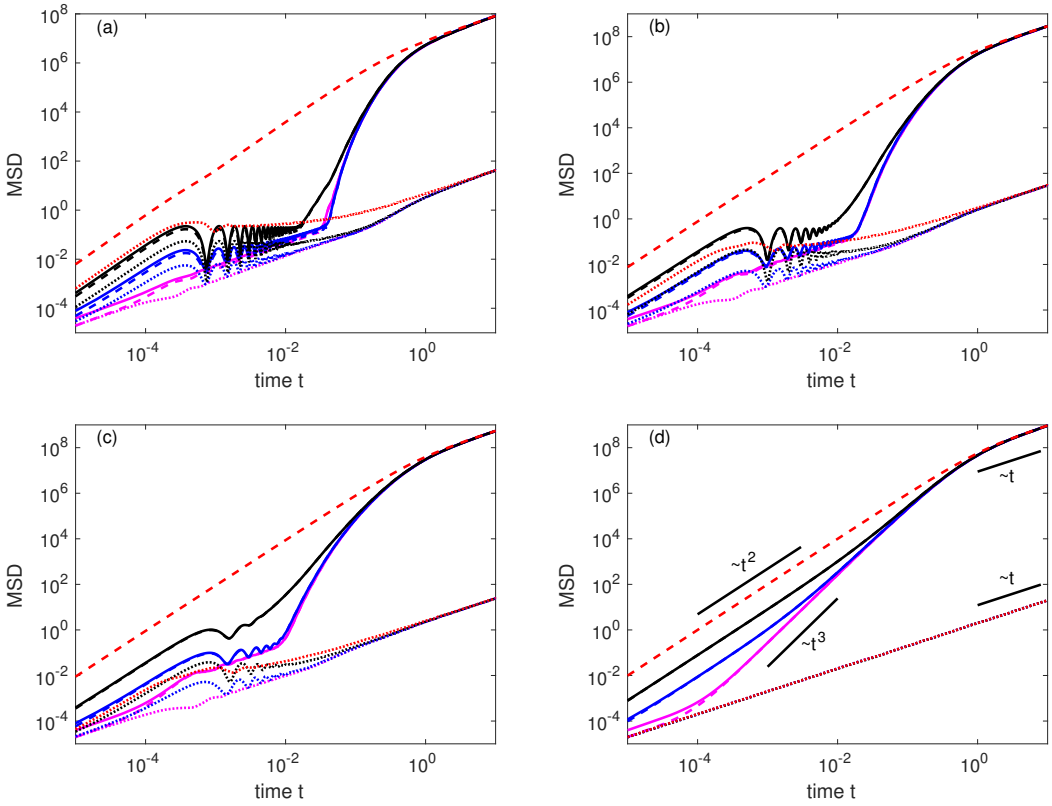

Figure 4.8: Same as Fig. 4.7 with (a) $A = 0.5$, (b) $A = 0.75$, (c) $A = 0.9$, and (d) $A = 1$. Note, that at $A = 1$ there are no eddies. Their former centers lie on the straight lines which consist of degenerate equilibria. Here aging for tracers that start on these lines is shown.

case when starting at the center of an eddy.

We have seen the results of extensive numerical simulations of the particle transport by the cat's eye flow concentrating on the mean squared displacement (MSD) of the particles from their initial positions in a broad time domain. We have investigated the intermediate time behavior of the MSD, the influence of initial conditions, and aging. The results of the simulations confirm theoretical results for the long time behavior of the MSD, and the applicability of the Lévy walk scheme for intermediate times, including the prediction about the connection between the transport velocities in the short- and intermediate-time ballistic regimes. They also show a variety of possible aging behaviors, depending on initial conditions, including an oscillatory one which is observed when particles start inside the eddies. This oscillatory MSD is due to the rotation of the particles in an eddy during the trapping phase, and is not captured by the Lévy walk scheme.

Chapter 5

Particle reactions in the eddy lattice flow

5.1 Introduction

Reaction-diffusion processes are found in many scientific fields, especially in chemistry. For a good introduction to the topic, see [48]. This family of theoretical models is typically used to describe situations in which particles are moving at least partially random in space, while there exists a part of the space in which they can meet, in order to combine, dissociate or enter another state. Different kinds of reactions typically behave in very different ways. Reversible reactions of single species, i.e. $A + A \leftrightarrow A$, have been examined in [49]. Also annihilation processes of single species $A + A \rightarrow 0$ have been analysed in more then two dimensions, see [50]. Furthermore, the effect of density fluctuations on reactions $A + B \rightarrow C$ has been researched, see [51], as well as its breakdown, see [52].

In order to gain a deeper insight into the inner dynamics of a flow, one can turn to particle reactions. This way one obtains information about when (and where) particles are more often closer together, because only then can particles react with each other. In this chapter we want to revisit the eddy lattice flow from chapter 3, but this time with added particle reactions. For numerical simplicity, we only want to consider the most simple reaction, i.e. the coagulation or accumulation of particles described by

$$A + A \rightarrow A. \tag{5.1}$$

This means, we allow the particles to stick together with a certain probability, when they are close enough to each other. However, we still assume all particles to remain passive tracers, i.e. they do not influence the flow. This might be violated in reality - especially after a long time, when several thousand particles have gathered and have become one large ball.

Again, like in our previous consideration of the eddy lattice flow, we simulate 10^4 particles. This time however, we only consider the flooded case, i.e. starting homogeneously distributed over one square cell. We check, if two particles are closer to each other than the *reaction radius* R, always after integer multiples of the *checking time* t_c. We go into further detail about the model used for the numerical simulations in the next section.

Before that, we recall the definition of the system: The equations of motion are

given by

$$\dot{x} = \mathrm{Pe}\sin(x)\cos(y) + \sqrt{2}\xi_x \tag{5.2}$$
$$\dot{y} = -\mathrm{Pe}\cos(x)\sin(y) + \sqrt{2}\xi_y, \tag{5.3}$$

which results in the particles moving around in closed orbits for most of the time inside quadratic cells with length π, where the velocity is of the order of Pe. Rarely, transitions to neighboring cells occur. With the help of the stretched and rotated variables $x_\pm = x \pm y$ we can write these equations in the simpler form

$$\dot{x}_+ = \mathrm{Pe}\sin x_- + 2\xi_{x_+} \tag{5.4}$$
$$\dot{x}_- = \mathrm{Pe}\sin x_+ + 2\xi_{x_-}, \tag{5.5}$$

where we have to note, that the two Gaussian noises do not add up linearly, but according to the law of the propagation of uncertainties, i.e. the resulting standard deviation is the square root of the sum of the squares of the standard deviations for each spatial dimension.

The remainder of this chapter is organised as follows: First, in Sect. 5.2 we look at the definition of the numerical model. Afterwards, in Sect. 5.3 we consider some general thoughts about reactions, leading to a fit function. It is used in the consequent two sections. Sect. 5.4 focuses on some details about the numerical simulations and the fits, whereas Sect. 5.5 presents the results of these simulations. Section 5.6 highlights the effect, that reactions occur more likely where the velocity gradients are larger. Finally, in Sect. 5.7 we summarise the findings. The results of this chapter have not been published yet. Here preliminary results are presented.

5.2 Definition of the numerical model

The numerical model is essentially the same as the previous eddy lattice model, see section 3.3. However, each particle now is labelled by an index. After the particles have been introduced into the system, they move without interaction until the checking time t_c. Then we go through the list of all particles in order of the index and test for each particle, if others are close enough to react, i.e. if the distance to another particle is smaller than the reaction radius R. We actually only check, if out of all particles we have not checked yet, the nearest one is within the reaction radius. If so, we let them merge with a probability of 50%. If not, then the particle does not react with any particle in this time step. We then move on to the next particle and compare its position to the ones with larger indices in the list and so on. If two particles react, the one with larger index, i.e. standing lower in the list of the particles, is deleted.

We choose these rules in this particular way, in order not to lose too many particles too quickly and also in order to reduce the computational effort for the simulations.

5.3 Theory: diffusion-reaction equation

In this section we want to consider the theoretical description of reacting, diffusing particles. When neglecting the flow, i.e. for Pe = 0, the particle concentration p for the reaction $A + A \to A$ obeys a diffusion-reaction equation

$$\frac{\partial p}{\partial t} = D\nabla^2 p - kp^2, \tag{5.6}$$

respectively in one dimension

$$\frac{\partial p}{\partial t} = D\frac{\partial^2 p}{\partial x^2} - kp^2. \tag{5.7}$$

Here, the diffusivity D is always set to unity, i.e. $D = 1$. The parameter k is the reaction rate and describes how fast the particles are reacting. The known exact analytical solution

$$p(t) = \frac{1}{1/p_0 + kt} \tag{5.8}$$

to the one-dimensional equation can be integrated over space, in order to yield the function for the decrease of the particle number over time. This is given by

$$N(t) = \frac{N_0}{1 + Kt}, \tag{5.9}$$

where N_0 is the initial particle number and $K = p_0 k$ has been defined, with p_0 being the initial particle concentration.

The function (5.9) can now easily be used to compare it to the simulations, when keeping the initial particle number constant, in our case $N_0 = 10^4$, since then the function only depends on the single parameter K.

5.4 Fitting numerical data to the theory

It is clear, that the dynamics of each particle itself is the same as in the eddy lattice flow without reactions. This includes e.g. the MSD. Note however, that this is not trivial to see from the simulations, since after most particles have reacted with each other, there are only so few left, that the simulated MSD looks very erratic. The only fundamentally different quantity now is the number of particles $N(t)$ decreasing over time instead of being constant.

According to the theory, the number of particles depending on time is supposed to be the simple sigmoid shaped function (5.9). In Fig. 5.1 this function is compared to the results of two simulations. The function is approximately a logistic function in logarithmic time. Its beginning is flat at the initial particle number, bends smoothly before and after a rapid decrease, and finally approaches zero in a very flat way. One slight difference between the simulations and the theory is, that the function (5.9) converges very quickly to zero, whereas actually at least one particle has to be left at the end for all eternity, since the particles do not decay, but only coagulate. This minor detail is neglected by the theory.

5.4.1 Individual measure for fit quality

Motivation

In this section we want to look at the criteria for fitting a curve of approximate sigmoid shape to another one. Let us first realise a subtle issue. The curves, per definition, usually all start at very large values, i.e. at 10^4 or a bit lower, if the simulations are very long and we only look at later orders of magnitude in time. Then around the time $1/K$ the curves typically rapidly decrease and eventually converge to zero. Let us suppose, we have two sigmoid curves looking almost identical. They both begin at 10^4 particles and after half the regarded orders of magnitude in time, they rapidly

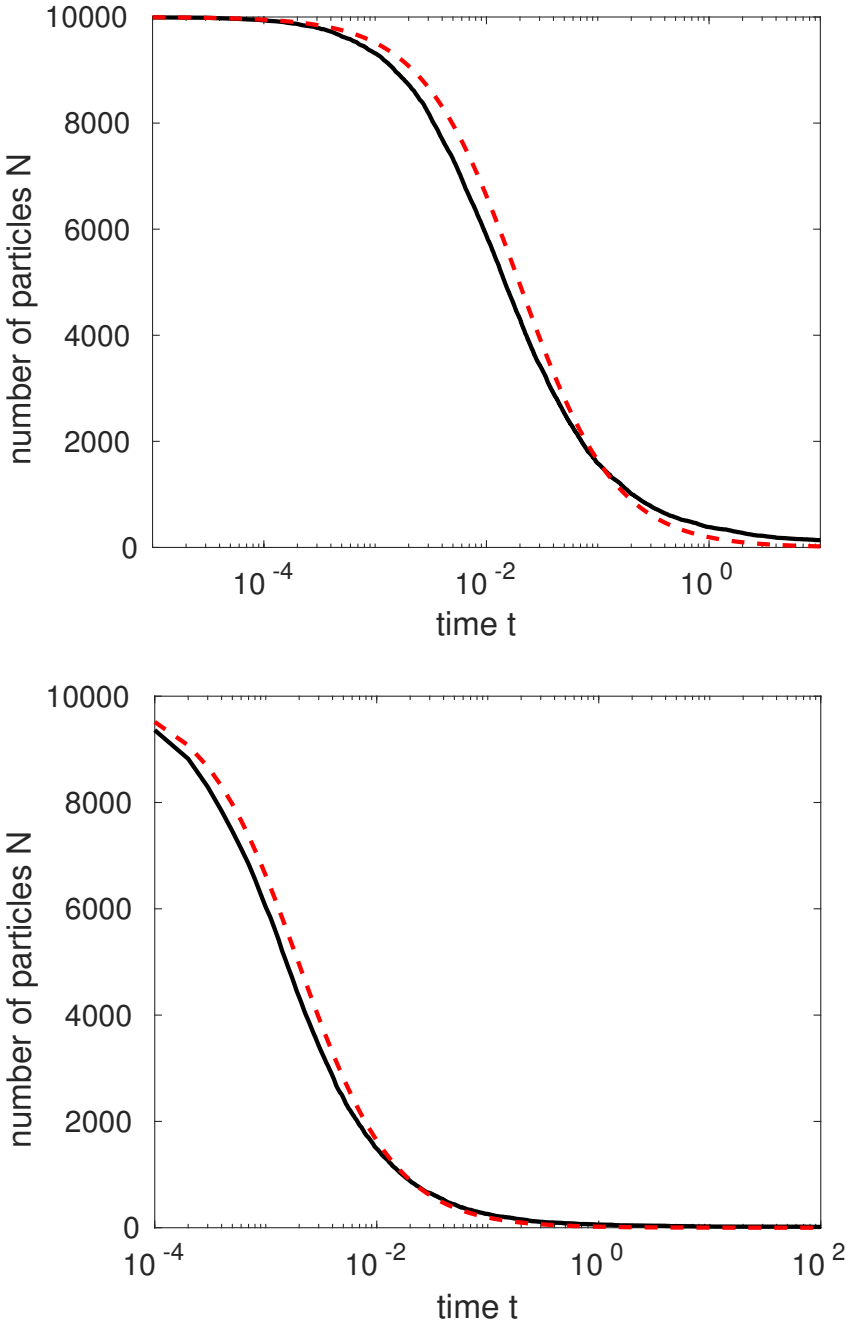

Figure 5.1: Simulated number of particles decreasing over time (black curves) compared to theory (5.9) (red dashed) for $N_0 = 10^4$, Pe $= 0$, $R = 10^{-3}$, $t_c = 10^{-5}$ and $\Delta t = 10^{-6}$ (upper plot), respectively $R = 10^{-2}$ and $t_c = 10^{-4}$ (lower plot). The reaction rate is about $K \approx 50$ for the upper plot, respectively $K \approx 500$ in the lower plot. The values for the P-score are 2.2% (upper) respectively 1.7% (lower). Note that $1/K$ is about the time, where the particle number displays its steepest decrease.

decrease to a value around unity. However, let both of them have slightly different asymptotic values, say for one curve it is unity, for the other curve it is two. In the semi-logarithmic plot, the curves look almost identical and at the very beginning they actually coincide. However, in the latter half of the considered orders of magnitude in time, they are deviating so much from each other, that one is 50% of the other, respectively 200%, when using the other curve as a reference. Additionally to not being a symmetrical measure, i.e. the quality of the fit depends strongly on which one is used as a reference, this method results in very large numbers for the deviations, although the two curves look very similar. One could have expected the numbers to better represent the genuinely good result. Hopefully, this example could illustrate, why a specialised non-standard measure for the quality of a curve fit is adequate in this situation.

Because of this, let us define a quantity for measuring how similar two positive curves are to each other, knowing that they both are bound from above by the same constant value. This measure is symmetric and it does not prefer large function values over small ones. It basically simply measures how similar the two curves look in a semi-logarithmic plot over six orders of magnitude in time, because this is the data always considered, and with a linear vertical axis going from zero to 10^4, because this is the only used initial number of particles. Because of a lack of a better name, let us call the measure *P-score*. Please note, that in different scientific fields there are several completely different metrics called exactly the same.

Definition

For this system it is reasonable to define this measure for semi-logarithmic plots, because other ways of plotting are hardly utilisable for evaluating the results. For example, in the linear plot the number of particles seems to be constant at zero.

The P-score of two curves is then defined in the following way: We measure the area in semi-logarithmic representation between the two curves via integration in units of orders of magnitude in time multiplied by the number of particles. Then we normalise this area by the value 6×10^4, because the only regarded interval is six orders of magnitude in time multiplied by 10^4 particles.

Properties

In order to illustrate the properties of this metric, it is reasonable to look at some extreme situations. If two curves are exactly the same, then the P-score vanishes. That means, zero is the best possible value. The other extreme is, when one curve is constant at 10^4 particles, while the other one is constant zero. Then the P-score is unity, or 100%. Of course, this large deviation is only hypothetical, since no fit would yield such a result. It never matters which curve is the data and which one is the fit. The score is the same when interchanging both curves. Very vertical areas between two curves are weighted much more than horizontal ones. This is intended, since getting a slightly different asymptotic value results in very lengthy horizontal difference areas, whereas not getting the right value for the more important parameter $1/K$, typically results in very vertical areas between the curves. Experience in using the P-score tells us, that for these kinds of plots, two curves look identical to the human eye, if the P-score equals 0.1% or less. For values in the range $0.1\% < \mathrm{P-score} < 1\%$, the curves still look almost identical. P-scores from 1% to about 4% or 5% correspond to curves usually looking roughly similar and typically qualitatively the same. With a P-score of larger than 5%, the curve fit should look very unsatisfactory. Finally, we have to keep

in mind, that one can also reasonably use this measure in other situations, e.g. in linear plots and double-logarithmic plots and other ranges with minimal modifications.

5.4.2 Considered parameter values

Before we come to the numeric results, let us gain a quick overview of which simulation parameters we look at, and why. In the following, we derive these values from the computational limitations. As mentioned before, we can integrate the deterministic part of the equations (3.4) of the eddy lattice flow with our algorithm to acceptable accuracy, if the time step of the integration obeys $\Delta t = 10^{-3}\mathrm{Pe}^{-1}$. We want to give the particles time to diffuse before letting them react, so that they do not all accumulate too quickly, since then only few particles would be left. But on the other hand, we do not want to give them too much time, since then they hardly react at all, and long trajectories would have to be simulated for hardly changing particle numbers. That is, why we check, if the particles might react every 10th, respectively every 100th step, i.e. $t_c = 10\Delta t$, respectively $t_c = 100\Delta t$. Due to computational limitations, i.e. limited time to wait for the simulation results, each trajectory shall not exceed 10^8 integration steps, i.e. the maximal time of simulation is given by $t_{\max} \leq 10^8\Delta t$. Since the particle number does only change every 10th to 100th step, we only have to save the particle numbers at these time steps. Furthermore, we only want to save 10^6 of such time steps. The initial number of particles N_0 should not be too small, since then the number of particles evolving over time would not be very smooth. Of course, it should also not be too large, because then the simulations take very long. The arbitrarily chosen value $N_0 = 10^4$, which is the standard value of the number of walks for the simulations of all flows in this thesis, turned out to be good. Taking all these conditions into account, we end up with the parameter values, for which the results are presented in the following subsection.

5.5 Numeric results

In this section we want to look at the results obtained from the curve fits of the data from the simulations. We want to focus on the flooded case only. First of all, we have to note, that the simulation gives a good sigmoid curve of the kind the theory predicts only, if the checking time t_c is small enough. There is a reaction-diffusion time $t_{\mathrm{RD}} = R^2/D = R^2$. This is a characteristic time particles need to diffusive through each other. If $t_c > t_{\mathrm{RD}}$, i.e. if we look whether particles may react less often than they diffuse through each other, then we miss many reactions that would have actually taken place. In this case, the number of particles is decreasing very slowly for very long times. This almost constant behavior can then be described by $N(t) \simeq c_1 - c_2 \ln(t)$. Determining a reaction rate K in this case is not easy, since technically it is ill-defined in this situation.

Let us look at the reasonable results, in this sense, for the simulations first without deterministic flow, i.e. $\mathrm{Pe} = 0$. The other parameters are $t_c = 10^{-4}$, respectively 10^{-5} with R ranging from 10^{-4} to 10^{-1}. The results can be summarised as

$$K \approx \frac{5R}{t_c} \quad ; t_c < t_{\mathrm{RD}}, \tag{5.10}$$

where $N_0 = 10^4$ always.

The results for the case including the deterministic flow, i.e. $\mathrm{Pe} \neq 0$, can be easily summarised as well. The parameter t_c ranged from 10^{-4} to 10^{-6} with the Péclet number

being Pe = 10^3, respectively 10^4. Again, the reaction rate is fully described by (5.10). In the other case, when t_c is too large, it can not be determined and the very slow logarithmic decrease can be seen. This means, that the Péclet number or the flow itself hardly seems to make any difference for the reactions, at least in the regarded parameter regime.

5.6 Velocity gradient

In this section we want to look at which places the particles react more often. Theoretically, this should happen where the velocity is changing the most. In order to illustrate this idea, consider the following two simple examples.

Imagine a two-dimensional shear flow, where the velocity is always pointing in the same horizontal direction and does not depend on the value of the horizontal axis. Suppose the velocity depends on the vertical coordinate in a non-linear way. In a relatively small surrounding of the streamline, where the velocity is changing the most, there are slower and faster particles moving parallel to each other on closely neighboring streamlines. The faster particles will approach the slower ones approximately in front of them. Keeping in mind, that all particles have a finite reaction radius and there is small noise in our system, we know that these particles, with different velocities moving on slightly different streamlines, are still able to react with each other. On the other hand, the situation that the faster particle is approximately in front of the slower one and thus running away, is not likely to occur, since these particles should have met and thus reacted in the past. That means, it should be only one of these two particles left. This can be an explanation for why the particles should react more likely where the velocity is changing the most in space. In particular this corresponds directly to the off-diagonal elements of the vector gradient of the velocity being large.

However, an even stronger effect of this kind can be observed in the following even simpler example. Consider one straight line, say in the horizontal direction. Suppose the velocity always points parallel to the line. If this velocity is changing in one place more than in the surrounding, this means that particles are running away from each other at one end and are hitting each other on the other end of this peak in the velocity change. All that happens while simply moving on the same streamline. For these situations, reactions are even more likely to occur. They correspond to the diagonal elements of the vector gradient of the velocity being large.

Fig. 5.2 compares the theory of this effect with simulations. What has been plotted in the first plot of this figure, is the Euclidean norm of the diagonal of the velocity gradient of the eddy lattice flow, i.e.

$$\sqrt{2}|\cos(x)\cos(y)| \tag{5.11}$$

as a measure for the spatial change of the velocity.

In the second plot of this figure a simulated density of reactions is shown for parameter values for which this effect is pronounced, i.e. for large Péclet numbers Pe, since in that situation the difference between the fastest and slowest locations in the flow is very large. The effect is overall very weak. That is, why one has to turn to large Pe and average over many simulations, in order to see it well. Similar plots are easily obtained for even larger Péclet numbers. The plot can be explained in the following way: The particles rotate in counter-clockwise motion. They slow down approximately when they are about to approach one of the two diagonals inside the cell. Due to this

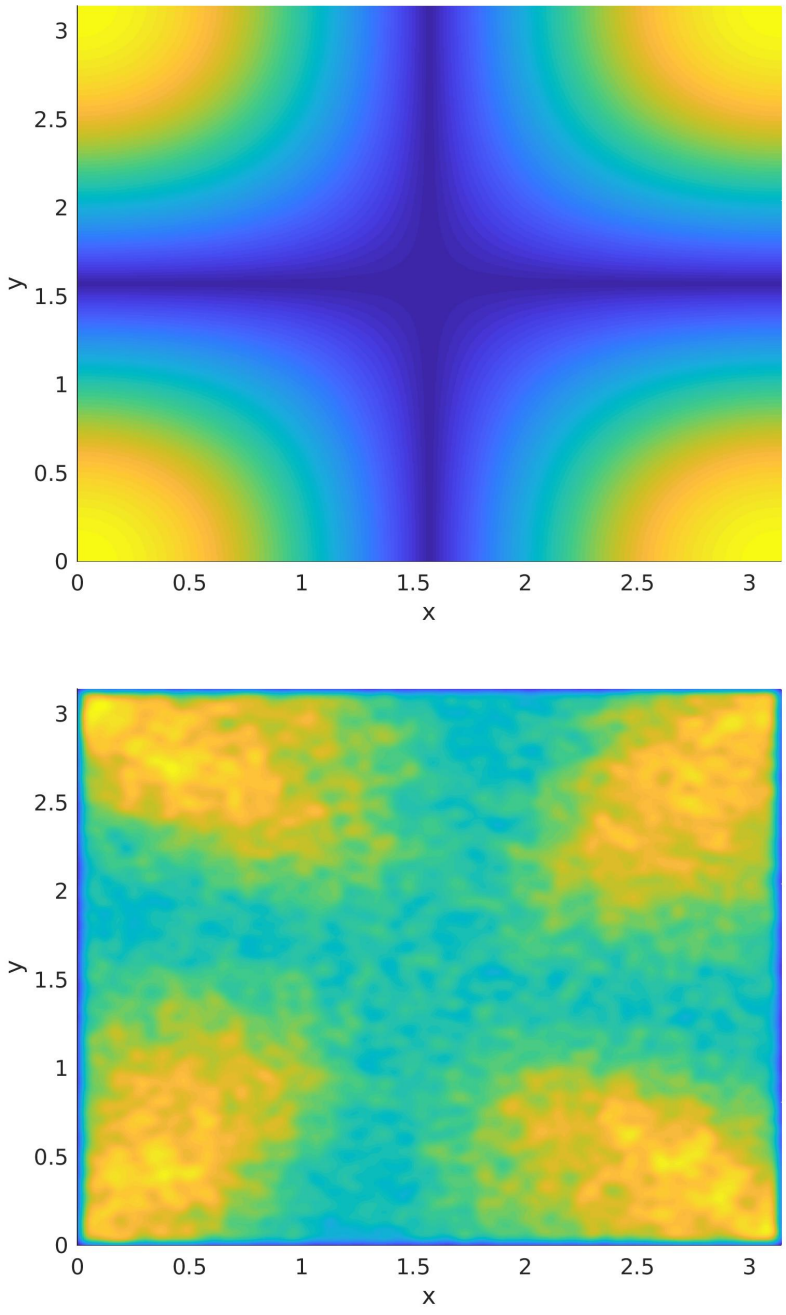

Figure 5.2: Upper plot: Norm (5.11) of the diagonal of the vector gradient of the velocity of the eddy lattice flow in one cell. Lower plot: Density of the positions of the reactions smoothed with Gaussian functions with standard deviation equal to the reaction radius $R = 3 \times 10^{-2}$ averaged over 100 simulations for $N_0 = 10^4$, Pe $= 10^6$, $t_c = 10^{-7}$ and $t_{\max} = 10^{-5}$. The motion of the particles is counter-clockwise. The reactions occur more often at positions where the velocity gradient of the flow is larger.

deceleration, the particles in the front get hit by the faster particles behind them. They react and merge. Now, there are fewer particles left and the velocity increases again. This decreases the probability of further reactions after a diagonal has been crossed. That is, why the reaction density has only rotational symmetries, contrary to the velocity gradient, which has the same symmetry group as a square. In order to make the numerical results less erratic, a Gaussian kernel function with a standard deviation equal to the reaction radius has been used. Furthermore, this smoothed reaction density has been averaged over 100 simulations.

5.7 Summary

We have considered an extension of a simple cellular flow - the eddy lattice flow with particle reactions, allowing coagulation of particles, i.e. particles can absorb each other when being close enough together. Since the particles absorb each other over time, the number of particles decreases. The theory of reaction-diffusion equations predicts a solution describing this decrease via a function, which can be imagined as approximately a logistic function in logarithmic time, i.e. a smooth step function from the initial particle number to zero at about the time equal to the inverse reaction rate.

For fitting this theory to numerical data, a specialised measure for the fit quality turned out to be useful. It is designed to consider both, the very large values at the beginning and the almost vanishing values for large times.

The numeric results reveal, that the reaction rate is simply proportional to the ratio of the reaction radius of the particles and the time after which we look, if particles react. This holds true, as long as we look often enough, in order not to miss too many reactions. In the complementary case, the observed decrease of the particles is logarithmic in time. This decrease would be so slow, that it almost looks like as if it was converging to a final constant particle number. Interestingly, these results for the reaction rate and the number of particles seem to be independent of how fast the particles are moving around in closed orbits within the cells of the flow.

Another observed effect is, that reactions take place significantly more often where the velocity of the flow is changing the most. At these places, slow particles are hit by faster particles following them. Although this effect is relatively weak, we found clear evidence for it in the simulations. This research subject promises further insights and deserves more attention in the future.

Chapter 6

Conclusion

Quantities that behave in a random or seemingly random way can be found in abundance in many natural and artificial systems. Often one does not possess enough information or computational power to describe these systems in a full deterministic way. In these cases a description using random variables and random numbers might be reasonable. One such system is the Brownian motion. It describes particles suspended in fluids like water or air. In these systems particles frequently collide with molecules of the fluid and consequently often change their direction of motion. The particles might also react in one way or another. If winds or streams are absent in the fluids, a description using solely random variables is often sufficient. However, if a mean drift is present, one has to take both effects into account: the random and the deterministic part of the motion.

We investigated the influence of molecular diffusion on the transport of passive tracer particles in two-dimensional laminar flows and obtained various numerical and several analytical results. The flows are of interest, because they are good approximations to experimentally realisable systems. These flows consist of the most basic building blocks, namely jet regions in which particles are transported with an approximately constant speed, as well as cells each containing an eddy. The cells in the examined models possess either the shape of squares or of cat's eyes. One model, the eddy lattice flow, consists of an infinitely large chess board pattern of square cells, each containing an eddy rotating either clockwise or counter-clockwise. Another flow contains a row of eddies between two walls - the Young-Pumir-Pomeau flow. The third one, the cat's eye flow, comprises meandering jets between infinitely many parallel rows of nearly elliptic eddies. A very convenient property of the last one is, that by the change of just one single parameter, one can vary the relative size, and thus the influence, of the jets and the eddies. This family of flows contains even the two extreme cases of the eddies lattice flow, possessing no jets, on one hand and a shear flow consisting of jets moving in opposite directions on the other hand. As already known, without thermal noise the particles inside the flow are trapped inside an eddy forever, whereas adding small molecular diffusion leads to largely enhanced normal diffusion for long times. In the past, these flows were often referred to as typical examples of systems showing subdiffusion, among other properties.

With the numerical simulations performed in this work, we have confirmed some of the previous theoretical predictions, like several intermediate anomalous diffusion exponents and final diffusion coefficients. However, the predicted subdiffusive motion on intermediate times is only present when particles start at the separatrix between two cells - the only case considered in depth in the past - and is less pronounced or

even absent for other initial conditions, or in cases when jet regions between cells can not be neglected, or in aged situations. The short and intermediate time regimes were less investigated until now. We were able to obtain analytical expressions derived from continuous time random walk models for the intermediate time subdiffusive regime, which are in accordance with predictions of former studies. Furthermore, we derived a Lévy walk model for a ballistic intermediate time regime in accordance with our numerical results. Nonetheless, these models do not grasp the details of the motion inside a single eddy on the time scale too small for the random walk models to be applicable. The complex dynamic inside an eddy is especially well visible when looking at aged systems, i.e. when starting the observation after an aging time. The oscillations of the aged mean squared displacement originate from the rotations of the particles around the center of an eddy.

Furthermore, we considered an extension of the eddy lattice flow, allowing coagulation reactions. Over time the particles assemble to one cluster, which however is considered to have the same properties as a single passive tracer particle. Thus effectively, the number of particles is simply decreasing in a way predicted by the exact solution of the corresponding reaction-diffusion equation. The resulting reaction rate depends in a simple way on the reaction radius, measuring the effective size of the particles, and the time describing how often we look, if the particles are close enough to react. This result is preserved as long as we look often enough in order not to miss too many reactions. Interestingly, the reaction rate hardly seems to depend on how fast the particles are rotating in the flow cells. In addition to that, we could see that the reactions occur more often at positions where the velocity of the flow is changing the most, resulting in slow particles being hit by faster ones following them. This research subject promises further insights and deserves more attention in the future.

The work in this thesis had to be done now, after several theoretical predictions have been made about flows, since now we have the computational power to make extensive numerical simulations in order to confirm or falsify these theoretical predictions and also in order gain a deeper and more detailed insight into the dynamics of these systems, especially in situations for which analytical results are hard to find.

Appendix A

Fast implementation of the stochastic Heun scheme for the cat's eye flow

In this section the essential part of a fast implementation of the stochastic Heun algorithm for the iteration of the cat's eye flow in Matlab © code shall be given. The code solves the two coupled stochastic differential equations

$$\dot{U} = \mathrm{Pe}\,(1+A)\sin(V) + \sqrt{2}\xi_U \tag{A.1}$$

$$\dot{V} = \mathrm{Pe}\,(1-A)\sin(U) + \sqrt{2}\xi_V \tag{A.2}$$

for the two rescaled variables $U = x + y$ and $V = x - y$ with ξ being independent Gaussian random numbers with $\langle \xi_i \rangle = 0$ and $\langle \xi_i \xi_{i'} \rangle = 2\delta(t_i - t_{i'})$ for $i = U, V$. The prefactor stems from the fact that one adds two normally distributed variables. Also note that replacing $A = 0$ turns this system into the eddy lattice flow.

Experience showed that a time step of $\Delta t = 10^{-3}\mathrm{Pe}^{-1}$ resulted in negligible deviations of the trajectories of the deterministic part from the exact solution, conserving the value of the stream function Ψ, for simulations being long enough to see all important regimes, i.e. until simulation time $t_{\max} = 100$. Since there are no interactions of the particles, it turned out to be very efficient to iterate all 10^4 particles at the same time in a vectorised way.

```
% given constants
% Pe ... Pe number
% A ... parameter of cat's eye flow
% dt ... constant time step
% N ... number of iteration steps
% walks ... number of particles

% derived constants
sigma=2*sqrt(dt); % factor sqrt(2) more than usual
% because of unconventional variables

% reserve data space
W1=zeros(walks,1);
W2=zeros(walks,1);
Up=zeros(walks,1);
Vp=zeros(walks,1);
Au=zeros(walks,1);
Av=zeros(walks,1);
```

```
U=zeros(walks,2); % old and new U=x+y, V=x-y
V=zeros(walks,2);

x=zeros(walks,1);
y=zeros(walks,1);

% initial conditions (replace with respective values)
% X0(:)=...;
% Y0(:)=...;

U0=X0+Y0;
V0=U0-V0;
U(:,1)=U0(:);
V(:,1)=V0(:);

% iteration for all particles vectorised at same time
for I=1:N
    % stochastic Heun algorithm
    % stochastic part
    W1(:)=randn(walks,1).*sigma;
    W2(:)=randn(walks,1).*sigma;
    % predicted values (same as Euler algorithm)
    Au(:)=(1+A).*sin(V(:,1));
    Av(:)=(1-A).*sin(U(:,1));
    Up(:)=U(:,1)+Au(:).*Pe.*dt+W1(:);
    Vp(:)=V(:,1)+Av(:).*Pe.*dt+W2(:);
    % corrected values (Heun)
    U(:,2)=U(:,1)+((1+A).*sin(Vp(:)) + Au(:)).*Pe.*dt/2+W1(:);
    V(:,2)=V(:,1)+((1-A).*sin(Up(:)) + Av(:)).*Pe.*dt/2+W2(:);
    U(:,1)=U(:,2);
    V(:,1)=V(:,2);

    % saving trajectory
    x(:,I)=(U(:,1)+V(:,1))./2;
    y(:,I)=(U(:,1)-V(:,1))./2;
end
```

Appendix B

Alternative representations of PDF of EL flow

In this section we want to give the derivation of the Fourier-Laplace representation of the probability density function (3.37)

$$p(x,t) = \int_0^\infty \frac{1}{2\pi\sqrt{K\omega t}} \exp\left(-\frac{x^2}{4K\omega} - \frac{\omega^2}{4t}\right) d\omega \tag{B.1}$$

used in chapter 3. Afterwards we will give an alternative representation of the PDF in the formalism of the Fox H-functions. In addition to integral transforms and Taylor series, this is a third common way of expressing PDFs.

B.1 Derivation of the Fourier-Laplace representation

In this section we will Fourier and Laplace transform the PDF of the particles in the EL flow and thus show that it possesses essentially the same form as the YPP flow with a different exponent as mentioned in the text. This is an exercise in integral transforms. They can be looked up e.g. in [15].

Starting with the integral representation in real space and time

$$\begin{aligned} p(x,t) &= \int_0^\infty \frac{1}{2\pi\sqrt{K\omega t}} \exp\left(-\frac{x^2}{4K\omega} - \frac{\omega^2}{4t}\right) d\omega & \text{(B.2)} \\ &= \int_0^\infty \frac{1}{\sqrt{4\pi K\omega}} \exp\left(-\frac{x^2}{4K\omega}\right) \frac{1}{\sqrt{\pi t}} \exp\left(-\frac{\omega^2}{4t}\right) d\omega, & \text{(B.3)} \end{aligned}$$

we use the fact that a Fourier transform in space x of a Gaussian distribution is again Gaussian

$$p(k,t) = \int_0^\infty \exp\left(-K\omega k^2\right) \frac{1}{\sqrt{\pi t}} \exp\left(-\frac{\omega^2}{4t}\right) d\omega. \tag{B.4}$$

Taking the Laplace transform in time t of this yields

$$\begin{aligned} p(k,s) &= \int_0^\infty \exp\left(-K\omega k^2\right) \frac{1}{\sqrt{s}} \exp\left(-\omega\sqrt{s}\right) d\omega & \text{(B.5)} \\ &= \frac{1}{\sqrt{s}} \int_0^\infty \exp\left(-(Kk^2 + \sqrt{s})\omega\right) d\omega. & \text{(B.6)} \end{aligned}$$

by solving this standard integral we obtain

$$p(k,s) = \frac{1}{\sqrt{s}} \frac{1}{Kk^2 + \sqrt{s}} = \frac{s^{-1/2}}{Kk^2 + s^{1/2}}, \tag{B.7}$$

which is of the form (3.34) of $p(k,s)$ with $\alpha = 1/2$, if $K \approx \pi^2 a^2/(2\sqrt{\pi t_1})$.

B.2 Definition of the H-function

The basic idea behind the formalism of H-functions is to use certain parameter values in order to place poles at different positions in the complex plane and then integrating around them. Thus, instead of having to look up differential and integral theorems for many typical special functions, one can simply manipulate the parameters. Before we can apply this formalism, we will briefly mention the definition and the properties relevant for us. The interested reader is referred to [53] for a more detailed introduction to the topic.

The H-function is defined via an inverse Mellin-Barnes transformation.

$$\begin{aligned} \mathrm{H}(x) &= \mathrm{H}^{m,n}_{p,q}\left[x\big|^{(a_p,A_p)}_{(b_q,B_q)}\right] = \mathrm{H}^{m,n}_{p,q}\left[x\big|^{(a_1,A_1),\ldots,(a_p,A_p)}_{(b_1,B_1),\ldots,(b_q,B_q)}\right] \\ &= \frac{1}{2\pi i}\int_{c-i\infty}^{c+i\infty} \frac{\left[\prod_{j=1}^{m}\Gamma\left(b_j + B_j s\right)\right]\left[\prod_{j=1}^{n}\Gamma\left(1-a_j-A_j s\right)\right]x^{-s}}{\left[\prod_{j=m+1}^{q}\Gamma\left(1-b_j-B_j s\right)\right]\left[\prod_{j=n+1}^{p}\Gamma\left(a_j+A_j s\right)\right]}\,ds \end{aligned} \tag{B.8}$$

Here i is the imaginary unit, $i^2 = -1$. The indices m, n, p and q are natural numbers. Empty products, i.e. a product from one to zero or a product from $m+1$ to m, are interpreted as unity.

There are some subtleties concerning the exact shape of the integration contour in the complex plane. The contour must separate the poles

$$s_{j\nu} = -\frac{b_j + \nu}{B_j}, \quad j = 1,\ldots,m, \quad \nu \in \mathbb{N} \tag{B.9}$$

of $\Gamma(b_j + B_j s)$ from the poles of $\Gamma(1 - a_\lambda - A_\lambda s)$ which are

$$s_{\lambda k} = \frac{1 - a_\lambda + k}{A_\lambda}, \quad \lambda = 1,\ldots,m, \quad k \in \mathbb{N}. \tag{B.10}$$

Often this can be achieved by using the contour as in Eq. (B.8) with a suitable choice of the constant c.

In the definition of the H-function appears the gamma function $\Gamma(x)$, see [16]. It is defined as

$$\Gamma(x) = \int_0^\infty t^{x-1} e^{-t}\,dt. \tag{B.11}$$

In the following we will use two properties of the H-function. These show the elegant manipulation of the parameters. First there is a formula for the inverse Laplace transform of an H-function, see Eq. (2.21) in [53],

$$\mathscr{L}^{-1}\left\{s^{-\varrho}\,\mathrm{H}^{m,n}_{p,q}\left[as^{\sigma}\big|^{(a_p,A_p)}_{(b_q,B_q)}\right]\right\} = t^{\varrho-1}\,\mathrm{H}^{m,n}_{p+1,q}\left[at^{-\sigma}\Big|^{(a_p,A_p),(\varrho,\sigma)}_{(b_q,B_q)}\right], \tag{B.12}$$

where $\mathrm{Re}(s) > 0$, $\varrho \in \mathbb{C}$ and $0 < \sigma \in \mathbb{R}$. A similar formula holds for the Laplace transform. Another identity exits for scaling with a power, (1.60) in [53],

$$x^{\sigma}\mathrm{H}^{m,n}_{p,q}\left[x\big|^{(a_p,A_p)}_{(b_q,B_q)}\right] = \mathrm{H}^{m,n}_{p,q}\left[x\big|^{(a_p+\sigma A_p,A_p)}_{(b_q+\sigma B_q,B_q)}\right], \tag{B.13}$$

where $\sigma \in \mathbb{C}$. Now we are going to apply this knowledge.

B.3 Applying the H-function to the PDF

Beginning with the Fourier-Laplace representation of the PDF (B.7)

$$p(k,s) = \frac{1}{K\sqrt{s}}\frac{1}{k^2 + \frac{\sqrt{s}}{K}} \tag{B.14}$$

and taking the inverse Fourier transform we obtain

$$\begin{aligned} p(x,s) &= \frac{1}{2\sqrt{K}} s^{-3/4} \exp\left(-\frac{|x|}{\sqrt{K}} s^{1/4}\right) && \text{(B.15)} \\ &= \frac{1}{2\sqrt{K}} s^{-3/4}\, \mathrm{H}_{0,1}^{1,0}\left[\frac{|x|}{\sqrt{K}} s^{1/4}\middle|_{(0,1)}\right]. && \text{(B.16)} \end{aligned}$$

Inverse Laplace transforming, using (B.12), results in

$$p(x,t) = \frac{1}{2\sqrt{K}} t^{-1/4} \mathrm{H}_{1,1}^{1,0}\left[\frac{|x|}{\sqrt{K}} t^{-1/4}\middle|_{(0,1)}^{\left(\frac{3}{4},\frac{1}{4}\right)}\right], \tag{B.17}$$

or alternatively by absorbing a power, (B.13),

$$p(x,t) = \frac{1}{2|x|} \mathrm{H}_{1,1}^{1,0}\left[\frac{|x|}{\sqrt{K}} t^{-1/4}\middle|_{(1,1)}^{\left(1,\frac{1}{4}\right)}\right]. \tag{B.18}$$

Unfortunately, this is not easily representable as a known special function.

Appendix C

Derivation of the intermediate time asymptotic for the cat's eye flow

In this section we derive the asymptotic expression for the MSD, Eq. (4.21), for intermediate times when starting at the separatrix. Since the MSD is dominated by the longitudinal motion along the axis of the system, a one-dimensional model is sufficient. We use *Lévy walks interrupted by rests* as a theoretical description. The derivation follows the one in [14].

Let $P_1(x,t)$ be the probability density of a tracer being at position x at time t when starting in a ballistic mode and alternating between ballistic motions with velocity $\pm v$ and rests. Given the probability densities of waiting times inside a jet (without index), for resting times (with index r) as well as for the last, incomplete step respectively rest (upper-case symbols), we obtain

$$\begin{aligned} P_1(x,t) &= \Phi(x,t) + \int_0^t \phi(x,t')\Phi_r(t-t')\,dt' \\ &\quad + \int_{-\infty}^{\infty} dx' \int_0^{\infty} dt' \int_0^{t'} dt'' \phi(x',t'')\phi_r(t-t')\Phi(x-x',t-t') + \ldots, \end{aligned} \tag{C.1}$$

where the first term is the probability density for starting at the origin and moving to position x in one single ballistic motion event. The second term corresponds to starting and moving in a ballistic motion until time t' reaching the final position x and then resting for at least as long as the observation time t. The third term corresponds to reaching the final position in two ballistic motions interrupted by one rest. More and more such convolution integrals follow ad infinitum, since the tracer can reach the position x in any number of motions and rests. Fortunately, in Fourier-Laplace representation all convolution integrals become simple products.

$$\begin{aligned} P_1(k,s) &= \Phi(k,s) + \phi(k,s)\Phi_r(s) \\ &\quad + [\phi(k,s)\phi_r(s)]^1\Phi(k,s) + [\phi(k,s)\phi_r(s)]^1\phi(k,s)\Phi_r(s) + \ldots \\ &\quad + [\phi(k,s)\phi_r(s)]^n\Phi(k,s) + [\phi(k,s)\phi_r(s)]^n\phi(k,s)\Phi_r(s) + \ldots \end{aligned} \tag{C.2}$$

Summing up the terms with an even, respectively odd, number of factors separately, we obtain

$$P_1(k,s) = \sum_{n=0}^{\infty} [\phi(k,s)\phi_r(s)]^n \Phi(k,s) + \sum_{n=0}^{\infty} [\phi(k,s)\phi_r(s)]^n \phi(k,s)\Phi_r(s). \tag{C.3}$$

Because of the normalisation, the probability densities are always smaller than unity and thus the geometric series

$$\sum_{n=0}^{\infty} cx^n = \frac{c}{1-x} \tag{C.4}$$

with $|x| < 1$ can be applied in order to obtain

$$P_1(k,s) = \frac{\Phi(k,s)}{1-\phi(k,s)\phi_r(s)} + \frac{\phi(k,s)\Phi_r(s)}{1-\phi(k,s)\phi_r(s)} = \frac{\Phi(k,s)+\Phi_r(s)\phi(k,s)}{1-\phi_r(s)\phi(k,s)}. \tag{C.5}$$

We have to average this result with one from a similar derivation. Let $P_2(k,s)$ be the Fourier-Laplace transformed probability density of arriving at (x,t) when starting in a resting mode. The probability density we need, will then be the arithmetic mean of P_1 and P_2, since both situations are equally probable. In a completely analog way to the previous calculation we obtain

$$\begin{aligned} P_2(k,s) &= \Phi_r(s) + \phi_r(s)\Phi(k,s) + \\ &\quad +[\phi_r(s)\phi(k,s)]^1\Phi_r(s) + [\phi_r(s)\phi(k,s)]^1\phi_r(s)\Phi(k,s) + \dots \\ &\quad +[\phi_r(s)\phi(k,s)]^n\Phi_r(s) + [\phi_r(s)\phi(k,s)]^n\phi_r(s)\Phi(k,s) + \dots, \end{aligned} \tag{C.6}$$

where the first term ($\delta(x)\Phi_r(t)$ in space-time representation) is the probability of starting at the origin and staying there for at least as long as the observation time t. The second term corresponds to beginning with a rest and afterwards reaching (x,t) in one ballistic motion and so on. Again, summing up over odd and even terms and using the geometric series yields

$$P_2(k,s) = \sum_{n=0}^{\infty}[\phi_r(s)\phi(k,s)]^n\Phi_r(s) + \sum_{n=0}^{\infty}[\phi_r(s)\phi(k,s)]^n\phi_r(s)\Phi(k,s) \tag{C.7}$$

$$= \frac{\Phi_r(s)}{1-\phi_r(s)\phi(k,s)} + \frac{\phi_r(s)\Phi(k,s)}{1-\phi_r(s)\phi(k,s)} = \frac{\Phi_r(s)+\Phi(k,s)\phi_r(s)}{1-\phi_r(s)\phi(k,s)}. \tag{C.8}$$

Putting everything together, we obtain

$$P(k,s) = \frac{1}{2}P_1(k,s) + \frac{1}{2}P_2(k,s) \tag{C.9}$$

$$= \frac{\Phi(k,s)+\Phi_r(s)\phi(k,s)}{2(1-\phi_r(s)\phi(k,s))} + \frac{\Phi_r(s)+\Phi(k,s)\phi_r(s)}{2(1-\phi_r(s)\phi(k,s))} \tag{C.10}$$

$$P(k,s) = \frac{\Phi(k,s)(1+\phi_r(s)) + \Phi_r(s)(1+\phi(k,s))}{2(1-\phi_r(s)\phi(k,s))} \tag{C.11}$$

for the probability density of being at time t at position x on the axis Fourier-transformed in space and Laplace-transformed in time. Numerics show, that the waiting time densities of a tracer inside a jet respectively a vortex can roughly be approximated by a power law

$$\phi(t) = \phi_r(t) = \frac{1}{2}\sqrt{t_1}t^{-3/2} = \frac{1}{2}\sqrt{\frac{\tau}{\pi}}t^{-3/2}, \tag{C.12}$$

if the parameter A is not too small, as expected by theory. Hence, we get for the PDF for the resting phase, see (2.16),

$$\phi_r(s) = \mathscr{L}\{\phi_r(t)\} = 1 - \sqrt{\tau s}, \tag{C.13}$$

respectively for the last incomplete rest, see 2.29,

$$\Phi_r(s) = \mathscr{L}\left\{\int_t^\infty \phi_r(t')\,dt'\right\} = \frac{1-\phi_r(s)}{s} = \sqrt{\frac{\tau}{s}}. \tag{C.14}$$

Furthermore, we obtain for the PDF of the last incomplete ballistic motion

$$\begin{aligned}
\Phi(k,s) &= \mathscr{L}\left\{\mathscr{F}\left[\frac{1}{2}\delta(|x|-vt)\right]\int_t^\infty \phi(t')\,dt'\right\} && \text{(C.15)}\\
&= \mathscr{L}\left\{\frac{1}{2}\int_{-\infty}^{\infty}\delta(|x|-vt)e^{ikx}\,dx\int_t^\infty \phi(t')\,dt'\right\} && \text{(C.16)}\\
&= \mathscr{L}\left\{\int_t^\infty \phi(t')\,dt'e^{-ikvt}\right\} = \mathrm{Re}\left\{\left.\frac{1-\phi(s')}{s'}\right|_{s'=s+ivk}\right\} && \text{(C.17)}\\
&= \mathrm{Re}\left\{\sqrt{\frac{\tau}{s+ivk}}\right\} = \frac{\sqrt{\tau}\cos\left(\frac{1}{2}\arctan\left(\frac{vk}{s}\right)\right)}{(s^2+v^2k^2)^{1/4}}, && \text{(C.18)}
\end{aligned}$$

respectively for the PDF of all other ballistic motions

$$\phi(k,s) = \mathscr{L}\left\{\mathscr{F}\left[\frac{1}{2}\delta(|x|-vt)\right]\phi(t)\right\} = \frac{1}{2}\sqrt{\frac{\tau}{\pi}}\int_{\tau/\pi}^\infty t^{-3/2}\cos(kvt)e^{-st}\,dt. \tag{C.19}$$

Note, that the lower boundary of the Laplace transform in (C.19) is not zero, since $\phi(t)$ possesses a lower cutoff at $t = t_1$. Writing the cosine complex, one obtains

$$\begin{aligned}
\phi(k,s) &= e^{-\frac{\tau}{\pi}s}\cos\left(\frac{\tau}{\pi}kv\right) && \text{(C.20)}\\
&\quad + \frac{\sqrt{s+ikv}}{2}\left[-\sqrt{\tau}+\mathrm{erf}\left(\sqrt{\frac{\tau}{\pi}(s+ikv)}\right)\right]\\
&\quad + \frac{\sqrt{s-ikv}}{2}\left[-\sqrt{\tau}+\mathrm{erf}\left(\sqrt{\frac{\tau}{\pi}(s-ikv)}\right)\right].
\end{aligned}$$

Here erf denotes the error function, [16]. Substituting (C.13), (C.14), (C.18) and (C.20) into (C.11) and expanding both its numerator and its denominator separately first in k until second order and then in s until first order, keeping only the highest order terms in s in each coefficient of the series in k, yields

$$P(k,s) = \frac{4\sqrt{\frac{\tau}{s}} - \frac{3\sqrt{\tau}v^2}{4s^{5/2}}k^2}{4\sqrt{\tau s} + \frac{\sqrt{\tau}v^2}{4s^{3/2}}k^2} = \frac{1}{s}\frac{\left[1-\frac{3}{16}\left(\frac{vk}{s}\right)^2\right]}{\left[1+\frac{1}{16}\left(\frac{vk}{s}\right)^2\right]}, \tag{C.21}$$

i.e.

$$P(k,s) = \frac{1}{s}\left[1-\frac{1}{4}\left(\frac{vk}{s}\right)^2\right] \tag{C.22}$$

in second order in k. From the probability density follows the MSD, see 2.24,

$$\mathrm{MSD}(s) = \frac{1}{2}v^2 s^{-3}, \tag{C.23}$$

which, according to Tauberian theorems for the inverse Laplace-transform, corresponds to (4.21) in real time.

List of Figures

Index of symbols and abbreviations

a	length scale
A	parameter of the cat's eye flow
Ai	Airy function
c	a constant
Cat	cat's eye (flow)
CDF	cumulative distribution function
CTRW	continuous time random walk
D	diffusivity, i.e. noise intensity
D^*	final diffusivity, i.e. final diffusion coefficient
EL	eddy lattice (flow)
erf	error function
f	a function
$\mathscr{F}$	Fourier transform from space x to wave number k
FPE	Fokker-Planck equation
g	a function
H	Fox H-function
i	the imaginary unit, an index
k	one-dimensional Fourier variable
K	a constant, reaction rate
$K(m)$	complete elliptic integral of first kind
$\mathscr{L}$	Laplace transform from time t to frequency s
LW	Lévy walk
M_n	the nth moment of a PDF
MSD	mean squared displacement
$\mathrm{MSD}^{\mathrm{sim}}$	MSD obtained from simulation
n	index, constant
N	number of particles
N_0	initial number of particles
PDF, p, P, P_1, P_2	probability density functions
Pe	Péclet number
r	radius, position in one- or two-dimensional space
R	reaction radius
Re	real part
RMSD	root mean squared displacement
rot	curl/rot operator

s	Laplace variable
SDE	stochastic differential equation
t	time
t_1, t_2, t_3	characteristic times
t_a	aging time
t_c	checking time (time after one looks, if particles may react)
$t_{\max}$	total observation time
t_{RD}	reaction-diffusion time (time particles need to diffuse through each other)
T	time period, total observation time
TAMSD	time averaged mean squared displacement
u, v	characteristic velocity of the flow, other velocities
U, V	rescaled and rotated (and shifted) coordinates
w	width of the jet in the cat's eye flow
WTD	waiting time probability density function
YPP	Young-Pumir-Pomeau (flow)
x, y	coordinates in two-dimensional position space
x_+, x_-	rescaled and rotated coordinates
z	coordinate perpendicular to the streamlines
α, γ	exponents
Γ	gamma function
δ	Dirac-delta function, a distance
Δ	time delay
Δt	time step for numeric integration
ϕ, Φ	(waiting time) probability density functions
ξ	Gaussian white noise
π	circumference of a circle with unit diameter
ρ	rescaled distance
τ	a normalisation constant
ψ	stream function
Ψ	stream function in rescaled units
ω, Ω	frequencies
$\langle\rangle$	ensemble average, i.e. arithmetic mean over particles
$\parallel$	parallel to the main axis of the cat's eye flow
$\perp$	perpendicular to the main axis of the cat's eye flow

Bibliography

[1] A. Fick, *Über Diffusion*, Ann. Phys. **94**, 59-86 (1855). https://doi.org/10.1002/andp.18551700105

[2] A. Einstein, *Über die von der molekularkinetischen Theorie der Wärme geforderte Bewegung von in ruhenden Flüssigkeiten suspendierten Teilchen*, Ann. Phys. **17**, 549-560 (1905). https://doi.org/10.1002/andp.200590005

[3] S. Chandrasekhar, *Stochastic Problems in Physics and Astronomy*, Rev. Mod. Phys. **15**, 1-89 (1943). https://doi.org/10.1103/RevModPhys.15.1

[4] P. Romanczuk, M. Bär, W. Ebeling, B. Lindner, and L. Schimansky-Geier, *Active Brownian Particles: From Individual to Collective Stochastic Dynamics*, Eur. Phys. J. Spec. Top. **202**, 1-162 (2012). https://doi.org/10.1140/epjst/e2012-01529-y

[5] G. E. Uhlenbeck and L. S. Ornstein, *On the Theory of the Brownian Motion*, Phys. Rev. **36**, 823-841 (1930). https://doi.org/10.1103/PhysRev.36.823

[6] C. Weber, P. K. Radtke, L. Schimansky-Geier, and Peter Hänggi, *Active motion assisted by correlated stochastic torques*, Phys. Rev. E **84**, 011132 (2011). https://doi.org/10.1103/PhysRevE.84.011132

[7] C. Van den Broeck, *Taylor dispersion revisited*, Physica A **168**, 677-696 (1990). https://doi.org/10.1016/0378-4371(90)90023-L

[8] L. Haeggqwist, L. Schimansky-Geier, I. M. Sokolov, and F. Moss, *Hopping on a zig-zag course*, Eur. Phys. J. Spec. Top. **157**, 33-42 (2008). http://dx.doi.org/10.1140/epjst/e2008-00628-8

[9] D. Takagi, A. B. Braunschweig, J. Zhang, and M. J. Shelley, *Dispersion of Self-Propelled Rods Undergoing Fluctuation-Driven Flips*, Phys. Rev. Lett. **110**, 038301 (2013). https://doi.org/10.1103/PhysRevLett.110.038301

[10] S. Havlin, and D. Ben-Avraham, *Diffusion in disordered media*, Adv. in Phys. **51**, 187-292 (2002). https://doi.org/10.1080/00018730110116353

[11] T. H. Solomon, E. R. Weeks, and H. L. Swinney, *Observation of Anomalous Diffusion and Lévy Flights in a Two-Dimensional Rotating Flow*, Phys. Rev. Lett. **71**, 3975-3978 (1993). https://doi.org/10.1103/PhysRevLett.71.3975

[12] T. H. Solomon, E. R. Weeks, and H. L. Swinney, *Chaotic advection in a two-dimensional flow: Lévy flights and anomalous diffusion*, Physica D **76**, 70-84 (1994). https://doi.org/10.1016/0167-2789(94)90251-8

[13] E. R. Weeks, J. S. Urbach, and H. L. Swinney, *Anomalous diffusion in asymmetric random walks with a quasi-geostrophic flow example*, Physica D **97**, 291-310 (1996). https://doi.org/10.1016/0167-2789(96)00082-6

[14] J. Klafter and I. M. Sokolov, *First steps in Random Walks* (Oxford University Press, Oxford, 2011).

[15] I. N. Bronstein, K. A. Semendjajew, G. Musiol and H. Mühlig, *Taschenbuch der Mathematik*, (Verlag Harri Deutsch, Frankfurt on Main, 2008). https://doi.org/10.1002/piuz.19800110415

[16] M. Abramowitz and I. A. Stegun, *Handbook of Mathematical Functions With Formulas, Graphs, and Mathematical Tables* (U.S. Gov. Print. Off., Washington D.C., 1964).

[17] S. N. Majumdar, *Universal first-passage properties of discrete-time random walks and Lévy flights on a line: Statistics of the global maximum and records*, Physica A **389**, 4299-4316 (2010). https://doi.org/10.1016/j.physa.2010.01.021

[18] J. P. Bouchaud and A. Georges, *Anomalous diffusion in disordered media: Statistical mechanisms, models and physical applications*, Phys. Rep. **195**, 127-293 (1990). http://dx.doi.org/10.1016/0370-1573(90)90099-N

[19] M. B. Isichenko, *Percolation, statistical topography, and transport in random media*, Rev. Mod. Phys. **64**, 961-1043 (1992). https://doi.org/10.1103/RevModPhys.64.961

[20] Y. Meroz, I. M. Sokolov, and J. Klafter, *Unequal twins: probability distributions do not determine everything*, Phys. Rev. Lett. **107**, 260601 (2011). https://doi.org/10.1103/PhysRevLett.107.260601

[21] W. Young, A. Pumir, and Y. Pomeau, *Anomalous diffusion of tracer in convection rolls*, Phys. Fluids A **1**, 462-469 (1989). http://dx.doi.org/10.1063/1.857415

[22] S. Childress, *Alpha-effect in flux ropes and sheets*, Phys. Earth Planet. Inter. **20**, 172-180 (1979). https://doi.org/10.1016/0031-9201(79)90039-6

[23] A. M. Soward, *Fast dynamo action in a steady flow*, J. Fluid Mech. **180**, 267-295 (1987). https://doi.org/10.1017/S0022112087001800

[24] B. I. Shraiman, *Diffusive transport in a Rayleigh-Bénard convection cell*, Phys. Rev. A **36**, 261-267 (1987). https://doi.org/10.1103/PhysRevA.36.261

[25] M. N. Rosenbluth, H. L. Berk, I. Doxas, and W. Horton, *Effective diffusion in laminar convective flows*, Phys. Fluids, **30**, 2636-2647 (1987). http://dx.doi.org/10.1063/1.866107

[26] A. J. Majda and P. R. Kramer, *Simplified models for turbulent diffusion: Theory, numerical modelling, and physical phenomena*, Phys. Rep. **314**, 237-574 (1999). https://doi.org/10.1016/S0370-1573(98)00083-0

[27] P. H. Haynes and J. Vanneste, *Dispersion in the large-deviation regime*, J. Fluid Mech. **745**, 321 (2014); **745**, 351 (2014).
https://doi.org/10.1017/jfm.2014.64
https://doi.org/10.1017/jfm.2014.65

[28] T. Miyaguchi and T. Akimoto, *Ultraslow convergence to ergodicity in transient subdiffusion*, Phys. Rev. E **83**, 062101 (2011).
https://doi.org/10.1103/PhysRevE.83.062101

[29] T. Miyaguchi and T. Akimoto, *Ergodic properties of continuous-time random walks*, Phys. Rev. E **87**, 032130 (2013).
https://doi.org/10.1103/PhysRevE.87.032130

[30] O. Cardoso and P. Tabeling, *Anomalous Diffusion in a Linear Array of Vortices*, Europhys. Lett. **7**, 225-230, (1988).
https://doi.org/10.1209/0295-5075/7/3/007

[31] T. H. Solomon and J. P. Gollub, *Passive transport in steady Rayleigh-Bénard convection*, Phys. Fluids **31**, 1372-1379 (1988).
http://dx.doi.org/10.1063/1.866729

[32] L. Bergougnoux, G. Bouchet, D. Lopez, and É. Guazzelli, *The motion of solid spherical particles falling in a cellular flow field at low Stokes number*, Phys. Fluids **26**, 093302 (2014). http://dx.doi.org/10.1063/1.4895736

[33] P. Pöschke, I. M. Sokolov, A. A. Nepomnyashchy, and M. A. Zaks, *Anomalous transport in cellular flows: The role of initial conditions and aging*, Phys. Rev. E **94**, 032128 (2016). https://doi.org/10.1103/PhysRevE.94.032128

[34] G. Iyer and A. Novikov, *Anomalous diffusion in fast cellular flows at intermediate time scales*, Probab. Theory Relat. Fields **164**, 707-740 (2016).
http://dx.doi.org/10.1007/s00440-015-0617-9

[35] R. Mannella, in *Stochastic processes in physics, chemistry, and biology* (Springer, Berlin Heidelberg, 2000), p. 353-364.
http://dx.doi.org/10.1007/3-540-45396-2_32

[36] I. M. Sokolov, *Models of anomalous diffusion in crowded environments*, Soft Matter **8**, 9043-9052 (2012). http://dx.doi.org/10.1039/C2SM25701G

[37] W. Thomson (Lord Kelvin), *On a disturbing infinity in Lord Rayleigh's solution for waves in a plane vortex stratum*, Nature **23**, 45 (1880).
http://dx.doi.org/10.1038/023045a0

[38] S. Childress and A. M. Soward, *Scalar transport and alpha-effect for a family of cat's-eye flows*, J. Fluid. Mech. **205**, 99-133 (1989).
https://doi.org/10.1017/S0022112089001965

[39] A. Fannjiang, *Time Scales in Homogenization of Periodic Flows with Vanishing Molecular Diffusion*, J. Diff. Eq. **179**, 433-445 (2002).
https://doi.org/10.1006/jdeq.2001.4039

[40] M. Hairer et al., *A fractional kinetic process describing the intermediate time behaviour of cellular flows*, Ann. Prob. (to be published). https://arxiv.org/abs/1607.01859

[41] A. Fannjiang and G. Papanicolaou, *Convection enhanced diffusion for periodic flows*, SIAM: J. Appl. Math. **54**, 333-408 (1994). http://doi.org/10.1137/S0036139992236785

[42] V. Zaburdaev, S. Denisov, and J. Klafter, *Lévy walks*, Rev. Mod. Phys. **87**, 483-530 (2015). https://doi.org/10.1103/RevModPhys.87.483

[43] D. Froemberg and E. Barkai, *Time-averaged Einstein relation and fluctuating diffusivities for the Lévy walk*, Phys. Rev. E **87**, 030104(R), (2013). https://doi.org/10.1103/PhysRevE.87.030104

[44] M. Magdziarz and T. Zorawik, *Aging ballistic Lévy walks*, Phys. Rev. E **95**, 022126 (2017). https://doi.org/10.1103/PhysRevE.95.022126

[45] P. Pöschke, I. M. Sokolov, M. A. Zaks, and A. A. Nepomnyashchy, *Transport on intermediate time scales in flows with cat's eye patterns*, Phys. Rev. E **96**, 062128 (2017). https://doi.org/10.1103/PhysRevE.96.062128

[46] E. A. Novikov, *Concerning a Turbulent Diffusion in a Stream with a Transverse Gradient of Velocity*, J. Appl. Math. Mech. **22**, 576-579 (1958). https://doi.org/10.1016/0021-8928(58)90074-1

[47] R. T. Foister and T. G. M. Van De Ven, *Diffusion of Brownian particles in shear flows*, J. Fluid Mech. **96**, 105-132 (1980). https://doi.org/10.1017/S0022112080002042

[48] D. Ben-Avraham and S. Havlin, *Diffusion and Reactions in Fractals and Disordered Systems*, (Cambridge University Press, Cambridge, 2000). https://doi.org/10.1017/CBO9780511605826

[49] N. Kumar and G. Tripathy, *Velocity and diffusion coefficient of $A+A \leftrightarrow A$ reaction fronts in one dimension*, Phys. Rev. E **74**, 011109 (2006). https://doi.org/10.1103/PhysRevE.74.011109

[50] E. Ben-Naim and P. L. Krapivsky, *Escape and finite-size scaling in diffusion-controlled annihilation*, J. Phys. A: Math. Theor. **49**, 504004 (2016). https://doi.org/10.1088/1751-8113/49/50/504004

[51] A. A. Ovchinnikov and Y. B. Zeldovich, *Role of density fluctuations in bimolecular reaction kinetics*, Chem. Phys. **28**, 215-218 (1978). https://doi.org/10.1016/0301-0104(78)85052-6

[52] G. Zumofen, J. Klafter, and M. F. Shlesinger, *Breakdown of Ovchinnikov-Zeldovich Segregation in the $A + B \rightarrow 0$ Reaction under Lévy Mixing*, Phys. Rev. Lett. **77**, 2830-2833 (1996). https://doi.org/10.1103/PhysRevLett.77.2830

[53] A. M. Mathai, R. K. Saxena and H. J. Haubold, *The H-function: Theory and Applications*, (Springer, New York Dordrecht Heidelberg London 2010).

List of Publications and Presentations

- P. Pöschke, I. M. Sokolov, A. A. Nepomnyashchy, and M. A. Zaks, *Anomalous transport in cellular flows: The role of initial conditions and aging*, Phys. Rev. E **94**, 032128 (2016). https://doi.org/10.1103/PhysRevE.94.032128
- P. Pöschke, I. M. Sokolov, M. A. Zaks, and A. A. Nepomnyashchy, *Transport on intermediate time scales in flows with cat's eye patterns*, Phys. Rev. E **96**, 062128 (2017). https://doi.org/10.1103/PhysRevE.96.062128
- 2nd Haifa Probability School, Haifa, Israel, *talk* (2017). https://hps2.net.technion.ac.il/

Acknowledgements

First of all, I have to thank my three supervisors Prof. Igor Sokolov, PD Michael Zaks and Prof. Alexander Nepomnyashchy very, very much for explaining the theory to me, for always finding the mistakes in my calculations and for teaching me how we scientists work. Furthermore, I thank Robert Ronge, Jörg Nötel, Martin Rückl and other colleagues for telling me one or the other trick about programming and for proofreading my thesis. Also I have to thank the German-Israeli Foundation for Scientific Research and Development for financing the research conducted for writing this thesis and thus giving me the opportunity to obtain the doctoral degree. Finally, I must thank my parents for giving me the opportunity of focusing solely on my study over all those years and for allowing me to dedicate the majority of my time to working on this thesis!

Tools

This thesis was written with LaTeX. Numerical simulations and plots were done using *Matlab* ® R2017a version 9.2. Some analytical calculations were performed using *Mathematica* ® 2017 version 11.1.

Selbstständigkeitserklärung

Hiermit erkläre ich, dass ich die Dissertation selbstständig und nur unter Verwendung der von mir gemäß §7 Abs. 3 der Promotionsordnung der Mathematisch-Naturwissenschaftlichen Fakultät, veröffentlicht im Amtlichen Mitteilungsblatt der Humboldt-Universität zu Berlin Nr. 126/2014 am 18.11.2014 angegebenen Hilfsmittel angefertigt habe.

Ich erkläre, dass die von mir in der Universitätsbibliothek abgegebene schriftliche und elektronische Version der Dissertationsschrift mit der angenommenen Dissertation übereinstimmt. Ich habe nur die Mängel beseitigt und die Auflagen erfüllt, die mir bei der Verteidigung mitgeteilt und deren Erfüllung der Vorsitzende der Promotionskommission bestätigt hat.

Patrick Pöschke	Ort, Datum